

ABSTRACT

Title of Dissertation: ESTIMATION AND CONTROL OF
A DISTRIBUTED PARAMETER SYSTEM BY
A TEAM OF MOBILE SENSORS AND ACTUATORS

Sheng Cheng
Doctor of Philosophy, 2021

Dissertation Directed by: Professor Derek A. Paley
Department of Aerospace Engineering
Institute for Systems Research

The recent development of mobile robots has dramatically extended the scenarios where robots can be deployed to complete tasks autonomously. One of the tasks is monitoring and controlling large-scale spatiotemporal processes, e.g., oil spills and forest fires, which is mainly conducted by human operators. These tasks can pose health threats, cause severe environmental issues, and incur substantial financial costs. Autonomous robots can free human operators from danger and complete tasks in a timely and economically efficient manner. In this dissertation, estimation and control of spatiotemporal processes using mobile sensors and actuators are studied. Spatiotemporal processes vary in both space and time, whose dynamics can be characterized by partial differential equations (PDEs). Since the state space of a PDE is infinite-dimensional, a system with PDE dynamics is also known as a distributed parameter system (DPS). The performance of the estimation and control of a DPS can be enhanced (compared to stationary sensors and

actuators) due to the additional degree of freedom induced from the mobility of the sensors and actuators. However, the vehicles carrying sensors and actuators usually have limited onboard resources (e.g., fuels and batteries) whose usage requires judicious decisions. Hence, we propose a new optimization framework that addresses the goal of estimation and control of a spatiotemporal process while considering the limited onboard resources.

In the first part of this dissertation, an optimization framework is proposed to control a DPS modeled by a 2D diffusion-advection equation using a team of mobile actuators. The framework simultaneously seeks optimal control of the DPS and optimal guidance of the mobile actuators such that a cost function associated with both the DPS and the mobile actuators is minimized subject to the dynamics of each. We establish conditions for the existence of a solution to the proposed problem. Since computing an optimal solution requires approximation, we also establish the conditions for convergence to the exact optimal solution of the approximate optimal solution. That is, when evaluating these two solutions by the original cost function, the difference becomes arbitrarily small as the approximation gets finer. Two numerical examples demonstrate the performance of the optimal control and guidance obtained from the proposed approach.

In the second part of this dissertation, an optimization framework is proposed to design guidance for a possibly heterogeneous team of multiple mobile sensors to estimate a spatiotemporal process modeled by a 2D diffusion-advection process. Owing to the abstract linear system representation of the process, we apply the Kalman-Bucy filter for estimation, where the sensors provide linear outputs. We

propose an optimization problem that minimizes the sum of the trace of the covariance operator of the Kalman-Bucy filter and a generic mobility cost of the mobile sensors, subject to the sensors' motion modeled by linear dynamics. We establish the existence of a solution to this problem. Moreover, we prove convergence to the exact optimal solution of the approximate optimal solution. That is, when evaluating these two solutions using the original cost function, the difference becomes arbitrarily small as the approximation gets finer. To compute the approximate solution, we use Pontryagin's minimum principle after approximating the infinite-dimensional terms originating from the diffusion-advection process. The approximate solution is applied in simulation to analyze how a single mobile sensor's performance depends on two important parameters: sensor noise variance and mobility penalty. We also illustrate the application of the framework to multiple sensors, in particular the performance of a heterogeneous team of sensors.

In the third part of this dissertation, a cooperative framework for estimating and controlling a spatiotemporal process using collocated mobile sensors and actuators is proposed. We model the spatiotemporal process by a 2D diffusion equation that represents the dynamics. Measurement and actuation of the process dynamics are performed by mobile agents whose motion is described by single-integrator dynamics. The estimation and control framework is formulated using a Kalman filter and an optimization problem. The former uses sensor measurements to reconstruct the process state, while the latter uses the estimated state to plan the actuation and guidance of the mobile agents. The optimization problem seeks the actuation and guidance that minimize the sum of the quadratic costs of the process state,

actuation input, and guidance effort. Constraints include the process and agent dynamics as well as actuation and speed bounds. The framework is implemented with the optimization problem solved periodically using a nonlinear program solver. Numerical studies analyze and evaluate the performance of the proposed framework using a nondimensional parameterization of the optimization problem. The framework is also implemented on an outdoor multi-quadrotor testbed with a simulated spatiotemporal process and synthetic measurement and actuation.

ESTIMATION AND CONTROL OF A DISTRIBUTED
PARAMETER SYSTEM BY A TEAM OF
MOBILE SENSORS AND ACTUATORS

by

Sheng Cheng

Dissertation submitted to the Faculty of the Graduate School of the
University of Maryland, College Park in partial fulfillment
of the requirements for the degree of
Doctor of Philosophy
2021

Advisory Committee:
Professor Derek A. Paley, Chair/Advisor
Professor John S. Baras
Professor André L. Tits
Professor Pratap Tokekar
Professor Nikhil Chopra

© Copyright by
Sheng Cheng
2021

Dedication

I dedicate this dissertation to my parents.

Acknowledgments

I want to thank Professor Derek Paley for being an enlightening, supportive, and knowledgeable advisor during my Ph.D. studies. I would like to thank Professors John Baras, André Tits, Pratap Tokekar, and Nikhil Chopra for agreeing to serve on my defense committee and their suggestions on my work. I would also like to express my gratitude to Professor Artur Wolek, Ezra Bregin, Curtis Merrill, Charles Flanagan, Joshua Yuan, Aniket Goel, Kenneth Kroeger, and Patrick Nolan for their help on setting up the multi-quadrotor testbed and conducting the experimental demonstrations at the Fearless Flight Facility of the University of Maryland. I am also thankful to the research opportunities funded by DARPA under Contract No. HR001118C0142 and by Northrop Grumman under a seed grant.

I want to thank my girlfriend Jinuan for being my safe harbor and supporting me whenever life is happy or tough. I'm sincerely grateful to my parents, Dr. Cheng and Mrs. Li, for being my strongest backing and selfless love.

And finally, I want to thank the lab members at the Collective Dynamics and Control Laboratory for the time we spent together at Kim 3247. I would also like to thank my friends for accompanying me during trips and adventures.

Table of Contents

Dedication	ii
Acknowledgements	iii
Table of Contents	iv
List of Tables	vi
List of Figures	vii
List of Abbreviations	x
Chapter 1: Introduction	1
1.1 Survey of the relevant literature	2
1.2 Contributions to the state-of-the-art	12
1.3 Outline of the dissertation	13
Chapter 2: Notation, terminology, and supporting Lemmas	16
2.1 Notation and terminology	16
2.2 Dynamics of the mobile actuators and sensors	17
2.3 Deterministic abstract linear system and linear-quadratic regulation	19
2.4 Abstract linear system with Gaussian noise and the Kalman filter	25
2.5 Finite-dimensional approximations	30
Chapter 3: Optimal cooperative control of a 2D diffusion-advection process	38
3.1 Problem formulation	40
3.2 Computation of optimal control and guidance	44
3.2.1 Checking assumptions (C4)–(C12)	49
3.2.2 Gradient-descent for solving problem (APc)	49
3.3 Numerical examples	50
3.3.1 Diffusion-advection process with Dirichlet boundary condition	51
3.3.2 Diffusion-advection process with Neumann boundary condition	56
Chapter 4: Optimal cooperative estimation of a 2D diffusion-advection process	61
4.1 Problem formulation	63
4.2 Solving optimal guidance using approximation	68
4.3 Simulation results	72

4.3.1	Single sensor results	75
4.3.2	Team of homogeneous sensors	81
4.3.3	Team of heterogeneous sensors	83
Chapter 5:	Cooperative estimation and control: simulations and experiments	86
5.1	Cooperative estimation and control framework	92
5.2	Numerical studies	95
5.2.1	An example of optimal guidance and actuation	96
5.2.2	Nondimensional analysis of the parameter space	99
5.2.3	Monte Carlo simulations	108
5.3	Experimental demonstration of the framework	110
5.3.1	Survey of multi-quadrotor testbed in the literature	110
5.3.2	Multi-quadrotor testbed in this work	112
5.3.3	Setup and procedure of the experiments	113
5.3.4	Results and discussion	116
Chapter 6:	Conclusion	123
6.1	Summary of contributions	123
6.2	Ongoing and future work	126
Appendix A:	Proofs	128
A.1	Proof of Lemma 2.3	128
A.2	Proof of Lemma 2.5	132
A.3	Proof of Lemma 2.7	134
A.4	Proof of Lemma 2.9	134
A.5	Proof of Theorem 3.1	135
A.6	Proof of Theorem 3.2	140
A.7	Proof of Theorem 3.3	141
A.8	Proof of Theorem 3.4	141
A.9	Proof of Theorem 4.1	150
A.10	Proof of Theorem 4.2	155
A.11	Proof of Theorem 4.3	155
Bibliography		165

List of Tables

3.1	Cost comparison of control and guidance strategies in the case of Dirichlet boundary condition. All costs are normalized with respect to the total cost of the case with no control.	56
3.2	Cost comparison of control and guidance strategies in the case of Neumann boundary condition. All costs are normalized with respect to the total cost of the case with no control.	60
4.1	Coordinates of initial sensor locations	84
5.1	Model parameters and their physical units	100

List of Figures

3.1	Evolution of the diffusion-advection process with Dirichlet boundary condition under the optimal feedback control \bar{u}^* . The actuators are steered by the optimal guidance p^* . Snapshots at $t = 0.05$ and 0.2 s show the transient stage, whereas the one at $t = 1$ s shows the relatively steady stage. The mobile disturbance is shown in gray. . . .	53
3.2	Optimal feedback control \bar{u}^* of each actuator in the case of Dirichlet boundary condition. The circles along the horizontal axis correspond to the snapshots in Fig. 3.1.	54
3.3	Norm of the PDE state in the case of Dirichlet boundary condition with pairs of control and guidance in Table 3.1. The circles along the horizontal axis correspond to the snapshots in Fig. 3.1.	54
3.4	Evolution of the process with Neumann boundary condition under the optimal feedback control \bar{u}^* . The actuators are steered by the optimal guidance p^* . Snapshots at $t = 0.05$ and 0.2 s show the transient stage, whereas the one at $t = 1$ s shows the relatively steady stage. The mobile disturbance is shown in gray.	58
3.5	Optimal feedback control \bar{u}^* of each actuator in the case of Neumann boundary condition. The circles along the horizontal axis correspond to the snapshots in Fig. 3.4.	59
3.6	Norm of the PDE state in the case of Neumann boundary condition with pairs of control and guidance in Table 3.2. The circles along the horizontal axis correspond to the snapshots in Fig. 3.4.	59
3.7	Approximate optimal costs $J_{(\text{APc1})}^*(p_N^*)$ normalized with respect to the optimal cost for $N^2 = 400$	60
4.1	Approximate optimal costs $J_{(\text{APe})}^*(p_N^*)$ normalized with respect to the optimal cost for $N^2 = 400$	73
4.2	Optimal trajectories for various values of the sensor noise variance R	76
4.3	Norm of the terminal estimation error for various values of sensor noise variance R . The color bar shows the mean value; the error bar shows the standard deviation. The value of mobility penalty γ is fixed at 0.5 , whereas the sensor noise's variance R takes values in the set $\{0.2, 0.4, 0.6, 0.8, 1\}$	77
4.4	Optimal trajectories for various values of the mobility penalty γ . . .	78

4.5	Norm of the terminal estimation error for various values of the mobility penalty γ . The color bar shows the mean value; the error bar shows the standard deviation. The value of sensor noise's variance R is fixed at 0.2, whereas the mobility penalty γ takes values in the set $\{0.5, 1, 1.5, 2, 2.5\}$	78
4.6	Trajectory of the sensor following the optimal guidance. The contours represent the level curves of pointwise variance of the estimation error on a uniform grid within the domain, computed from the Monte Carlo simulations.	80
4.7	Trajectories of multiple homogeneous sensors following the optimal guidance. The contours represent the level curves of pointwise variance of the estimation error on a uniform grid within the domain.	82
4.8	Normalized optimal total cost and uncertainty cost of a heterogeneous team with m_p poor sensors and $8 - m_p$ superior sensors.	85
5.1	Snapshots of a diffusion process and the trajectories of the mobile agent with Dirichlet BC and Neumann BC. The process and agent location (dot) are depicted at the middle of the interval shown on top left.	98
5.2	Reduction of the state norm. The vertical dashed lines correspond to the time of snapshots in Fig. 5.1.	99
5.3	Optimal control and speed solved from (Pexp). The vertical dashed lines correspond to the time of snapshots in Fig. 5.1.	99
5.4	Performance of the optimal solution to problem (Pexp) for diffusivity a in the range of 10^{-5} to 10^{-2} m ² /s.	103
5.5	Performance of problem (Pexp)'s optimal solution as bivariate heat maps of the nondimensional parameters (Dirichlet BC).	105
5.6	Performance of problem (Pexp)'s optimal solution as bivariate heat maps of the nondimensional parameters (Neumann BC).	107
5.7	Results for Monte Carlo simulations. Smaller values of the state norm $\ Z_N(T)\ $ in (a) and (b) indicate more effective actuation, whereas bigger values of the RPA in (c) and (d) indicate more efficient actuation.	111
5.8	Quadrotors in the testbed with the DJI F450 frame (left) and the Tarot 650 frame (right)	113
5.9	Block diagram of hardware and software architecture of the multi-quadrotor testbed	114
5.10	Software architecture for the experiments. Dashed arrows indicate synthetic values.	115
5.11	Snapshots of a virtual diffusion process and the trajectories of the actual quadrotors in Experiment 1. The process and the quadrotor locations (dots) are taken at the middle of the interval shown on top left.	118

5.12	Snapshots of a virtual diffusion process and the trajectories of the actual quadrotors in Experiment 2. The process and the quadrotor locations (dots) are taken at the middle of the interval shown on top left.	119
5.13	Optimal actuation in experiments. The unit for the vertical axes is kg/m ² s. The vertical dashed lines correspond to the time of snapshots in Figs. 5.11 and 5.12.	120
5.14	Reduction of the state norm in experiments. The vertical dashed lines correspond to the time of snapshots in Figs. 5.11 and 5.12.	122

List of Abbreviations

AE	Actuation effectiveness
BC	Boundary condition
DPS	Distributed parameter system
FIM	Fisher information matrix
F3	Fearless Flight Facility
HAB	Harmful algal blooms
KF	Kalman-Bucy filter
LQ	Linear-quadratic
LQR	Linear-quadratic regulator
NS	Nondimensional speed
PDE	Partial differential equation
RPA	Average norm reduction per unit actuation
TD	Total diffusion

Chapter 1: Introduction

The recent development of mobile robots has dramatically extended the scenarios where robots can be deployed to complete tasks autonomously. One of the tasks is monitoring and controlling large-scale spatiotemporal processes, e.g., oil spills, harmful algal blooms, and forest fires, which currently relies on human operators. These tasks can pose health threats, cause severe environmental issues, and incur substantial financial costs. A heterogeneous pool of autonomous agents with diverse sensors and actuators is an effective tool for understanding and/or influencing a dynamical spatiotemporal process. For example, a forest fire is an example of a dynamical and spreading process that may be influenced by onboard actuation, i.e., targeted application of fire retardant. Another example is chemical- or biological-contamination in the air or water, where one or multiple toxic sources can be detected with sensor measurements, and the plume can be contained and eliminated by reactive counter-measures. However, operational and resource constraints, such as time, energy, or the number of agents, may prohibit simultaneous estimation and/or control of these processes, especially when the agents are simultaneously performing other tasks. To overcome this limitation, agents should be adaptively deployed to leverage their unique dynamics and sensing and actuation abilities.

This dissertation aims to solve the problem raised in the scenarios described above by proposing an optimization framework that addresses the goal of estimating and controlling a spatiotemporal process and takes into consideration the limitations of the mobile agents. Specifically, the following three problems are formulated and studied in this dissertation:

1. How to control a spatiotemporal process using mobile actuators with limited onboard resources? Specifically, what trajectories do the actuators follow, and how much actuation do the actuators implement along such trajectories to control the spatiotemporal process to a zero state?
2. How to estimate a spatiotemporal process using mobile sensors with limited onboard resources? Specifically, what trajectories do the sensors follow to improve the quality of estimation using a given estimation scheme?
3. How good is the proposed framework that controls a spatiotemporal process using the estimated state information with mobile sensors and actuators? What are the advantages and disadvantages of the proposed framework?

1.1 Survey of the relevant literature

Spatiotemporal processes vary in both space and time, and they often span a large domain. Earlier work has focused on sampling the spatiotemporal process using stationary or mobile sensor networks, where the so-called coverage problem has been extensively investigated. Such a problem studies how to place the sensors with

limited sensing range to cover the domain for sampling and to maintain communications among each other. Lloyd’s algorithm and its variations are frequently used to solve the coverage problem, where the key is to partition the (non)uniform domain [8]. In [77], a multi-vehicle sampling algorithm is proposed to generate trajectories for nonuniform coverage of a nonstationary spatiotemporal field. A nonlinear coordinate transformation is applied to turn the field locally stationary (such that uniform coverage algorithms are applied) and subsequently inversely transformed to obtain the vehicles’ sampling trajectories. The authors of [72] propose a distributed control algorithm to steer a group of agents to provide adaptive sampling of the environment. Coverage of the field and online learning of sampling priority are conducted simultaneously. The algorithm provides provable guarantees on error bounds of the estimation of the field and convergence of the robots to their locally optimal sensing positions. Experiments were conducted to demonstrate the algorithm with ground robots that sample spatially distributed luminous intensity as the environment.

Modeling the spatiotemporal field by (non-parametric) Gaussian process [91] or artificial sampling surfaces [77, 89] has shown satisfactory results for estimation and sampling purposes. However, such models may not characterize well the control or impact to the spatiotemporal field due to its lack of expression for inputs. An alternative model is the partial differential equation (PDE). A PDE varies both in space and time that matches the nature of spatiotemporal fields. An example is the diffusion-advection PDE that characterizes mass transportation (harmful algal blooms [71]) or heat transfer (temperature distribution control [69]). The control

input takes effect in a PDE-modeled system by serving as an inhomogeneous term in the differential equation. Measurement or sampling of the PDE is done through the observation equation which provides local information of the PDE.

The fundamentals about PDEs in the context of control and estimation have been studied since the 1960s. The textbooks [5, 21] provide a comprehensive review on the subject. The sensors/actuators can be placed on the boundary which results in boundary estimation/control [36, 48, 74]. For sensors placed on the boundary, one may design observers based on boundary measurements. The challenge in using boundary measurements is that the output operator is unbounded when characterized in an abstract linear system. A tutorial paper [36] reviews the conditions for the well-posedness of the dual control problem with boundary inputs. One approach to boundary observer design is backstepping [42, 73], which stabilizes the observer using a Volterra transformation that transforms the original system to a stable target system and passes on the stability to the observer via its inverse transformation. Optimization techniques, e.g., a linear-quadratic estimator [62], have been proposed for boundary sensors using the method of variation. For boundary control, backstepping may also be applied to design stabilizing control [74].

The estimation can be categorized into estimation of the parameters in the model and the state of the process. The former is also known as parameter identification, in which the sensors are guided to collect information about the process and use the model's structure to infer unknown parameters. A common procedure adopted from the field of optimal experiment design is based on the Fisher Information Matrix (FIM), whose inverse is an approximation of the covariance matrix of

any unbiased estimator of the unknown parameters [81]. The FIM is constructed by the partial derivative of the process state with respect to the unknown parameters. Hence, the FIM characterizes parameter sensitivity. Many scalar-valued criteria can be applied with various goals [81], for example, D-optimality, which maximizes the log-determinant of the FIM, achieves the minimum volume of the confidence ellipsoid of the estimation; E-optimality, which maximizes the smallest eigenvalue of the FIM, achieves minimal length of the longest axis of the same ellipsoid. Various criteria have been proposed for sensors' guidance design, for example, D-optimality [75, 79], minimum time [82], or the Frobenius number of the Hessian of the least square [83].

Among the parameter identification problems, the one that aims to detect the source(s) has been extensively studied due to broad applications that fit into the problem's definition. It is also known as source localization or source identification. Generally speaking, the source will generate a spatially distributed field (also known as a plume) in which the sensors can detect the source using the gradient information. But in reality this is not always the case since the field may not be stationary: a dynamical process is likely possible. Furthermore, multiple sources may exist and they could be mobile. In such complex scenarios, the model-based methods provide systematic guidance for sensors to track the sources. The authors of [46] propose a systematic approach for active source identification in a steady-state advection-diffusion process using mobile sensors. The approach iterates between two subproblems: motion planning and source identification. The motion planning places the sensors at locations that maximize the minimum eigenvalue of the FIM. The source identification is formulated as a PDE-constrained optimization

problem that minimizes a regularized least-squares cost. The method is compared with other methods in simulations and shows advantage in different scales of the Péclet number of the diffusion-advection process. Experimental demonstration is conducted where the mobile sensor locates an ethanol source within a nonconvex domain. In the case where a source may represent intruder which leaves behind trackable plumes, a gradient ascent method has been used in [31, 32] to track a mobile source which yields relatively big errors in the estimated state variable. In [30], a Lyapunov-based scheduling guidance law is proposed for a mobile sensor network to estimate the proximity of an intruder modeled as a mobile source.

It is generally impossible to completely identify the state of a PDE-modeled system with a finite number of sensors. Hence, an observer for such a system is necessary. For the estimation of the state, since linear partial differential equations can be treated as abstract linear systems, Luenberger observer and Kalman filter (KF) [3] can be applied. The key to an infinite-dimensional KF is the evolution of the estimation error's covariance, which is operator-valued and can be solved via Riccati equations whose properties have been discussed in [11, 12]. For numerical approximation and computational issues, approximation results are summarized in [13] for the infinite-dimensional algebraic Riccati equations of a linear-quadratic regulator. However, often the disturbance to a system may not be Gaussian, in which case H_2 - or H_∞ -observer design is favorable [61, 86]. For a comparison of various observer designs for the heat equation, see [1].

For static in-domain sensors, a network can be deployed for estimating a PDE-modeled system. The problem is how to place the sensors to yield effective estima-

tion, which is referred to as sensor placement. The solution is to select the sensor placement that yields optimal performance for a certain criterion. The trace of the covariance operator of the KF, which quantifies the uncertainty of the estimate, is a common choice of the cost function to be minimized [4]. A similar problem is investigated in [96], which establishes the well-posedness of the sensor placement problem and its approximation with the cost function being the trace of the covariance operator. The same criterion has been applied to sensor placement of the Boussinesq equation [40]. In [66], a randomized observability constant is minimized by choosing suitable shapes and locations of the sensors. Other criteria, e.g., enhanced observability, optimal state estimation, and robust input-output mapping, are discussed for a parabolic PDE in [29]. Geometric approaches can also be applied to sensor placement, e.g., using the centroidal Voronoi tessellation [27] and combining the transfer-function model with geometric rules [84].

A variation of the sensor placement problem includes mobility of the sensors. In this scenario, a guidance policy is necessary to take advantage of the additional degree of freedom induced by mobility, which also makes the problem more complicated by introducing the dynamics of the mobile sensors. One may design sensor guidance using Lyapunov-based methods, where the guidance is constructed to make the derivative of the Lyapunov function negative. The Lyapunov function is usually designed to contain (quadratic) terms of the PDE state and the sensor guidance [22, 23, 33]. The Lyapunov-based guidance can further be used in monitoring a hazardous environment where the regions of high information density reduce sensor longevity. Such guidance is combined with a switching policy to balance the con-

flicting needs of information collection and sensor life span [26]. A similar approach uses the gradient of estimation error to guide sensors to the region that has large estimation error [24].

Optimization can also be applied to design sensor guidance, where the guidance (or the trajectory) of the sensor is selected to minimize a cost function. An early work [14] proposes an optimization problem that minimizes the weighted sum of the guidance effort for steering a sensor and the mean-square estimation error at a terminal time. In [25], the sensors are guided to the location that yields a maximum value of the estimation kernel. In [41], receding horizon guidance is proposed to find the sensor path that maximizes mutual information between sensor measurements and the predicted state of the PDE.

Since control of a PDE is the dual of estimation, the approaches reviewed above have been applied for designing actuators' scheduling, placement, or guidance. The problem of determining the location of stationary actuators is called the actuator placement problem. Actuator placement has been studied for optimality in the sense of linear-quadratic (LQ) [57], H_2 [58], and H_∞ [43]. The author of [57] studies the actuator placement problem with the LQ performance criterion. The actuators' locations are chosen to minimize the operator norm or trace norm of the Riccati operator solved from an algebraic Riccati equation associated with an infinite-dimensional system. If the input operator is compact and continuous with respect to actuator location in the operator norm, then a solution exists for the problem minimizing the operator norm of the Riccati operator [57, Theorem 2.6], under stabilizability and detectability assumptions. When computing the optimal

actuator locations, if the approximated Riccati operator converges to the original Riccati operator at each actuator location, then the approximate optimal actuator locations converge to the exact optimal locations [57, Theorem 3.5]. For the above results to hold when minimizing the trace-norm of the Riccati operator, the input and output spaces have to be finite-dimensional [57, Theorems 2.10 and 3.9] in addition to the assumptions stated above.

The authors of [58] design optimal actuator placement by minimizing the H_2 -control performance criterion, which minimizes the L_2 -norm of the linear output of a linear system, subject state disturbances. Roughly speaking, H_2 -control performance reduces the response to the disturbances while setting a zero initial condition, whereas the LQ performance reduces the response to the initial condition in a disturbance-free setting. For disturbances with known or unknown spatial distribution, the trace of the Riccati solution (scaled by the disturbance's spatial distribution) or operator norm of the Riccati solution are minimized, respectively, where the existence of a solution and convergence to the exact optimal solution of the approximate optimal solution are guaranteed. In [43], the H_∞ -performance criterion is minimized for actuator placement. Specifically, the actuators are placed in the locations that yield infimum of the attenuation bound (upper bound of the infinity norm of the closed-loop disturbance-to-output transfer function). The conditions for the existence of a solution and convergence to the exact optimal placement of the approximate optimal placement are provided.

Geometric approaches have also been proposed for actuator placement. For example, a modified centroidal Voronoi tessellation (mCVT) yields locations of ac-

tuators and sensors that yields least-squares approximate control and estimation kernels for a parabolic PDE [27]. The input operator is designed by maximizing the H_2 -norm of the input-to-state transfer function, whereas the kernel of the state feedback is obtained using the Riccati solution. Next, mCVT determines the partition such that the actuator and sensor locations achieve optimal performance (in the sense of least-squares) to the input operator and state feedback kernel, respectively. A comparison of various performance criteria for actuator placement has been conducted for controlling a simply supported beam [59] and a diffusion process [60]. It has been analyzed that maximizing the minimum eigenvalue of the controllability gramian is not a useful criterion. Because the lower bound of the eigenvalue is zero, the minimum eigenvalue approaches zero as the dimension of approximation increases [59, 60].

The guidance of mobile actuators is designed to improve the control performance in comparison to stationary actuators. Various performance criteria have been proposed for guidance. In [34], a mobile heat source is steered to maintain a spatially uniform temperature distribution in 1D using the optimal control method. The formulation uses a finite-dimensional approximation for modeling the process and evaluating performance. Additionally, the admissible locations of the heat source are chosen within a discrete set that yields approximate controllability requirements. Algorithms are provided to solve the proposed problem with considerations in real-time implementation and hardware constraints. Experimental results demonstrate the performance of the proposed scheme. The authors of [35] propose an optimization framework that steers mobile actuators to control a reaction-

diffusion process. A specific cost function, consisting of norms of control input and measurement of the DPS and the steering force, is minimized subject to dynamics of the actuator's motion and the PDE, and bounds on the control input and state of the DPS. The implementation of the framework is emphasized by discrete mechanics and model predictive control which yield computationally tractable solutions, in addition to an approximation of the PDE and a discrete set of admissible actuator locations.

The problem of ultraviolet curing using a mobile radiant actuator is investigated in [95], where the curing process is modeled by a 1D nonlinear PDE. Both the radiant power and scanning velocity of the actuator are computed for reaching a target curing state. A dual extended Kalman filter is applied to estimate the state and parameters of the curing process for feedback control, based on the phases of curing. In [28], a navigation problem is studied in which a mobile agent moves through a diffusion process represented by a hazardous field with given initial and terminal positions. Such a formulation may be applied to emergency evacuation guidance from an indoor environment with carbon monoxide. Both problems with minimum time and minimum accumulated effects of hazards are formulated, and closed-form solutions are derived using the Hamiltonian. A Lyapunov-based guidance strategy for collocated sensors and actuators to estimate and control a diffusion process is proposed in [23]. The decentralized guidance of the actuators for controlling a diffusion process to a zero state is derived by constructing suitable Lyapunov functions. The same methodology is applied to construct a distributed consensus filter via the network among agents to improve state estimation.

1.2 Contributions to the state-of-the-art

This dissertation provides research contributions in the general areas of estimation and control of PDE-modeled systems and multi-agent systems. The main results of this dissertation have been submitted for publication in archival journals [16, 17, 19]. Earlier research results related to this dissertation appeared in conference proceedings [15, 18, 20].

First, *we propose an optimization framework for controlling a PDE-modeled system using a team of mobile actuators.* The framework incorporates both controlling the process and steering the mobile actuators. We establish the existence conditions of a solution of the proposed problem. It turns out that the conditions are generally satisfied in engineering problems, which allows the results to be applied to a wide range of applications. Most importantly, we prove the conditions for the convergence to the exact optimal solution of the approximated optimal solution. The convergence is in the sense that the cost function of the exact problem evaluated at these two solutions becomes arbitrarily close as the dimension of the approximation goes to infinity. The convergence is verified in numerical studies and confirms the appropriateness of the optimal solution of the approximation.

Second, *we formulate an optimization problem to generate a guidance policy for a team of mobile sensors to estimate a 2D diffusion-advection process.* The optimization problem minimizes the trace of the covariance operator plus a generic cost of the sensors' motion subject to sensor platform dynamics. The formulation with a generic mobility cost applies to a wide range of applications, e.g., accumulated

exposure to hazards, guidance effort, or distance to terminal rendezvous locations. We establish conditions for the existence of a solution to the proposed problem and conditions for convergence to an exact optimal solution of the approximate optimal solution. When evaluating these two solutions using the original cost function, the difference gets arbitrarily small as the approximation gets finer.

Thirdly, *we propose a framework for cooperative estimation and control of a spatiotemporal process using a team of mobile collocated sensors and actuators.* The actuators' guidance and actuation are obtained by periodically solving an optimization problem. We identify key parameters for the optimization problem, use nondimensional analysis to reduce the size of the parameter space, and conduct extensive numerical analysis on how the performance of the optimal solution changes when the nondimensional parameters change. The overall framework is evaluated using the Monte Carlo simulations with comparisons to naive strategies. We demonstrate the framework on an outdoor multi-quadrotor testbed, which confirms the framework's capability and also suggests ongoing and future directions to improve the feasibility of the framework in practice with real spatiotemporal processes.

1.3 Outline of the dissertation

The organization of the dissertation is as follows. Chapter 2 introduces the notation and terminology in this dissertation. Background knowledge is reviewed in terms of the dynamics of the mobile sensors and actuators, 2D diffusion-advection equation and its abstract linear system representation, the associated linear-quadratic

regulator and the Kalman filter, and finite-dimensional approximations to the infinite-dimensional components.

Chapter 3 describes an optimization framework for controlling a DPS that is modeled by a 2D diffusion-advection equation using a team of mobile actuators. The framework simultaneously seeks optimal control of the DPS and optimal guidance of the mobile actuators such that a cost function associated with both the DPS and the mobile actuators is minimized subject to the dynamics of each. We establish conditions for the existence of a solution to the proposed problem. Since computing an optimal solution requires approximation, we also establish the conditions for convergence to the exact optimal solution of the approximate optimal solution. That is, when evaluating these two solutions by the original cost function, the difference becomes arbitrarily small as the approximation gets finer. Two numerical examples demonstrate the performance of the optimal control and guidance obtained from the proposed approach.

Chapter 4 describes an optimization framework for designing guidance for a possibly heterogeneous team of multiple mobile sensors to estimate a DPS modeled by a 2D diffusion-advection process. We propose an optimization problem that minimizes the sum of the trace of the covariance operator of the Kalman-Bucy filter and a generic mobility cost of the mobile sensors, subject to the sensors' motion modeled by linear dynamics. We establish the existence of a solution to this problem. Moreover, we prove convergence to the exact optimal solution of the approximate optimal solution. That is, when evaluating these two solutions using the original cost function, the difference becomes arbitrarily small as the approximation gets

finer. The approximate solution is applied in simulation to analyze how a single mobile sensor’s performance depends on two important parameters: sensor noise variance and mobility penalty. We also illustrate the application of the framework to multiple sensors, particularly the performance of a heterogeneous team of sensors.

Chapter 5 describes a framework for cooperative estimation and control of a 2D diffusion process with collocated mobile actuators and sensors. We plan for the actuators’ guidance and actuation using the estimation of the state. The guidance and actuation are solved from an optimization problem that has the same structure as the problem studied in Chapter 3 but with additional constraints on the maximum speed and maximum actuation of the actuators. The problem is formulated with approximated PDE components and solved using a nonlinear optimal control solver. Extensive numerical studies have been conducted to analyze and evaluate the performance of the framework under varying parameters. The framework was demonstrated on an outdoor multi-quadrotor testbed with four quadrotors. The advantages and disadvantages of the framework are discussed.

Chapter 6 summarizes the contributions of the dissertation and lists ongoing and future work.

Chapter 2: Notation, terminology, and supporting Lemmas

2.1 Notation and terminology

The dissertation adopts the following notation. The symbols \mathbb{R} , \mathbb{R}^+ , and \mathbb{N} denote the sets of real numbers, nonnegative real numbers, and nonnegative integers, respectively. The boundary of a set M is denoted by ∂M . The n -ary Cartesian power of a set M is denoted by M^n . The notation $X_1 \hookrightarrow X_2$ means that the space X_1 is densely and continuously embedded in X_2 . The norm in a finite- and infinite-dimensional space is denoted by $|\cdot|$ and $\|\cdot\|$, respectively, with subscripts indicating its type. The space of all bounded linear operators from space X to space Y is denoted by $\mathcal{L}(X; Y)$ or $\mathcal{L}(X)$ if $Y = X$. We define the space of continuous mappings by $C(I; X) = \{F : I \rightarrow X \text{ such that } t \mapsto F(t) \text{ is continuous in } \|\cdot\|_X\}$ with the sup norm $\|F(\cdot)\|_{C(I; X)} = \sup_{t \in I} \|F(t)\|_X$. For a Hilbert space \mathcal{H} equipped with inner product $\langle \cdot, \cdot \rangle$ and $\phi_1, \phi_2 \in \mathcal{H}$, define $\phi_1 \circ \phi_2 \in \mathcal{L}(\mathcal{H})$ by $(\phi_1 \circ \phi_2)\psi = \phi_1 \langle \phi_2, \psi \rangle$ for all $\psi \in \mathcal{H}$. The superscript $*$ denotes an optimal variable, whereas $*$ denotes the adjoint of a linear operator. The transpose of a matrix A is denoted by A^\top . An $n \times n$ -dimensional diagonal matrix with elements of vector $[a_1, a_2, \dots, a_n]$ on the main diagonal is denoted by $\text{diag}(a_1, a_2, \dots, a_n)$. The i th element of a vector v is $[v]_i$. An $n \times n$ -dimensional identity matrix is denoted by I_n . We denote by $0_{n \times m}$ and

$1_{n \times m}$ an $n \times m$ -dimensional matrix with all entries being 0 and 1, respectively. The term *guidance* refers to the steering of the mobile agents, whereas the term *control* refers to the control input to the DPS. For an optimization problem

$$\begin{aligned} & \underset{x}{\text{minimize}} && J(x) \\ & \text{subject to} && x \in C, \end{aligned} \tag{P0}$$

we use $J_{(\text{P0})}(x)$ to denote the cost function of (P0) evaluated at x . Specifically, $J_{(\text{P0})}^*(x^*)$ indicates that the optimal value of (P0) is attained when the cost function is evaluated at an optimal solution x^* .

2.2 Dynamics of the mobile actuators and sensors

Assume each of the m_a mobile actuators has linear dynamics, so that the dynamics of actuator i are

$$\dot{\xi}_i(t) = \alpha_i \xi_i(t) + \beta_i p_i(t), \quad \xi_i(0) = \xi_{i,0}, \tag{2.1}$$

where $\xi_i(t) \in \mathbb{R}^n$ ($n \geq 2$) and $p_i(t) \in P_i \subset \mathbb{R}^m$ are the state and guidance at t , respectively, for $i \in \{1, 2, \dots, m\}$. Assume that system (2.1) is controllable. The first two elements of $\xi_i(t)$ are the horizontal and vertical position, $x_i(t)$ and $y_i(t)$, of the actuator in the 2D domain. One special case would be a single integrator, where $\xi_i(t) \in \mathbb{R}^2$ is the position, $p_i(t) \in \mathbb{R}^2$ is the velocity commands, $\alpha_i = 0_{2 \times 2}$, and $\beta_i = I_2$.

For conciseness, we concatenate the states and guidance of all actuators, respectively, and use one dynamical equation to characterize the dynamics of all actuators:

$$\dot{\xi}(t) = \alpha\xi(t) + \beta p(t), \quad \xi(0) = \xi_0, \quad (2.2)$$

where matrices α and β are assembled from α_i and β_i for $i \in \{1, 2, \dots, m_a\}$, respectively and are consistent with the concatenation for ξ and p . With a slight abuse of notation, we use n for the dimension of $\xi(t)$ and m for the dimension of $p(t)$. Define the admissible set of guidance $P = P_1 \times P_2 \times \dots \times P_{m_a}$ such that $p(t) \in P$ for $t \in [0, t_f]$. Let $M \in \mathbb{R}^{2m_a \times n}$ be a matrix such that $M\xi(t)$ is a vector of locations of the actuators.

Assume each of the m_s mobile sensors has the linear dynamics

$$\dot{\zeta}_i(t) = \alpha_i\zeta_i(t) + \beta_i p_i(t), \quad \zeta_i(0) = \zeta_{i,0}, \quad (2.3)$$

where $\zeta_i(t) \in \mathbb{R}^n$ and $p_i(t) \in P_i \subset \mathbb{R}^m$ are the state and the guidance of sensor i at time t , respectively. With a slight abuse of notation, we do not distinguish the notation for α_i , β_i , and p_i in the dynamics of the actuators (2.1) and of the sensors (2.3) as they are clear from the context. The state ζ_i contains the 2D location of sensor i and hence $n \geq 2$. Assume that system (2.3) is controllable. One special case of (2.3) would be a single integrator, where $\zeta_i(t) \in \mathbb{R}^2$ is the location, $p_i(t) \in \mathbb{R}^2$ is the velocity command, and α_i and β_i are zero matrix and identity matrix, respectively.

For conciseness, we concatenate the states and guidance of all m_s sensors,

respectively, and use one dynamical equation to describe the dynamics of all sensors:

$$\dot{\zeta}(t) = \alpha\zeta(t) + \beta p(t), \quad \zeta(0) = \zeta_0, \quad (2.4)$$

where matrices α and β are assembled from α_i and β_i for $i \in \{1, 2, \dots, m_s\}$, respectively, and are consistent with the concatenation for ζ and p . The controllability of the concatenated system (2.4) inherits that of each individual system (2.3). We use n for the dimension of $\zeta(t)$ and m for the dimension of $p(t)$. Define the admissible set of guidance $P = P_1 \times P_2 \times \dots \times P_{m_s}$ such that $p(t) \in P$ for $t \in [0, t_f]$.

2.3 Deterministic abstract linear system and linear-quadratic regulation

This dissertation is motivated by the problem of controlling the following diffusion-advection process on a two-dimensional spatial domain $\Omega = [0, 1] \times [0, 1]$ with a team of m_a mobile actuators:

$$\frac{\partial z(x, y, t)}{\partial t} = a\nabla^2 z(x, y, t) - \mathbf{v} \cdot \nabla z(x, y, t) + \sum_{i=1}^{m_a} (\mathcal{B}_i u_i)(x, y, t), \quad (2.5)$$

$$z(\cdot, \cdot, t)|_{\partial\Omega} = 0, \quad (2.6)$$

$$z(x, y, 0) = z_0(x, y), \quad (2.7)$$

where $z(\cdot, \cdot, t)$ is the state at time t , $\mathbf{v} \in \mathbb{R}^2$ is the velocity field for advection, and u_i is the control implemented by actuator i , with the actuation characterized

spatially by \mathcal{B}_i . The state z lives in the state space $L^2(\Omega)$. A representative model of the actuation dispensed by each actuator is Gaussian-shaped and centered at the actuator i 's location (x_i, y_i) with a bounded support such that

$$\mathcal{B}_i(x, y) = \begin{cases} \frac{1}{2\pi\sigma_i^2} \exp\left(-\frac{(x-x_i)^2}{\sigma_i^2} - \frac{(y-y_i)^2}{\sigma_i^2}\right) & \text{if } |x-x_i| \leq \sigma_i \text{ and } |y-y_i| \leq \sigma_i, \\ 0 & \text{otherwise,} \end{cases} \quad (2.8)$$

where the parameter σ_i determines the spatial influence of the actuation, which is concentrated mostly at the location of the actuator and disperses to the surrounding with an exponential decay.

To describe the dynamics of PDE (2.5)–(2.7), consider the following abstract linear system:

$$\dot{\mathcal{Z}}(t) = \mathcal{A}\mathcal{Z}(t) + \mathcal{B}(M\xi(t), t)u(t), \quad \mathcal{Z}(0) = \mathcal{Z}_0, \quad (2.9)$$

where $\mathcal{Z}(\cdot)$ is the state within state space $\mathcal{H} = L^2(\Omega)$ and $u(\cdot)$ is the control within the control space $u(t) \in U \subseteq \mathbb{R}^{m_a}$ for $t \in [0, t_f]$. In the case of diffusion-advection process (2.5), for $\phi \in \mathcal{H}$,

$$(\mathcal{A}\phi)(x, y) = a\nabla^2\phi(x, y) - \mathbf{v} \cdot \nabla\phi(x, y), \quad (2.10)$$

where the operator \mathcal{A} has domain $\text{Dom}(\mathcal{A}) = H^2(\Omega) \cap H_0^1(\Omega)$. The input operator $\mathcal{B}(M\xi(t), t) \in \mathcal{L}(U, \mathcal{H})$ is a function of the actuator locations such that $\mathcal{B}(M\xi(t), t) = [\mathcal{B}_1(M\xi_1(t), t), \dots, \mathcal{B}_{m_a}(M\xi_{m_a}(t), t)]^\top$, where $\mathcal{B}_i(\cdot, t) \in L^2(\Omega)$ for all $t \in [0, t_f]$ and

$i \in \{1, 2, \dots, m_a\}$. A special case is the time-invariant input operator in (2.8). Since the actuator state $\xi(t)$ is a function of time t , we sometimes use $\mathcal{B}(t)$ for brevity.

The operator $\mathcal{A} : \text{Dom}(\mathcal{A}) \rightarrow \mathcal{H}$ is an infinitesimal generator of a strongly continuous semigroup $\mathcal{S}(t)$ on \mathcal{H} . Subsequently, the dynamical system (2.9) has a unique mild solution $\mathcal{Z} \in C([0, t_f]; \mathcal{H})$ for any $\mathcal{Z}_0 \in \mathcal{H}$ and any $u \in L^2([0, t_f]; U)$ such that $\mathcal{Z}(t) = \mathcal{S}(t)\mathcal{Z}_0 + \int_0^t \mathcal{S}(t - \tau)\mathcal{B}(\xi(\tau), \tau)u(\tau)d\tau$.

Similar to a finite-dimensional linear system, a linear-quadratic regulator (LQR) problem can be formulated with respect to (2.9), which looks for a control $u(\cdot) \in L^2([0, t_f]; U)$ that minimizes the following quadratic cost:

$$J(\mathcal{Z}, u) = \int_0^{t_f} \langle \mathcal{Z}(t), \mathcal{Q}(t)\mathcal{Z}(t) \rangle + u(t)^\top R u(t) dt + \langle \mathcal{Z}(t_f), \mathcal{Q}_f \mathcal{Z}(t_f) \rangle, \quad (2.11)$$

where $\mathcal{Q}(t) \in \mathcal{L}(\mathcal{H})$ and $\mathcal{Q}_f \in \mathcal{L}(\mathcal{H})$ are self-adjoint and nonnegative, which evaluates the running cost and terminal cost of the PDE state. The coefficient R is an $m_a \times m_a$ -dimensional symmetric and positive definite matrix that evaluates the control effort. We refer to $J(\mathcal{Z}, u)$ as the *PDE cost*.

Analogous to the finite-dimensional LQR, an optimal control u^* that minimizes the quadratic cost (2.11) is

$$u^*(t) = -R^{-1}\mathcal{B}^*(t)\Pi^c(t)\mathcal{Z}(t), \quad (2.12)$$

where Π^c is an operator that associates with the following backward differential

operator-valued Riccati equation:

$$\dot{\Pi}^c(t) = -\mathcal{A}^*\Pi^c(t) - \Pi^c(t)\mathcal{A} - \mathcal{Q}(t) + \Pi^c(t)\bar{\mathcal{B}}\bar{\mathcal{B}}^*(t)\Pi^c(t) \quad (2.13)$$

with terminal condition $\Pi^c(t_f) = \mathcal{Q}_f$, where $\bar{\mathcal{B}}\bar{\mathcal{B}}^*(t)$ is short for $\mathcal{B}(t)R^{-1}\mathcal{B}^*(t)$. Before we proceed to state the conditions for the existence of a unique solution of (2.13), we introduce the \mathcal{J}_q -class as follows.

Denote the trace of a nonnegative operator $A \in \mathcal{L}(\mathcal{H})$ by $\text{Tr}(A)$, where $\text{Tr}(A) = \sum_{k=1}^{\infty} \langle \phi_k, A\phi_k \rangle$ for any orthonormal basis $\{\phi_k\}_{k=1}^{\infty}$ of \mathcal{H} (the trace is independent of the choice of basis functions). For $1 \leq q < \infty$, let $\mathcal{J}_q(\mathcal{H})$ denote the set of all bounded operators $\mathcal{L}(\mathcal{H})$ such that $\text{Tr}((\sqrt{A^*A})^q) < \infty$ [11]. If $A \in \mathcal{J}_q(\mathcal{H})$, then the \mathcal{J}_q -norm of A is defined as $\|A\|_{\mathcal{J}_q(\mathcal{H})} = (\text{Tr}((\sqrt{A^*A})^q))^{1/q} < \infty$. The class $\mathcal{J}_1(\mathcal{H})$ and $\mathcal{J}_2(\mathcal{H})$ are known as the space of trace operators and the space of Hilbert-Schmidt operators, respectively. Note that a continuous embedding $\mathcal{J}_{q_1}(\mathcal{H}) \hookrightarrow \mathcal{J}_{q_2}(\mathcal{H})$ holds if $1 \leq q_1 < q_2 \leq \infty$. In other words, if $A \in \mathcal{J}_{q_1}(\mathcal{H})$, then $A \in \mathcal{J}_{q_2}(\mathcal{H})$ and $\|A\|_{\mathcal{J}_{q_2}(\mathcal{H})} \leq \|A\|_{\mathcal{J}_{q_1}(\mathcal{H})}$.

The existence of a mild solution of (2.13) is established via Lemma 2.1. We omit the proof of this lemma because it is a direct consequence of [11, Theorem 3.6].

Consider the following assumptions with $1 \leq q < \infty$:

(C1) $\mathcal{Q}_f \in \mathcal{J}_q(\mathcal{H})$ and \mathcal{Q}_f is nonnegative.

(C2) $\mathcal{Q}(\cdot) \in L^1([0, t_f]; \mathcal{J}_q(\mathcal{H}))$ and $\mathcal{Q}(t)$ is nonnegative for all $t \in [0, t_f]$.

(C3) $\bar{\mathcal{B}}\bar{\mathcal{B}}^*(\cdot) \in L^\infty([0, t_f]; \mathcal{L}(\mathcal{H}))$ and $\bar{\mathcal{B}}\bar{\mathcal{B}}^*(t)$ is nonnegative for $t \in [0, t_f]$.

Lemma 2.1. [11, Theorem 3.6] Let \mathcal{H} be a separable Hilbert space and let $\mathcal{S}(t)$ be a strongly continuous semigroup on \mathcal{H} . Suppose assumptions (C1)–(C3) hold. Then, the equation

$$\begin{aligned} \Pi^c(t) = \mathcal{S}^*(t_f - t)\mathcal{Q}_f\mathcal{S}(t_f - t) + \int_t^{t_f} \mathcal{S}^*(\tau - t) \\ (\mathcal{Q}(\tau) - \Pi^c(\tau)\bar{\mathcal{B}}\bar{\mathcal{B}}^*(\tau)\Pi^c(\tau))\mathcal{S}(\tau - t)d\tau \end{aligned} \quad (2.14)$$

provides a unique mild solution to (2.13) in the space $L^2([0, t_f]; \mathcal{J}_{2q}(\mathcal{H}))$. The solution also belongs to $C([0, t_f]; \mathcal{J}_q(\mathcal{H}))$ and is pointwise self-adjoint and nonnegative. Furthermore, if $\mathcal{Q}(\cdot) \in C([0, t_f]; \mathcal{J}_q(\mathcal{H}))$ and $\bar{\mathcal{B}}\bar{\mathcal{B}}^*(\cdot) \in C([0, t_f]; \mathcal{L}(\mathcal{H}))$, then Π^c is a weak solution to (2.13).

The equality introduced next in Lemma 2.2 allows for turning the optimal quadratic PDE cost into a quadratic term associated with the initial condition of the PDE and the Riccati operator. We state it without proof because it can be established by integrating $d\langle \mathcal{Z}(t), \Pi^c(t)\mathcal{Z}(t) \rangle/dt$ from 0 to t_f ; the differentiability of $\langle \mathcal{Z}(t), \Pi^c(t)\mathcal{Z}(t) \rangle$ is proven in [21, Theorem 6.1.9].

Lemma 2.2. Suppose $\Pi(t)$ is a mild solution to (2.13), given by (2.14). For every $\mathcal{Z}_0 \in \mathcal{H}$, the optimal PDE cost (2.11) satisfies the equality $J(\mathcal{Z}^*, u^*) = \langle \mathcal{Z}_0, \Pi^c(0)\mathcal{Z}_0 \rangle$, where \mathcal{Z}^* is the state that follows the dynamics (2.9) under optimal control u^* of (2.12), and $\Pi^c(0)$ is the solution (2.14) evaluated at $t = 0$.

The following assumption is vital to the main results in Chapter 3:

(C4) The input operator $\mathcal{B}_i(x, t)$ is continuous with respect to location $x \in \mathbb{R}^2$ [10,

Definition 4.5], that is, there exists a continuous function $l : \mathbb{R}^+ \rightarrow \mathbb{R}^+$ such that $l(0) = 0$ and $\|\mathcal{B}_i(x, t) - \mathcal{B}_i(y, t)\|_{L^2(\Omega)} \leq l(|x - y|_2)$ for all $t \in [0, t_f]$, all $x, y \in \mathbb{R}^2$, and all $i \in \{1, 2, \dots, m_a\}$.

The actuators' locations determine where the input is actuated and, furthermore, how $\Pi^c(\cdot)$ evolves through (2.14). Since the input operator $\mathcal{B}(\cdot, t)$ is a mapping of the actuators' locations at time t , the composite input operator $\bar{\mathcal{B}}\bar{\mathcal{B}}^*(\cdot)$ is a mapping of the actuator state in $[0, t_f]$ and so is $\Pi^c(0)$ by (2.14), although the actuator state is not explicitly reflected in the notation of $\bar{\mathcal{B}}\bar{\mathcal{B}}^*(\cdot)$ or $\Pi^c(0)$. Hence, we can define the optimal PDE cost $\langle \mathcal{Z}_0, \Pi^c(0)\mathcal{Z}_0 \rangle$ as a mapping of the actuator state. Let $K^c : C([0, t_f]; \mathbb{R}^n) \rightarrow \mathbb{R}^+$ such that $K^c(\zeta) = \langle \mathcal{Z}_0, \Pi^c(0)\mathcal{Z}_0 \rangle$. Assumption (C4) plays an important role in yielding the continuity of the mapping $K^c(\cdot)$ stated below in Lemma 2.3. .

Lemma 2.3. *Suppose $\mathcal{Z}_0 \in \mathcal{H}$. Let assumptions (C1)–(C3) hold with $q = 1$ and $\Pi^c \in C([0, t_f]; \mathcal{J}_1(\mathcal{H}))$ be defined as in (2.14). If assumption (C4) holds, then the mapping $K^c : C([0, t_f]; \mathbb{R}^n) \rightarrow \mathbb{R}^+$ such that $K^c(\xi) = \langle \mathcal{Z}_0, \Pi^c(0)\mathcal{Z}_0 \rangle$ is continuous.*

Proof. See Appendix A.1. □

2.4 Abstract linear system with Gaussian noise and the Kalman filter

Consider the following inhomogeneous diffusion-advection equation over a 2D spatial domain Ω :

$$\frac{\partial z(x, y, t)}{\partial t} = a \nabla^2 z(x, y, t) - \mathbf{v} \cdot \nabla z(x, y, t) + w(x, y, t) \quad (2.15)$$

$$z(x, y, 0) = \hat{z}(x, y, 0) + w_0(x, y) \quad (2.16)$$

$$z(x, y, t)|_{(x, y) \in \partial\Omega} = 0, \quad (2.17)$$

where $(x, y) \in \Omega$, $t \in [0, t_f]$, $a > 0$ is the diffusion coefficient, and $\mathbf{v} \in \mathbb{R}^2$ is the flow that yields advection. The initial condition $z(\cdot, \cdot, 0)$ is perturbed around its nominal value $\hat{z}(\cdot, \cdot, 0)$ by an additive zero-mean Gaussian noise $w_0(\cdot, \cdot)$. The dynamics (2.15) is subject to an additive zero-mean Gaussian noise $w(\cdot, \cdot, t)$ with variance $Q(t)$, which is nonnegative and self-adjoint. The state noise $w(\cdot, \cdot, t)$ and initial noise $w_0(\cdot, \cdot)$ are mutually independent for all t .

For simplicity, represent the PDE state in (2.15) by an abstract linear system whose state variable $\mathcal{Z}(t)$ represents $z(\cdot, \cdot, t)$ at time t , such that

$$\dot{\mathcal{Z}}(t) = \mathcal{A}\mathcal{Z}(t) + w(t), \quad \mathcal{Z}(0) = \hat{\mathcal{Z}}_0 + w_0, \quad (2.18)$$

where $\mathcal{Z} \in \mathcal{H}$ and the infinitesimal generator \mathcal{A} of a strongly continuous semigroup \mathcal{S} are as defined in Section 2.3.

The measurement by sensor i depends on the sensor's location such that

$$y_i(t) = \mathcal{C}_i^*(M_0\zeta_i(t), t)\mathcal{Z}(t) + v_i(t), \quad (2.19)$$

where M_0 is a matrix with appropriate dimension such that $M_0\zeta_i(t) \in \mathbb{R}^2$ is the location of sensor i and $\mathcal{C}_i^*(M_0\zeta_i(t), t) \in \mathcal{L}(\mathcal{H}, \mathbb{R})$ is the output operator that yields an integral kernel $\mathcal{C}_i(M_0\zeta_i(t), t) \in L^2(\Omega)$ such that

$$\mathcal{C}_i^*(M_0\zeta_i(t), t)\phi = \iint_{\Omega} \mathcal{C}_i(M_0\zeta_i(t), t)(x, y)\phi(x, y)dx dy$$

for $\phi \in \mathcal{H}$. Additive zero-mean Gaussian noise $v_i(t)$ with variance σ_i^2 is included in the measurement.

The measurement can have many types, e.g., pointwise [14, 44, 45], interval integral [12, 33], interval average [30], and Gaussian-type kernel [12]. Later in the simulation section, we will use a time-invariant kernel given by square-shaped average

$$\mathcal{C}_i(M_0\zeta_i(t))(x, y) = \begin{cases} \frac{1}{4r_i^2} & \text{if } \begin{bmatrix} x \\ y \end{bmatrix} - M_0\zeta_i(t) \in [-r_i, r_i] \times [-r_i, r_i] \\ 0 & \text{otherwise,} \end{cases} \quad (2.20)$$

where $2r_i$ is the length of the side of the square at time t .

The measurements $y(t) \in \mathbb{R}^{m_s}$ of all sensors are compactly written as

$$y(t) = \mathcal{C}^*(M\zeta(t), t)\mathcal{Z}(t) + v(t), \quad (2.21)$$

where $\mathcal{C}^*(M\zeta(t), t)$ is an operator-valued vector

$$\mathcal{C}^*(M\zeta(t), t) = [\mathcal{C}_1^*(M_0\zeta_1(t), t), \mathcal{C}_2^*(M_0\zeta_2(t), t), \dots, \mathcal{C}_{m_s}^*(M_0\zeta_{m_s}(t), t)]^\top$$

and $M \in \mathbb{R}^{2m_s \times n}$ is a matrix such that $M\zeta(t)$ is a vector of locations of the sensors, i.e.,

$$(M\zeta(t))^\top = \left[(M_0\zeta_1(t))^\top \quad \dots \quad (M_0\zeta_{m_s}(t))^\top \right].$$

We sometimes use $\mathcal{C}(t)$ for brevity instead of $\mathcal{C}(\zeta(t), t)$, because the sensor state $\zeta(t)$ is a function of t . The measurement noise $v(t)$ is a zero-mean Gaussian vector with covariance $R = \text{diag}(\sigma_1^2, \sigma_2^2, \dots, \sigma_{m_s}^2)$. Assume the noise $w_0(\cdot, \cdot)$, $w(\cdot, \cdot, t)$, and $v(t)$ are mutually independent for all t .

Analogous to a finite-dimensional linear system, the infinite-dimensional linear system (2.18) and (2.21) admits a Kalman-Bucy filter (KF). For the derivation of the KF of an abstract linear system, one may refer to [54, 65]. The estimation $\hat{\mathcal{Z}}(t)$ of the state $\mathcal{Z}(t)$ can be updated from the measurement $y(t)$ by

$$\dot{\hat{\mathcal{Z}}}(t) = \mathcal{A}\hat{\mathcal{Z}}(t) + \Pi^e(t)\mathcal{C}(M\zeta(t), t)R^{-1}(y(t) - \hat{y}(t)), \quad (2.22)$$

$$\hat{y}(t) = \mathcal{C}^*(M\zeta(t), t)\hat{\mathcal{Z}}(t), \quad (2.23)$$

with initial condition $\hat{\mathcal{Z}}(t_0) = \hat{\mathcal{Z}}_0$. The predicted observation of the estimated system is denoted by $\hat{y}(t)$. The covariance operator of the estimation error $\Pi^e(t) =$

$\mathbb{E}[(\mathcal{Z}(t) - \hat{\mathcal{Z}}(t)) \circ (\mathcal{Z}(t) - \hat{\mathcal{Z}}(t))]$ satisfies the following operator Riccati equation:

$$\dot{\Pi}^e(t) = \mathcal{A}\Pi^e(t) + \Pi^e(t)\mathcal{A}^* + Q(t) - \Pi^e(t)\bar{\mathcal{C}}\bar{\mathcal{C}}^*(t)\Pi^e(t), \quad (2.24)$$

where $\bar{\mathcal{C}}\bar{\mathcal{C}}^*(t)$ is a compact representation of $\mathcal{C}(t)R^{-1}\mathcal{C}^*(t)$. The initial condition $\Pi^e(0)$ is given as the covariance operator Π_0^e of the initial estimation error $\Pi_0^e = \mathbb{E}[(\mathcal{Z}(0) - \hat{\mathcal{Z}}(0)) \circ (\mathcal{Z}(0) - \hat{\mathcal{Z}}(0))]$ [96], which is the variance of w_0 and is nonnegative and self-adjoint.

Consider the following assumptions with $1 \leq q < \infty$:

(E1) $\Pi_0^e \in \mathcal{J}_q(\mathcal{H})$ and Π_0^e is nonnegative.

(E2) $Q(\cdot) \in L^1([0, t_f]; \mathcal{J}_q(\mathcal{H}))$ and $Q(t)$ is nonnegative for all $t \in [0, t_f]$.

(E3) $\bar{\mathcal{C}}\bar{\mathcal{C}}^*(\cdot) \in L^\infty([0, t_f]; \mathcal{L}(\mathcal{H}))$ and $\bar{\mathcal{C}}\bar{\mathcal{C}}^*(t)$ is nonnegative for $t \in [0, t_f]$.

The existence of a mild solution of (2.24) is established in Lemma 2.4 (which is the dual version of Lemma 2.1). The proof is omitted because the lemma follows directly from [11, Theorem 3.6].

Lemma 2.4. [11, Theorem 3.6] *Let \mathcal{H} be a separable Hilbert space. Suppose assumptions (E1)–(E3) hold. Then, the equation*

$$\Pi^e(t) = \mathcal{S}(t)\Pi_0^e\mathcal{S}^*(t) + \int_0^t \mathcal{S}(t-\tau) (Q(\tau) - \Pi^e(\tau)\bar{\mathcal{C}}\bar{\mathcal{C}}^*(\tau)\Pi^e(\tau)) \mathcal{S}^*(t-\tau) d\tau \quad (2.25)$$

provides a unique mild solution to (2.24) in the space $L^2([0, t_f]; \mathcal{J}_{2q}(\mathcal{H}))$. The solution is in $C([0, t_f]; \mathcal{J}_q(\mathcal{H}))$ and is pointwise self-adjoint and nonnegative.

The covariance operator $\Pi^e(t)$ characterizes the uncertainty of the estimation error. The expected value of the squared norm of the estimation error is the trace of the covariance operator $\Pi^e(t)$ [12, 96]:

$$\text{Tr}(\Pi^e(t)) = \mathbb{E}[\|\mathcal{Z}(t) - \hat{\mathcal{Z}}(t)\|_{\mathcal{H}}^2]. \quad (2.26)$$

The following assumption is vital to the main results in Chapter 4:

(E4) For each sensor $i \in \{1, 2, \dots, m_s\}$, the kernel of the output operator $\mathcal{C}_i(x, t)$ is continuous with respect to location $x \in \mathbb{R}^2$ [12, Definition 4.5]. That is, there exists a continuous function $l : \mathbb{R}^+ \rightarrow \mathbb{R}^+$ such that $l(0) = 0$ and

$$\|\mathcal{C}_i(x_1, t) - \mathcal{C}_i(x_2, t)\|_{L^2(\Omega)} \leq l(|x_1 - x_2|_2) \quad (2.27)$$

for all $t \in [0, t_f]$ and all $x_1, x_2 \in \mathbb{R}^2$.

Assumption (E4) is important in that, roughly speaking, it establishes the continuity of the covariance operator with respect to sensor state (Lemma 2.5), which further permits the existence of a solution to the optimization problem proposed in Chapter 4 (Theorem 4.1), its finite-dimensional approximation (Theorem 4.2), and the convergence to the exact optimal cost of the approximate optimal cost (Theorem 4.3).

Remark 2.1. *The time invariant kernel in (2.20) is continuous with respect to location, where $l(u) = (4r_i c_0 u + u^2)^{1/2} / (4r_i^2)$ for sensor i in assumption (E4) for $c_0 > 0$.*

The sensors' locations determine where the output is measured and, furthermore, how the covariance operator evolves through (2.25). We characterize this relation by a composite mapping. Since the output operator $\mathcal{C}^*(\cdot, t)$ is a mapping of the sensors' locations at time t , the composite output operator $\bar{\mathcal{C}}\bar{\mathcal{C}}^*(\cdot)$ is a mapping of the sensor state in $[0, t_f]$ and so is $\Pi^e(\cdot)$ by (2.25), although the sensor state is not explicitly reflected in the notation of the latter two mappings. Hence, we can define the uncertainty cost $\int_0^{t_f} \text{Tr}(\Pi^e(t))dt$ as a mapping of the sensor state. Let $K^e : C([0, t_f]; \mathbb{R}^n) \rightarrow \mathbb{R}^+$ such that $K^e(\zeta) = \int_0^{t_f} \text{Tr}(\Pi^e(t))dt$. Lemma 2.5 below shows when the uncertainty cost varies continuously with respect to the sensor state.

Lemma 2.5. *Let assumptions (E1)–(E3) hold with $q = 1$ and $\Pi^e \in C([0, t_f]; \mathcal{J}_1(\mathcal{H}))$ be defined in (2.25). If assumption (E4) holds, then the mapping $K^e(\cdot)$ is continuous.*

Proof. See Appendix A.2. □

2.5 Finite-dimensional approximations

Approximations to the infinite-dimensional terms (e.g., the PDE state \mathcal{Z} and its estimate $\hat{\mathcal{Z}}$ and the operators \mathcal{Q} , \mathcal{Q}_f , and Π_0^e) permit numerical computation. Consider a finite-dimensional subspace $\mathcal{H}_N \subset \mathcal{H}$ with dimension N . The inner product and norm of \mathcal{H}_N are inherited from that of \mathcal{H} . Let $P_N : \mathcal{H} \rightarrow \mathcal{H}_N$ denote the orthogonal projection of \mathcal{H} onto \mathcal{H}_N . Let $Z_N(t) = P_N\mathcal{Z}(t)$ and $S_N(t) = P_N\mathcal{S}(t)P_N$ denote the finite-dimensional approximation of $\mathcal{Z}(t)$ and $\mathcal{S}(t)$, respectively. A finite-

dimensional approximation of (2.9) is

$$\dot{Z}_N(t) = A_N Z_N(t) + B_N(M\xi(t), t)u(t), \quad (2.28)$$

$$Z_N(0) = Z_{0,N} = P_N Z_0, \quad (2.29)$$

where $A_N \in \mathcal{L}(\mathcal{H}_N)$ and $B_N(M\xi(t), t) \in \mathcal{L}(U, \mathcal{H}_N)$ are approximations of \mathcal{A} and $\mathcal{B}(M\xi(t), t)$, respectively. Since the actuator state $\xi(t)$ is a function of time t , we sometimes use $B_N(t)$ for brevity. Correspondingly, the finite-dimensional approximation of (2.14) is

$$\begin{aligned} \Pi_N^c(t) = & S_N^*(t_f - t)Q_{f,N}S_N(t_f - t) + \int_t^{t_f} S_N^*(\tau - t) \\ & (Q_N(\tau) - \Pi_N^c(\tau)\bar{B}_N\bar{B}_N^*(\tau)\Pi_N^c(\tau)) S_N(\tau - t)d\tau, \end{aligned} \quad (2.30)$$

where $Q_N = P_N Q P_N$, $Q_{f,N} = P_N Q_f P_N$, and $\bar{B}_N\bar{B}_N^*(\tau)$ is short for $B_N(\tau)R^{-1}B_N^*(\tau)$.

The optimal control u_N^* that minimizes the approximated PDE cost

$$\begin{aligned} J_N(Z_N, u_N) = & \langle Z_N(t_f), Q_{f,N}Z_N(t_f) \rangle \\ & + \int_0^{t_f} \langle Z_N(t), Q_N(t)Z_N(t) \rangle + u_N^\top(t)Ru_N(t)dt \end{aligned} \quad (2.31)$$

is analogous to (2.12):

$$u_N^*(t) = -R^{-1}B_N^*(M\xi(t), t)\Pi_N^c(t)Z_N(t), \quad (2.32)$$

where $\Pi_N^c(t)$ is a solution of (2.30).

The following assumptions are associated with the approximations:

(C5) Both \mathcal{Q}_f and sequence $\{Q_{f,N}\}_{N=1}^\infty$ are elements of $\mathcal{J}_q(\mathcal{H})$. Both \mathcal{Q}_f and $Q_{f,N}$ are nonnegative for all $N \in \mathbb{N}$ and $\|\mathcal{Q}_f - Q_{f,N}\|_{\mathcal{J}_q(\mathcal{H})} \rightarrow 0$ as $N \rightarrow \infty$.

(C6) Both $\mathcal{Q}(\cdot)$ and sequence $\{Q_N(\cdot)\}_{N=1}^\infty$ are elements of $L^1([0, t_f]; \mathcal{J}_q(\mathcal{H}))$. Both $\mathcal{Q}(\tau)$ and $Q_N(\tau)$ are nonnegative for all $\tau \in [0, t_f]$ and all $N \in \mathbb{N}$ and satisfy $\int_0^t \|\mathcal{Q}(\tau) - Q_N(\tau)\|_{\mathcal{J}_q(\mathcal{H})} d\tau \rightarrow 0$ for all $t \in [0, t_f]$ as $N \rightarrow \infty$.

(C7) Both $\bar{\mathcal{B}}\bar{\mathcal{B}}^*(\cdot)$ and sequence $\{\bar{B}_N\bar{B}_N^*(\cdot)\}_{N=1}^\infty$ are elements of $L^\infty([0, t_f]; \mathcal{L}(\mathcal{H}))$. Both $\bar{\mathcal{B}}\bar{\mathcal{B}}^*(t)$ and $\bar{B}_N\bar{B}_N^*(t)$ are nonnegative for all $t \in [0, t_f]$ and all $N \in \mathbb{N}$ and satisfy

$$\operatorname{ess\,sup}_{t \in [0, t_f]} \|\bar{\mathcal{B}}\bar{\mathcal{B}}^*(t) - \bar{B}_N\bar{B}_N^*(t)\|_{\operatorname{op}} \rightarrow 0 \quad (2.33)$$

as $N \rightarrow \infty$ ($\|\cdot\|_{\operatorname{op}}$ denotes the operator norm).

Note that the assumptions (C1), (C2), and (C3) are contained in (C5), (C6), and (C7), respectively.

The next Lemma states the convergence of an approximate solution of the Riccati equation, which is reproduced from [11, Theorem 3.5] and hence stated without a proof.

Lemma 2.6. *[11, Theorem 3.5] Suppose $\mathcal{S}(t)$ is a strongly continuous semigroup of linear operators over a Hilbert space \mathcal{H} and that $\{S_N(t)\}_{N=1}^\infty$ is a sequence of uniformly continuous semigroup over the same Hilbert space that satisfy, for each*

$\phi \in \mathcal{H}$

$$\|\mathcal{S}(t)\phi - S_N(t)\phi\| \rightarrow 0, \quad \|\mathcal{S}^*(t)\phi - S_N^*(t)\phi\| \rightarrow 0 \quad (2.34)$$

as $N \rightarrow \infty$, uniformly in $[0, t_f]$. Suppose assumptions (C5)–(C7) hold. If $\Pi^c(\cdot) \in C([0, t_f]; \mathcal{J}_q(\mathcal{H}))$ is a solution of (2.14) and $\Pi_N^c(\cdot) \in C([0, t_f]; \mathcal{J}_q(\mathcal{H}))$ is the sequence of solution of (2.30), then

$$\sup_{t \in [0, t_f]} \|\Pi^c(t) - \Pi_N^c(t)\|_{\mathcal{J}_q(\mathcal{H})} \rightarrow 0 \quad (2.35)$$

as $N \rightarrow \infty$.

The following assumption and lemma are analogous to (C4) and Lemma 2.3, respectively:

(C8) The approximated input operator $B_{i,N}(x, t)$ is continuous with respect to location $x \in \mathbb{R}^2$, that is, there exists a continuous function $l_N : \mathbb{R}^+ \rightarrow \mathbb{R}^+$ such that $l_N(0) = 0$ and $\|B_{i,N}(x, t) - B_{i,N}(y, t)\|_{L^2(\Omega)} \leq l_N(|x - y|_2)$ for all $t \in [0, t_f]$, all $x, y \in \mathbb{R}^2$, and all $i \in \{1, 2, \dots, m_a\}$.

Similar to the mapping $K^c(\cdot)$ in Lemma 2.3, the optimal approximated PDE cost can be characterized as a mapping of the actuator state through (2.30), where the continuity is established in Lemma 2.7

Lemma 2.7. *Suppose $Z_{0,N} \in \mathcal{H}_N$. Let assumptions (C5)–(C7) hold and $\Pi_N^c(t)$ be defined as in (2.30). If assumption (C8) holds, then the mapping $K_N^c : C([0, t_f]; \mathbb{R}^n) \rightarrow \mathbb{R}^+$ such that $K_N^c(\xi) = \langle Z_{0,N}, \Pi_N^c(0)Z_{0,N} \rangle$ is continuous.*

Proof. See Appendix A.3. □

The same approximation scheme can be applied to the Kalman filter of the system (2.22), i.e.,

$$\dot{\hat{Z}}_N(t) = A_N \hat{Z}_N(t) + \Pi_N^e(t) C_N(t) R^{-1} (y(t) - \hat{y}_N(t)), \quad (2.36)$$

$$\hat{y}_N(t) = C_N^*(t) \hat{Z}_N(t), \quad (2.37)$$

with initial condition $\hat{Z}_N(t_0) = P_N \hat{Z}_0$. The approximations $A_N \in \mathcal{L}(\mathcal{H}_N)$ and $C_N(t) \in \mathcal{L}(\mathbb{R}^{m_s}, \mathcal{H}_N)$ are of \mathcal{A} and $\mathcal{C}(t)$, respectively, and $\Pi_N^e(t)$ is the finite-dimensional approximation of $\Pi^e(t)$ such that

$$\begin{aligned} \Pi_N^e(t) = \int_0^t S_N(t-\tau) (Q_N(\tau) - \Pi_N^e(\tau) \bar{C}_N \bar{C}_N^*(\tau) \Pi_N^e(\tau)) S_N^*(t-\tau) d\tau \\ + S_N(t) \Pi_{0,N}^e S_N^*(t), \end{aligned} \quad (2.38)$$

where $\Pi_{0,N}^e = P_N \Pi_0^e P_N$ and $Q_N(t) = P_N Q(t) P_N$ are approximations of Π_0^e and $Q(t)$, respectively, and $\bar{C}_N \bar{C}_N^*(\tau)$ is short for $C_N R^{-1} C_N^*(\tau)$.

If the subspace \mathcal{H}_N is chosen such that it is spanned by the first N functions of the orthonormal basis $\{\phi_i\}_{i=1}^\infty$ that spans \mathcal{H} , then

$$\text{Tr}(\Pi_N^e(t)) = \text{Tr}(P_N \Pi^e(t) P_N) = \sum_{i=1}^N \langle \phi_i, \Pi^e(t) \phi_i \rangle. \quad (2.39)$$

To establish convergence of the approximate covariance operator $\Pi_N^e(\cdot)$ to the original operator $\Pi^e(\cdot)$, the following assumptions are made:

(E5) Both Π_0^e and sequence $\{\Pi_{0,N}^e\}_{N=1}^\infty$ are elements of $\mathcal{J}_q(\mathcal{H})$. Both Π_0^e and $\Pi_{0,N}^e$

are nonnegative for all $N \in \mathbb{N}$ and $\|\Pi_0^e - \Pi_{0,N}^e\|_{\mathcal{J}_q(\mathcal{H})} \rightarrow 0$ as $N \rightarrow \infty$.

(E6) Both $Q(\cdot)$ and sequence $\{Q_N(\cdot)\}_{N=1}^\infty$ are elements of $L^1([0, t_f]; \mathcal{J}_q(\mathcal{H}))$. Both

$Q(\tau)$ and $Q_N(\tau)$ are nonnegative for all $\tau \in [0, t_f]$ and all $N \in \mathbb{N}$ and satisfy

$$\int_0^t \|Q(\tau) - Q_N(\tau)\|_{\mathcal{J}_q(\mathcal{H})} d\tau \rightarrow 0 \quad (2.40)$$

for all $t \in [0, t_f]$ as $N \rightarrow \infty$.

(E7) Both $\bar{\mathcal{C}}\bar{\mathcal{C}}^*(\cdot)$ and sequence $\{\bar{C}_N\bar{C}_N^*(\cdot)\}_{N=1}^\infty$ are elements of $L^\infty([0, t_f]; \mathcal{L}(\mathcal{H}))$.

Both $\bar{\mathcal{C}}\bar{\mathcal{C}}^*(t)$ and $\bar{C}_N\bar{C}_N^*(t)$ are nonnegative for all $t \in [0, t_f]$ and all $N \in \mathbb{N}$ and

satisfy

$$\operatorname{ess\,sup}_{t \in [0, t_f]} \|\bar{\mathcal{C}}\bar{\mathcal{C}}^*(t) - \bar{C}_N\bar{C}_N^*(t)\|_{\operatorname{op}} \rightarrow 0 \quad (2.41)$$

as $N \rightarrow \infty$ ($\|\cdot\|_{\operatorname{op}}$ denotes the operator norm).

Note that assumptions (E1), (E2), and (E3) are contained within assumptions (E5), (E6), and (E7), respectively.

The convergence of the approximate covariance operator $\Pi_N^e(\cdot)$ is stated in the next theorem (which is the dual version of Lemma 2.6) whose proof is omitted since the Lemma is reproduced from [11, Theorem 3.5].

Lemma 2.8 ([11, Theorem 3.5]). *Suppose $\mathcal{S}(t)$ is a strongly continuous semigroup of linear operators over a Hilbert space \mathcal{H} and that $\{S_N(t)\}_{N=1}^\infty$ is a sequence of uniformly continuous semigroup over the same Hilbert space that satisfy, for each $\phi \in \mathcal{H}$,*

$$\|\mathcal{S}(t)\phi - S_N(t)\phi\| \rightarrow 0 \quad (2.42a)$$

$$\|\mathcal{S}^*(t)\phi - S_N^*(t)\phi\| \rightarrow 0 \quad (2.42b)$$

as $N \rightarrow \infty$, uniformly in $[0, t_f]$. Suppose assumptions (E5)–(E7) hold. If $\Pi^e(\cdot) \in C([0, t_f]; \mathcal{J}_q(\mathcal{H}))$ is a solution of (2.25) and $\Pi_N^e(\cdot) \in C([0, t_f]; \mathcal{J}_q(\mathcal{H}))$ is the sequence of solution of (2.38), then

$$\sup_{t \in [0, t_f]} \|\Pi^e(t) - \Pi_N^e(t)\|_{\mathcal{J}_q(\mathcal{H})} \rightarrow 0 \quad (2.43)$$

as $N \rightarrow \infty$.

The following assumption and lemma are related to the continuity with respect to location of the approximate output kernel and the continuity with respect to sensor state of the trace of the approximate covariance operator, which are analogous to assumption (E4) and Lemma 2.5, respectively.

(E8) The approximated input operator $C_{i,N}(x, t)$ is continuous with respect to location $x \in \mathbb{R}^2$, that is, there exists a continuous function $l_N : \mathbb{R}^+ \rightarrow \mathbb{R}^+$ such that $l_N(0) = 0$ and

$$\|C_{i,N}(x_1, t) - C_{i,N}(x_2, t)\|_{L^2(\Omega)} \leq l_N(|x_1 - x_2|_2)$$

for all $t \in [0, t_f]$, all $x_1, x_2 \in \mathbb{R}^2$, and all $i \in \{1, 2, \dots, m_s\}$.

Similar to the mapping $K^e(\cdot)$ in Lemma 2.5, we can characterize the approximate uncertainty cost as a mapping of the sensor state ζ , where continuity is established in Lemma 2.9.

Lemma 2.9. *Let assumptions (E5)–(E7) hold and $\Pi_N^e(t)$ be defined as in (2.38).*

If assumption (E8) holds, then the mapping $K_N^e : C([0, t_f]; \mathbb{R}^n) \rightarrow \mathbb{R}^+$ such that

$K_N^e(\zeta) = \int_0^{t_f} \text{Tr}(\Pi_N^e(t)) dt$ is continuous.

Proof. See Appendix A.4. □

Chapter 3: Optimal cooperative control of a 2D diffusion-advection process

In this chapter, an optimization framework is proposed that simultaneously solves for the guidance of a team of mobile actuators and the control of a DPS. We consider a 2D diffusion-advection process as the DPS for its capability of modeling a variety of processes governed by continuum mechanics and the convenience of the state-space representation. The framework minimizes an integrated cost function, evaluating both the control of the DPS and the guidance of the actuators, subject to the dynamics of the DPS and the mobile actuators. The problem addresses the mobile actuator and the DPS as a unified system, instead of solely controlling the DPS. Furthermore, the additional degree of freedom endowed by mobility yields improved control performance in comparison to using stationary actuators.

The problem formulation in this chapter includes a cost function that simultaneously evaluates controlling the PDE-modeled DPS, referred to as the *PDE cost*, and steering the mobile actuators, referred to as the *mobility cost*. The PDE cost is a quadratic cost of the PDE state and control, whose optimal value can be obtained by solving an operator-valued differential Riccati equation. Our results are based on the related work [11], which establishes Bochner integrable solutions of

finite-horizon Riccati integral equations (with values in Schatten p -classes) associated with infinite-dimensional systems. The existence conditions for the solution of exact and approximate Riccati integral equations are established in [11]. The significance of the Bochner integrable solution is that it allows the implementation of simple numerical quadratures for computing the approximated solution of Riccati integral equations. In [11], the Riccati solution is applied in a sensor placement problem, which computes optimal sensor locations that minimize the trace of the covariance operator of the Kalman filter of a diffusion-advection process. The same cost has been used in an optimization framework for mobile sensor's motion planning in [10]. The existence of a solution of the optimization problem is established under the assumption that the integral kernel of the output operator is continuous with respect to the location of the sensor [10, Definition 4.5]. This assumption permits the construction of a compact set of operators [10, Lemma 4.6] over which the cost function is continuous, and hence establishes the existence of a solution. The assumption is also made on the input operator in Chapter 2, which allows the derivation of a vital result on the Riccati operator's continuity with respect to the actuator trajectory (see Lemma 2.3). The continuity property plays a crucial role in establishing the existence of the proposed problem's solution and the convergence to the exact optimal solution of the approximate optimal solution. The existence of a solution is established in using the fact that a weakly sequentially lower semi-continuous function attains its minimum on a weakly sequentially compact set over a normed linear space. In addition to the assumptions made for the existence of a solution, a stringent (yet with reasonable physical interpretation) requirement is

placed on the admissible set to yield compactness, which leads to convergence of the approximate optimal solution. The convergence is in the sense that when evaluating the exact and approximate optimal solutions by the original cost function, the difference becomes arbitrarily small as the dimension of approximation increases.

The remainder of this chapter is organized as follows. Section 3.1 introduces the proposed optimization problem and its equivalent problem. Conditions for the existence of a solution are stated. Section 3.2 details the computation of an optimal solution using finite-dimensional approximations. Conditions for the convergence to the exact optimal solution of the approximate optimal solution are stated. A gradient-based method is applied to find an optimal solution. Section 3.3 provides two numerical examples to illustrate optimal guidance and control solved by the proposed method.

3.1 Problem formulation

This chapter seeks to derive the guidance and control input of each actuator such that the state \mathcal{Z} of the abstract linear system (2.9) can be driven to zero. Specifically, consider the following problem:

$$\begin{aligned}
 & \underset{\substack{u \in L^2([0, t_f]; U) \\ p \in L^2([0, t_f]; P)}}{\text{minimize}} && J(\mathcal{Z}, u) + J_m(\xi, p) \\
 & \text{subject to} && \dot{\mathcal{Z}}(t) = \mathcal{A}\mathcal{Z}(t) + \mathcal{B}(M\xi(t), t)u(t), \quad \mathcal{Z}(0) = \mathcal{Z}_0, \\
 & && \dot{\xi}(t) = \alpha\xi(t) + \beta p(t), \quad \xi(0) = \xi_0,
 \end{aligned} \tag{Pc}$$

where $J_m(\xi, p) = \int_0^{t_f} h(\xi(t), t) + g(p(t), t)dt + h_f(\xi(t_f))$ is the cost associated with the motion of the actuators, named the *mobility cost*, such that the mappings $h : \mathbb{R}^n \times [0, t_f] \rightarrow \mathbb{R}^+$ and $g : \mathbb{R}^m \times [0, t_f] \rightarrow \mathbb{R}^+$ evaluate the running state cost and running guidance cost, respectively, and the mapping $h_f : \mathbb{R}^n \rightarrow \mathbb{R}^+$ evaluates the terminal state cost.

The running state cost $h(\cdot, \cdot)$ may characterize restrictions to actuator state. For example, a Gaussian-type function with its peak in the center of the spatial domain, i.e.,

$$h\left(\begin{bmatrix} x \\ y \end{bmatrix}, t\right) = \frac{1}{2\pi\sigma_x(t)\sigma_y(t)} \exp\left(-\frac{(x-0.5)^2}{\sigma_x^2(t)} - \frac{(y-0.5)^2}{\sigma_y^2(t)}\right), \quad (3.1)$$

where $\sigma_x(t), \sigma_y(t) > 0$ and $x, y \in [0, 1]$, can model a hazardous field that may shorten the life span of an actuator. The integral of this function in the interval $[0, t_f]$ evaluates the accumulated exposure of the mobile actuator along its trajectory, which may need to be contained as small as possible (see [28]). Another example is the artificial potential field [39], cast as a soft constraint, that penalizes the trajectory when it passes an inaccessible region such as an obstacle. The running guidance cost $g(\cdot, \cdot)$ may be the absolute value or a quadratic function of the guidance, which characterizes the total amount (of fuel) or energy for steering, respectively. And the terminal state cost $h_f(\cdot)$ may characterize restrictions of the terminal state of the mobile actuators. For example, if an application specifies terminal positions, then $h_f(\cdot)$ may be a quadratic function that penalizes the deviation of the actual terminal positions.

The formulation in (Pc) provides an intermediate step for minimizing the PDE cost subject to mobility constraints, in addition to the dynamics constraints. The mobility constraints are characterized by inequalities of $h_f(\cdot)$ and the integrals of $h(\cdot, \cdot)$ and $g(\cdot, \cdot)$, because these constraints can be used to augment the cost function and turned into the form of (Pc) using the method of Lagrange multipliers.

An equivalent problem of (Pc) can be derived using Lemma 2.2. For an arbitrary admissible guidance p , the actuator trajectory ξ is determined following the dynamics (2.2), which also determines the input operator $\mathcal{B}(\xi(\cdot), \cdot)$. By Lemma 2.2, the control u that minimizes the cost function of (Pc)—specifically, the PDE cost $J(\mathcal{Z}, u)$ —is given by (2.12), and the minimum PDE cost is $\langle \mathcal{Z}_0, \Pi(0)\mathcal{Z}_0 \rangle$, where $\Pi(0)$ is the mild solution of (2.14) with actuator trajectory steered by guidance p . Note the Riccati operator $\Pi(\cdot)$ in this chapter is the operator $\Pi^c(\cdot)$ in Chapter 2 (the superscript c is dropped for simplicity). Hence, we derive the following problem equivalent to (Pc):

$$\begin{aligned} & \underset{p \in L^2([0, t_f]; P)}{\text{minimize}} && \langle \mathcal{Z}_0, \Pi(0)\mathcal{Z}_0 \rangle + J_m(\xi, p) \\ & \text{subject to} && \dot{\xi}(t) = \alpha\xi(t) + \beta p(t), \quad \xi(0) = \xi_0, \end{aligned} \tag{Pc1}$$

where $\Pi(0)$ is defined in (2.14) with $t = 0$.

To prove the existence of a solution to (Pc1), we make the following assumptions on the admissible set of guidance and the functions composing the mobility cost:

(C9) The set of admissible guidance $P \subset \mathbb{R}^m$ is closed and convex.

(C10) The mappings $h : \mathbb{R}^n \times [0, t_f] \rightarrow \mathbb{R}^+$, $g : \mathbb{R}^m \times [0, t_f] \rightarrow \mathbb{R}^+$, and $h_f : \mathbb{R}^n \rightarrow \mathbb{R}^+$ are continuous. For every $t \in [0, t_f]$, the function $g(\cdot, t)$ is convex.

(C11) There exists a constant $d_1 > 0$ with $g(p, t) \geq d_1 |p|_2^2$ for all $(p, t) \in P \times [0, t_f]$.

Assumptions (C9)–(C11) are generally satisfied in applications with vehicles carrying the actuators. Assumption (C9) is a physically reasonable characterization of the steering of a vehicle, where the admissible steering is generally a continuum with attainable limits within its range. Assumption (C10) places a general continuity requirement on the cost functions and a convexity requirement on the steering cost function. Assumption (C11) requires the function $g(p, t)$ to be bounded below by a quadratic function of the guidance p for all t , which is generally satisfied, e.g., with g itself being a quadratic function of p . These assumptions are applied in Theorem 3.1 below regarding the existence of a solution of (Pc1). Subsequently, the solution to (Pc1) can be used to reconstruct the solutions to (Pc), which is stated in Theorem 3.2.

Theorem 3.1. *Consider problem (Pc1) and let assumptions (C1)–(C4) and (C9)–(C11) hold. Then (Pc1) has a solution.*

Proof. See Appendix A.5. □

Theorem 3.2. *Consider problems (Pc) and (Pc1). Let assumptions (C4) and (C9)–(C11) hold. Let p^* be the optimal solution of (Pc1) and u^* be the optimal control obtained from (2.12) with actuator trajectory steered by p^* . Then u^* and p^* minimize problem (Pc).*

Proof. See Appendix A.6. □

The equivalent problem (Pc1) allows us to search for an optimal guidance p such that the mobility cost plus the optimal PDE cost is minimized. The control is no longer an optimization variable, because it is determined by the LQR of the abstract linear system for arbitrary trajectories of the mobile actuators.

3.2 Computation of optimal control and guidance

Approximation of the infinite-dimensional terms in problem (Pc) is necessary when computing the optimal control and guidance. Hence, we replace the PDE cost and dynamics of (Pc) by (2.31) and (2.28), respectively, and obtain the following approximate problem (APc):

$$\begin{aligned}
 & \underset{\substack{u \in L^2([0, t_f]; U) \\ p \in L^2([0, t_f]; P)}}{\text{minimize}} && J_N(Z_N, u) + J_m(\xi, p) \\
 & \text{subject to} && \dot{Z}_N(t) = A_N Z_N(t) + B_N(M\xi(t), t)u(t) \\
 & && Z_N(0) = Z_{0,N}, \\
 & && \dot{\xi}(t) = \alpha\xi(t) + \beta p(t), \\
 & && \xi(0) = \xi_0.
 \end{aligned} \tag{APc}$$

Similar to (Pc), problem (APc) can be turned into an equivalent form using

LQR results for a finite-dimensional system:

$$\begin{aligned} & \underset{p \in L^2([0, t_f]; P)}{\text{minimize}} && \langle Z_{0,N}, \Pi_N(0)Z_{0,N} \rangle + J_m(\xi, p) \\ & \text{subject to} && \dot{\xi}(t) = \alpha\xi(t) + \beta p(t), \quad \xi(0) = \xi_0, \end{aligned} \tag{APc1}$$

where $\Pi_N(0)$ is defined in (2.30) with $t = 0$. Analogous to Theorems 3.1 and 3.2, the existence of a solution of (APc1) and how to use its solution to reconstruct a solution for (APc) are stated in Theorem 3.3 below.

Theorem 3.3. *Consider problem (APc1) and let assumptions (C5)–(C8) and (C9)–(C11) hold. Then (APc1) has a solution, denoted by p_N^* . Let u_N^* be the optimal control obtained from (2.32) with actuator trajectory steered by p_N^* . Then u_N^* and p_N^* minimize problem (APc).*

Proof. See Appendix A.7. □

An extension to Theorem 3.3 is that an optimal feedback control can be obtained from (2.32) whenever the optimal guidance is solved from (APc) or (APc1). Basically, when the trajectory is determined via the optimal guidance, a feedback control can be implemented.

To establish convergence to the solution of (Pc1) of (APc1)'s solution, we need to restrict the set of admissible guidance to a smaller set as introduced below in assumption (C12).

- (C12) There exist $p_{\max} > 0$ and $a_{\max} > 0$ such that the set of admissible guidance is $\mathcal{P}(p_{\max}, a_{\max}) = \{p \in C([0, t_f]; P) : |p(t)| \text{ is uniformly bounded by } p_{\max} \text{ and}$

$$|p(t_1) - p(t_2)| \leq a_{\max}|t_1 - t_2|, \forall t_1, t_2 \in [0, t_f].$$

There are two perspectives to interpreting the assumption (C12). Mathematically, (C12) requires the admissible guidance to be a continuous function that is uniformly bounded and uniformly equicontinuous. These two properties yield the sequential compactness of the set $\mathcal{P}(p_{\max}, a_{\max})$ by the Arzelà-Ascoli Theorem [67]. Practically, (C12) requires the input signal to be continuous and have bounds p_{\max} and a_{\max} on the magnitude and the rate of change, respectively. This requirement is reasonable and checkable because a continuous signal is commonly used for smooth operation, and the bounds on magnitude and changing rate are due to the physical limits of the motion of a platform. For example, in the case of single integrator dynamics where p is the velocity command, p_{\max} and a_{\max} refer to the maximum speed and maximum acceleration, respectively. Moreover, since time discretization of the signal is applied when computing the optimal guidance, as long as the bound p_{\max} on the magnitude of the signal is determined, then the changing rate is bounded by $a_{\max} := 2p_{\max}/\Delta t_{\min}$ for the smallest discrete interval length Δt_{\min} . Theorem 3.4 below states the convergence of the approximate optimal solution.

Theorem 3.4. *Consider problem (Pc1) and its finite-dimensional approximation (APc1). Let assumptions (C4)–(C12) hold and let p^* and p_N^* denote the optimal guidance of (Pc1) and (APc1), respectively. Then*

$$\lim_{N \rightarrow \infty} |J_{(\text{APc1})}^*(p_N^*) - J_{(\text{Pc1})}^*(p^*)| = 0. \quad (3.2)$$

Furthermore, the cost function of (Pc1) evaluated at the guidance p_N^ converges to*

the optimal cost of (Pc1)

$$\lim_{N \rightarrow \infty} |J_{(\text{Pc1})}(p_N^*) - J_{(\text{Pc1})}^*(p^*)| = 0. \quad (3.3)$$

Proof. See Appendix A.8. □

Remark 3.1. *Two implications of Theorem 3.4 follow. First, (3.2) implies that the optimal cost of the approximated problem (APc1) converges to that of the exact problem (Pc1), which justifies the approximation in (APc1). Second, (3.3) implies that the approximate optimal guidance p_N^* , when evaluated by the cost function of (Pc1), yields a cost that is arbitrarily close to the exact optimal cost of (Pc1). Since p_N^* is computable and p^* is not, the convergence in (3.3) qualifies p_N^* as an appropriate optimal guidance.*

The convergence stated in Theorem 3.4 is established based on several earlier stated results, including

1. the input operator's continuity with respect to location (assumption (C4)), which leads to the continuity of the PDE cost with respect to actuator trajectory (Lemma 2.3);
2. existence of the Riccati operator (Lemma 2.1) and convergence of its approximation (Lemma 2.6); and
3. sequential compactness of the set of admissible guidance (assumption (C12)), which leads to the continuity of the cost function with respect to guidance (Lemma A.1 in the Appendix).

Notice that these key results, in an analogous manner, are also required in [57] when establishing the convergence to the exact optimal actuator locations of the approximate optimal locations [57, Theorem 3.5], i.e.,

1. continuity with respect to location and compactness of the input operator [57, Theorem 2.6], which lead to continuity of the Riccati operator with respect to actuator locations [57, Theorem 2.6];
2. existence of the Riccati operator [57, Theorem 2.3] and the convergence of its approximation [57, Theorem 3.1]; and
3. sequential compactness of the set of admissible locations, which is inherited from the setting that the spatial domain is closed and bounded in a finite-dimensional space.

Although the establishment of convergence is similar to the one in [57], the cost function and type of Riccati equation are different: we have the quadratic PDE cost plus generic mobility cost and differential Riccati equation in this chapter for control and actuator guidance versus the Riccati operator's norm as cost function and algebraic Riccati equation in [57] for actuator placement. The similarity comes from the infinite-dimensional nature of PDEs such that approximation is necessary for computation, and convergence in approximation qualifies the approximate optimal solutions.

3.2.1 Checking assumptions (C4)–(C12)

For the approximated optimal guidance to be a good proxy of the exact optimal guidance, by Theorem 3.4, assumption (C4)–(C12) have to be checked to ensure the convergence. We summarize methods for checking these assumptions here. (C4): examine the explicit form of \mathcal{B} ; (C5)–(C7): examine the explicit form of the operators \mathcal{Q} , \mathcal{Q}_f , and $\bar{\mathcal{B}}\bar{\mathcal{B}}^*$ and their approximations; (C8): examine the explicit form of B_N ; (C9)–(C11): examine the explicit form of J_m ; (C12): examining the bounds on the magnitude and changing rate of the admissible guidance.

3.2.2 Gradient-descent for solving problem (APc)

We apply a gradient-descent for solving problem (APc). Define the costates $\lambda(t) \in \mathcal{H}_N$ and $\mu(t) \in \mathbb{R}^n$ associated with $Z_N(t)$ and $\xi(t)$, respectively, for $t \in [0, t_f]$ and define the Hamiltonian:

$$\begin{aligned}
 & H(Z_N(t), \xi(t), u(t), p(t), \lambda(t), \mu(t)) \\
 &= \langle Z_N(t), Q_N(t)Z_N(t) \rangle + u^\top(t)Ru(t) + h(\xi(t), t) \\
 &\quad + g(p(t), t) + \lambda^\top(t) (A_N Z_N(t) + B_N(M\xi(t), t)u(t)) \\
 &\quad + \mu^\top(t) (\alpha\xi(t) + \beta p(t)). \tag{3.4}
 \end{aligned}$$

By Pontryagin's minimum principle [51], we can solve a two-point boundary value problem originated from (3.4) to find a local minimum of (APc). The iterative procedure for solving the two-point boundary value problem can be implemented in

a gradient-descent manner [47, 50].

3.3 Numerical examples

We demonstrate the performance of the optimal guidance and control in two numerical examples. The first example uses the diffusion-advection process with zero Dirichlet boundary condition (2.5)–(2.7). The second example uses the same process but with zero Neumann boundary condition.

The examples are motivated by and simplified from practical applications, e.g., removal of harmful algal blooms (HAB). In this case, the distribution of the HAB’s concentration on the water surface can be modeled by a 2D diffusion-advection process. The cases of zero Dirichlet and Neumann boundary conditions correspond to the scenarios where the surface is circumvented by absorbent and nonabsorbent materials, respectively. The control to the process is implemented by the surface vehicles that use physical methods (e.g., emitting ultrasonic waves or hauling algae filters) or chemical methods (by releasing algal treatment) [71], whose impact on the process can be characterized by the input operator (2.8). The magnitude of the control determines how fast the concentration is reduced at the location of the actuator. The optimal control and guidance minimize the cost such that the HAB concentration is reduced while the vehicles do not exercise too much control nor conduct aggressive maneuvers. And vehicles’ low-level control can track the optimal trajectories despite the model mismatch between the dynamics of the vehicles and those applied in the optimization problem (Pc).

We apply the following values in the numerical examples: $\Omega = [0, 1] \times [0, 1]$, $z_0(x, y) = 320(x - x^2)(y - y^2)$, $N = 13$, $m_a = 4$, $t_f = 1$, $\mathbf{v} = [0.1, -0.1]^\top$, $a = 0.05$, $U = \mathbb{R}^m$, $P_i = [-100, 100]$, $p_{\max} = a_{\max} = 100$, $R = 0.1I_4$, $\mathcal{Q} = \mathcal{Q}_f = \chi(x, y)$, $h(\xi(t), t) = h_f(\xi(t_f)) = 0$, $g(p(t), t) = 0.1p^\top(t)p(t)$, $\xi_1(0) = [0.1, 0.1]^\top$, $\xi_2(0) = [0.125, 0.1]^\top$, $\xi_3(0) = [0.125, 0.125]^\top$, $\xi_4(0) = [0.1, 0.125]^\top$, $b_i = 1$, $\sigma_i = 0.05$, $\alpha_i = 0_{2 \times 2}$, and $\beta_i = I_2$ for $i \in \{1, 2, \dots, m_a\}$, where the indicator function $\chi(x, y) = 1$ if $x = y$, and $\chi(x, y) = 0$ if $x \neq y$. We use (2.8) for the input operator of each actuator. The Péclet number of the process is $|\mathbf{v}|_2/a \approx 2.83$, which implies neither the diffusion or the advection dominates the process.

3.3.1 Diffusion-advection process with Dirichlet boundary condition

We use the dynamics in (2.5)–(2.7) with the Dirichlet boundary condition. We use the Galerkin scheme to approximate the infinite-dimensional variables. The orthonormal set of eigenfunctions of the Laplacian operator ∇^2 (with zero Dirichlet boundary condition) over the spatial domain $\Omega = [0, 1] \times [0, 1]$ is $\phi_{i,j}(x, y) = 2 \sin(\pi i x) \sin(\pi j y)$. We introduce a single index $k = (i - 1)N + j$ such that $\phi_k = \phi_{i,j}$. For brevity, we use \mathcal{H}_N to denote the N^2 -dimensional space spanned by the basis functions $\{\phi_k\}_{k=1}^{N^2}$. Recall the orthogonal projection $P_N : \mathcal{H} \rightarrow \mathcal{H}_N$. It follows that $P_N^* = P_N$ and $P_N^* P_N \rightarrow I$ strongly [11]. Let $\Phi_N = [\phi_1 \ \phi_2 \ \dots \ \phi_{N^2}]^\top$. We choose $N = 13$ because it is the smallest dimension such that the resulting optimal cost is within the 1% of the optimal cost evaluated with the maximum dimension $N = 20$ in the numerical studies (see Fig. 3.7).

Assumption (C4) holds for the choice of input operator. With the Galerkin approximation using the orthonormal eigenfunctions of the Laplacian operator ∇^2 with zero Dirichlet boundary condition, it can be shown that assumption (C8) holds for $l_N(\cdot) = N^2 l(\cdot)$. Assumptions (C5)–(C7) hold with $q = 1$ under the Galerkin approximation with aforementioned basis functions Φ_N [11]. Assumptions (C9)–(C11) and (C12) hold for the choice of functions in the mobility cost and parameters of the set of admissible guidance, respectively.

We use the forward-backward sweeping method [53] to solve the two-point boundary value problem originated from the Hamiltonian (3.4). The forward propagation of Z_N and ξ and backward propagation of λ and μ are computed using the Runge-Kutta method. The same method is also applied to propagate the approximate Riccati solution $\Pi(t)$. Spatial integrals are computed using Legendre-Gauss quadrature. To verify the convergence of the approximate optimal cost $J_{(\text{APc1})}^*(p_N^*)$ stated in (3.2), we compute $J_{(\text{APc1})}^*(p_N^*)$ for $N \in \{6, 7, \dots, 20\}$. Note that the total number of basis functions is N^2 . The result is shown in Fig. 3.7, where exponential convergence can be observed.

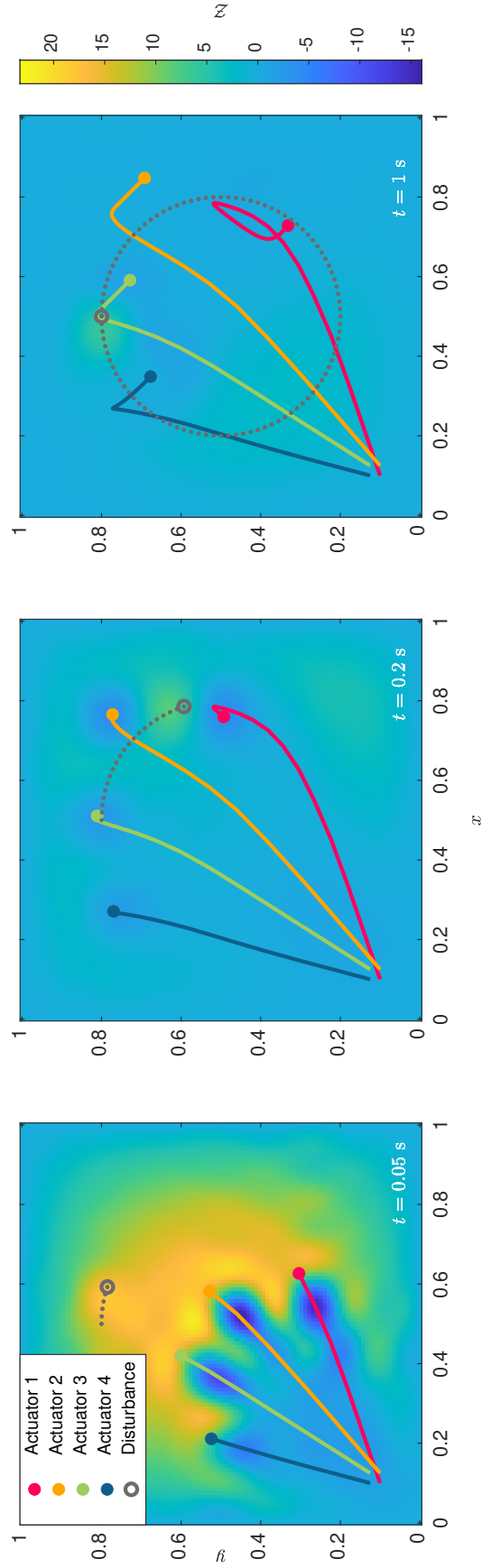


Figure 3.1: Evolution of the diffusion-advection process with Dirichlet boundary condition under the optimal feedback control \bar{u}^* . The actuators are steered by the optimal guidance p^* . Snapshots at $t = 0.05$ and 0.2 s show the transient stage, whereas the one at $t = 1$ s shows the relatively steady stage. The mobile disturbance is shown in gray.

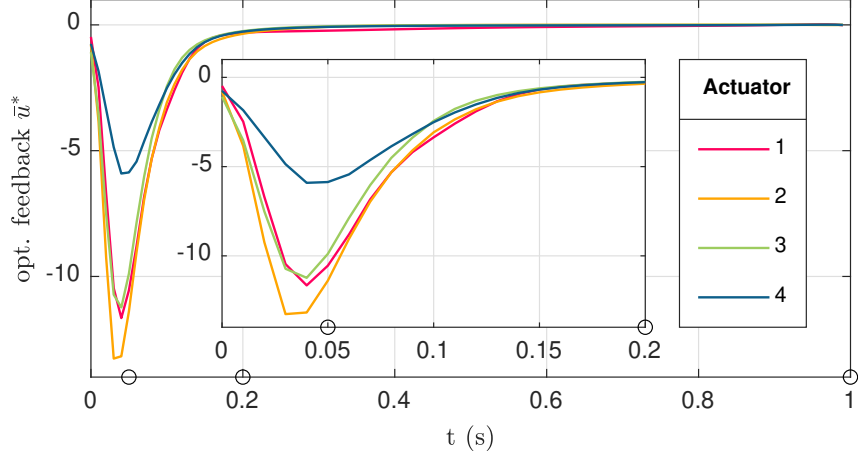


Figure 3.2: Optimal feedback control \bar{u}^* of each actuator in the case of Dirichlet boundary condition. The circles along the horizontal axis correspond to the snapshots in Fig. 3.1.

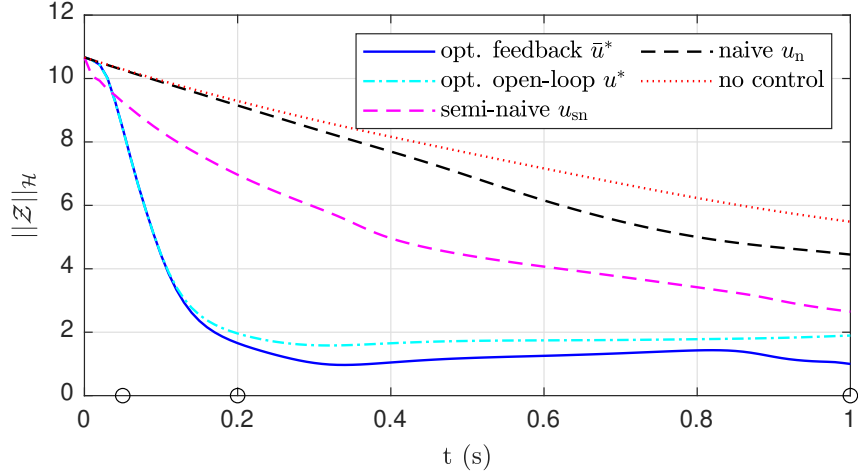


Figure 3.3: Norm of the PDE state in the case of Dirichlet boundary condition with pairs of control and guidance in Table 3.1. The circles along the horizontal axis correspond to the snapshots in Fig. 3.1.

In the simulation, a mobile disturbance $0.5\mathcal{B}(x_d(t), t)$, whose trajectory is $x_d(t) = [0.5 + 0.3 \sin(2\pi t), 0.5 + 0.3 \cos(2\pi t)]^\top$, is added to the right-hand side of the dynamics (2.5).

Denote the optimal open-loop control and optimal guidance solved using the gradient-descent method in the end of Section 3.2 by u^* and p^* , respectively. The

trajectory steered by p^* is denoted by ξ^* . Recall that an optimal feedback control, denoted by \bar{u}^* , can be synthesized using (2.32) based on the optimal trajectory ξ^* of the actuators.

Fig. 3.1 shows the evolution of the process controlled by the optimal feedback control and the optimal trajectories of the actuators. The actuation concentrates in the first 0.2 s, which is shown in Fig. 3.2. The actuators quickly pass the peak of the initial PDE at the center of the spatial domain and spread evenly in space in the first 0.2 s. Subsequently, the actuators 2–4 cease active steering and dispensing actuation. The flow field causes the actuators to drift until the terminal time.

To demonstrate the performance of the optimal feedback control \bar{u}^* , we compare it with semi-naive control u_{sn} and naive control u_{n} defined as local feedback controls: $u_{\text{sn}}(t) = -0.1z_{\text{sn}}(\xi^*(t), t)$ and $u_{\text{n}}(t) = -0.1z_{\text{n}}(\xi_{\text{n}}(t), t)$. The semi-naive actuators follow the optimal trajectory ξ^* , whereas the naive actuators follow the trajectory ξ_{n} , which moves at a constant speed from ξ_0 to $1_{n \times 1} - \xi_0$. Table 3.1 compares the cost breakdown of all the control and guidance strategies. The optimal feedback control yields a smaller cost than the optimal open-loop control due to the capability of feedback control in rejecting disturbances. Simulations with a disturbance-free model (not shown) yield identical total cost for optimal open-loop control and optimal feedback control, which justifies the correctness of the synthesis. Fig. 3.3 compares the norm of the PDE state controlled by pairs of control and guidance listed in Table 3.1. As can be seen, the PDE is effectively regulated using optimal feedback control. As a comparison, the norm associated with optimal open-loop control grows slowly after 0.3 s due the influence of the disturbance, although

	Control (C) and Guidance (G)		Cost		
	C	G	J_N	J_m	Total
opt. feedback	\bar{u}^*	ξ^*	13.7%	3.0%	16.7%
opt. open-loop	u^*	ξ^*	17.5%	3.0%	20.5%
semi-naive	u_{sn}	ξ^*	42.5%	3.0%	45.5%
naive	u_{n}	ξ_{n}	78.8%	0.5%	79.3%
no control	-	-	100.0%	0.0%	100.0%

Table 3.1: Cost comparison of control and guidance strategies in the case of Dirichlet boundary condition. All costs are normalized with respect to the total cost of the case with no control.

its reduction in the beginning is indistinguishable from that of the optimal feedback control.

3.3.2 Diffusion-advection process with Neumann boundary condition

The results derived in this chapter also apply to the operator \mathcal{A} defined in (2.10) with a Neumann boundary condition (BC), because a general second-order and uniformly elliptic operator with Neumann BC yields a strongly continuous analytic semigroup on $L^2(\Omega)$ [49]. In this example, we consider the diffusion-advection process (2.5) with initial condition (2.7) and zero Neumann BC: $\partial z(x, y, t)/\partial \mathbf{n} = 0$, where \mathbf{n} is the normal to the boundary $\partial\Omega$ and $(x, y) \in \partial\Omega$. Notice that the basis function applied for Galerkin approximation in this case are the eigenfunctions of the Laplacian with zero Neumann BC, $\phi_{i,j}(x, y) = 2 \cos(\pi i x) \cos(\pi j y)$ for $i, j \in \{0, 1, \dots\}$. All the parameters, disturbance, and pairs of control and guidance for comparison applied in this example are identical to those in Section 3.3.1. Exponential convergence in the approximate optimal cost can be observed in Fig. 3.7.

Fig. 3.4 shows the evolution of the process and the optimal trajectory of the

actuators. Similar to the case of Dirichlet BC, the actuators spread out to cover most of the domain in the initial 0.2 s, with most of the actuation implemented during the same interval, seen in Fig. 3.5. However, the actuators span a slightly larger area (Fig. 3.4) and the maximum amplitude of actuation is bigger (Fig. 3.5), compared to the case of Dirichlet BC in Fig. 3.1 and Fig. 3.2, respectively. The difference is a consequence of the fact that the zero Neumann BC does not contribute to the regulation of the process because it insulates the process from the outside. Contrarily, the zero Dirichlet BC acts as a passive control that can essentially regulate the process to a zero state when there is no inhomogeneous term in the dynamics (2.5). This difference can be observed when comparing the norm of the PDE state in Fig. 3.6 with Fig. 3.3. The norm of the uncontrolled state reduces slightly in the case of Neumann BC (Fig. 3.6) compared to the almost linear reduction in the case of Dirichlet BC (Fig. 3.3). Fig. 3.6 also shows the difference of norm reduction between the optimal feedback control and optimal open-loop control. Once again, the former yields a smaller terminal norm than the latter due to the feedback's capability of disturbance rejection. The cost breakdown of the pairs of control and guidance in comparison is shown in Table 3.2.

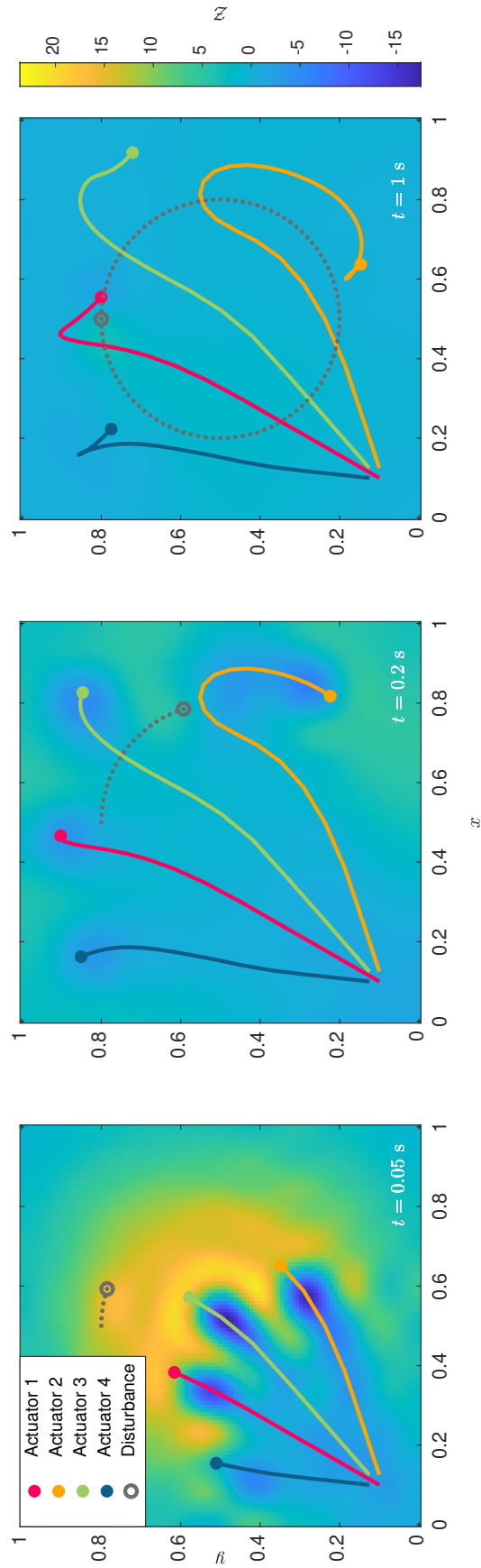


Figure 3.4: Evolution of the process with Neumann boundary condition under the optimal feedback control \bar{u}^* . The actuators are steered by the optimal guidance p^* . Snapshots at $t = 0.05$ and 0.2 s show the transient stage, whereas the one at $t = 1$ s shows the relatively steady stage. The mobile disturbance is shown in gray.

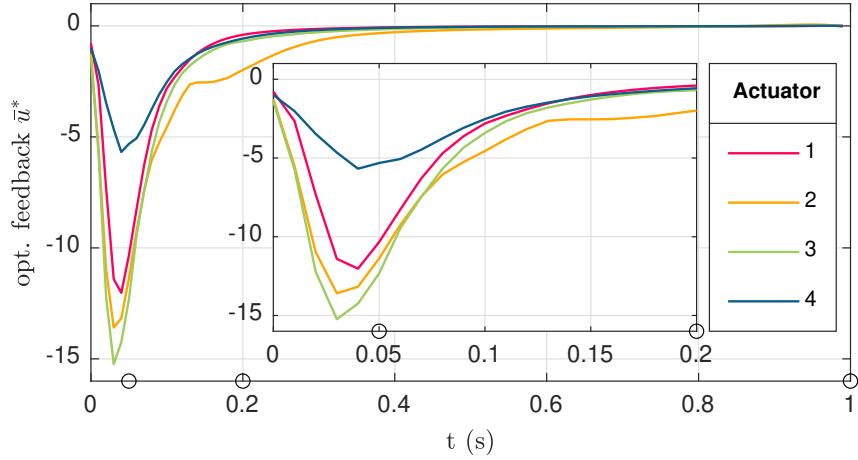


Figure 3.5: Optimal feedback control \bar{u}^* of each actuator in the case of Neumann boundary condition. The circles along the horizontal axis correspond to the snapshots in Fig. 3.4.

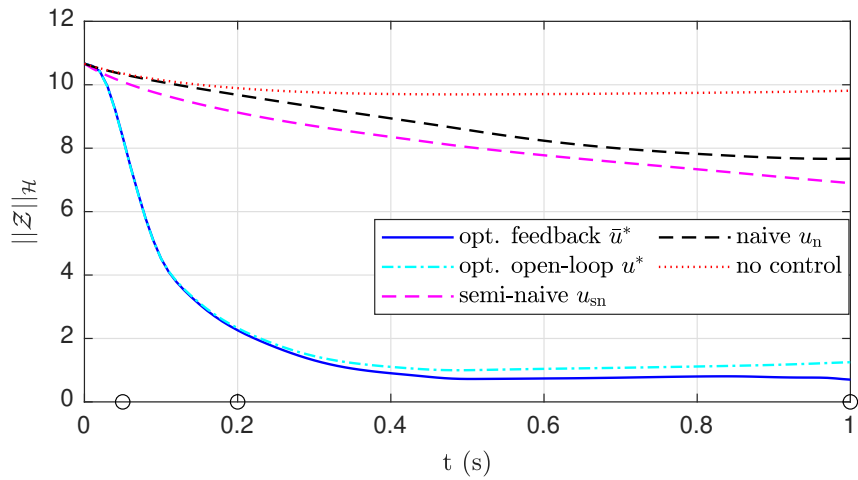


Figure 3.6: Norm of the PDE state in the case of Neumann boundary condition with pairs of control and guidance in Table 3.2. The circles along the horizontal axis correspond to the snapshots in Fig. 3.4.

	Control (C) and Guidance (G)		Cost		
	C	G	J_N	J_m	Total
opt. feedback	\bar{u}^*	ξ^*	6.4%	1.6%	8.0%
opt. open-loop	u^*	ξ^*	7.1%	1.6%	8.7%
semi-naive	u_{sn}	ξ^*	63.7%	1.6%	65.3%
naive	u_n	ξ_n	65.9%	0.2%	66.1%
no control	-	-	100.0%	0.0%	100.0%

Table 3.2: Cost comparison of control and guidance strategies in the case of Neumann boundary condition. All costs are normalized with respect to the total cost of the case with no control.

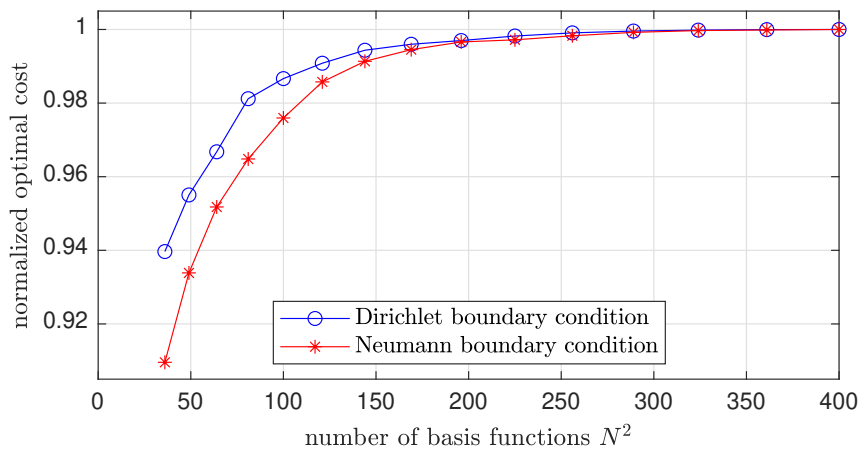


Figure 3.7: Approximate optimal costs $J_{(\text{APcl})}^*(p_N^*)$ normalized with respect to the optimal cost for $N^2 = 400$.

Chapter 4: Optimal cooperative estimation of a 2D diffusion-advection process

This chapter proposes an optimization framework that designs guidance for a team of mobile sensors to estimate a 2D diffusion-advection process using a centralized KF. The cost to be minimized is the sum of two terms: the trace of the covariance operator of the KF, called the *uncertainty cost*, which quantifies the uncertainty of the estimation error and the *mobility cost* associated with the sensors' motion. The covariance operator of the KF, which is the solution of an operator-valued Riccati equation, has been studied in [11]. Specifically, conditions for the existence of Bochner integrable solutions (with values in the Schatten p -class) of an operator-valued Riccati equation are established. The Bochner integrable solutions yield simple numerical quadratures for computation of the covariance operator, which is demonstrated in sensor placement [11] and sensor trajectory planning [12]. Both problems minimize the trace of a weighted covariance operator, whereas the latter has the sensors' dynamics as the constraint.

In our formulation, factors related to the mobile sensor platforms are integrated in addition to reducing the estimation uncertainty only [12]. Specifically, the integration is reflected by the mobility cost, which can be interpreted as the penalty

associated with motion. Our formulation supports various types of cost functions for evaluating the cost or penalty induced from mobility. In prior work, the mobility cost is either limited to a quadratic guidance effort [14] or cast as a general function of the guidance without detailed discussion [4,9]. Furthermore, the formulation permits treating the proposed problem as an optimal control problem, where we show both the uncertainty cost and the mobility cost are continuous mappings of the sensors' guidance. We use the techniques for the existence of an optimal control [88, Theorem 6.1.4] to establish the existence of a solution to our problem.

To compute an optimal solution, approximations of the infinite-dimensional terms are necessary. Our treatment of the proposed problem (and its approximation) permits the application of a two-point boundary value problem derived using Pontryagin's minimum principle. After restricting the admissible guidance functions to a stringent set (with a reasonable physical interpretation), we establish convergence to an exact optimal solution of an approximate optimal solution, i.e., the cost difference between the original and approximate solutions becomes arbitrarily small as the dimension of approximation increases. The convergence result justifies the use of the approximation and affirms that the performance of an approximate solution is arbitrarily close to the performance of an exact solution.

We implement the solution method numerically in simulations to evaluate and analyze the performance of a single sensor and multiple sensors. The flow field that yields advection is set to drift the sensor platforms under realistic conditions. It has been observed that the flow field is leveraged by the optimal guidance to reduce the mobility cost in both cases of a single sensor and a team of homogeneous

sensors. Simulations with a team of heterogeneous sensors suggest that such a team can reduce the cost of investment with only a minor degradation in the overall performance.

The remainder of the chapter is organized as follows. Section 4.1 states the problem formulation and establishes conditions for the existence of a solution to the problem. Section 4.2 proves the convergence to the exact optimal solution of the approximate optimal solution and introduces a solution method to obtain optimal guidance. Section 4.3 includes the simulation results of multiple parameter studies: a single sensor, a team of homogeneous sensors, and a team of heterogeneous sensors.

4.1 Problem formulation

We now introduce the formulation of the optimization problem. Given the dynamics and initial condition (2.4) of the sensors, the dynamics of the diffusion-advection process (2.18), and the second moment of the initial state noise $w_0(\cdot, \cdot)$, the process noise $w(\cdot, \cdot, t)$, and measurement noise $v(t)$, the problem below yields the optimal guidance for a team of mobile sensors to estimate a 2D diffusion-advection process.

The cost function consists of two parts: one part accounts for reducing the estimation uncertainty (*uncertainty cost*), and the other accounts for the motion of the sensors (*mobility cost*). Note the Riccati operator $\Pi(\cdot)$ in this chapter is the operator $\Pi^e(\cdot)$ in Chapter 2 (the superscript e is dropped for simplicity). The uncertainty cost is the integral of the trace of the covariance operator $\Pi(\cdot)$ over the

horizon $[0, t_f]$, i.e., $\int_0^{t_f} \text{Tr}(\Pi(t))dt$. The mobility cost $J_m(\zeta, p)$ is defined as

$$J_m(\zeta, p) = \int_0^{t_f} h(\zeta(t), t) + g(p(t), t)dt + h_f(\zeta(t_f)). \quad (4.1)$$

Here, $h : \mathbb{R}^n \times [0, t_f] \rightarrow \mathbb{R}^+$ is a continuous function that characterizes the cost associated with the state of the mobile sensors. For example, a hazardous field can be modeled by h , where $h(\zeta(t), t)$ evaluates the exposure of the mobile sensors, which can shorten the sensor's life span. The cost of the guidance is characterized by $g : \mathbb{R}^m \times [0, t_f] \rightarrow \mathbb{R}^+$. For example, quadratic guidance effort is $g(p(t), t) = p^\top(t)\gamma p(t)$, where $\gamma \in \mathbb{R}^{m \times m}$ is symmetric and positive definite. The guidance cost can address limited onboard resources, like fuel or batteries, by treating γ as the penalty coefficient.

The terminal state cost $h_f : \mathbb{R}^n \rightarrow \mathbb{R}^+$ evaluates the cost associated with the terminal state. An exemplary scenario is when the sensors are expected to come close to a set of pre-assigned terminal locations $x_f \in \Omega^{m_s}$, where $h_f(\zeta(t_f)) = |M\zeta(t_f) - x_f|_2^2$. The motion of the sensors follows from the dynamics (2.4), which constrain the optimization. Denote the admissible set of guidance functions as $\mathcal{P} = \{p \in L^2([0, t_f]; P)\}$, where P is the set of admissible guidance (values) defined at the end of Section 2.2.

The optimization problem is formulated as follows:

$$\begin{aligned} & \underset{p \in \mathcal{P}}{\text{minimize}} && \int_0^{t_f} \text{Tr}(\Pi(t)) + h(\zeta(t), t) + g(p(t), t)dt + h_f(\zeta(t_f)) \\ & \text{subject to} && \dot{\zeta}(t) = \alpha\zeta(t) + \beta p(t), \quad \zeta(0) = \zeta_0, \end{aligned} \quad (\text{Pe})$$

where $\Pi(t)$ is given by (2.25) with a given initial condition $\Pi(0) = \Pi_0$. It suffices to search for guidance p that minimizes the cost of (Pe), because the sensor state ζ is entirely determined by guidance p via the sensor dynamics and the given initial condition ζ_0 , which further determines $\Pi(\cdot)$ through (2.25) with a given initial covariance $\Pi(0)$.

A special case is considered in [18] where only a quadratic guidance effort is considered in the mobility cost. Such a formulation applies to the case of limited onboard resources of each mobile sensor when γ is diagonal. It minimizes the Lagrangian function of the optimization problem that minimizes the uncertainty cost subject to the constraints of bounded guidance effort and linear dynamics of the mobile sensors.

The following three assumptions are necessary for the existence of a solution to problem (Pe).

(E9) The set of admissible guidance $P \subset \mathbb{R}^m$ is closed and convex.

(E10) The mappings $h : \mathbb{R}^n \times [0, t_f] \rightarrow \mathbb{R}^+$, $g : \mathbb{R}^m \times [0, t_f] \rightarrow \mathbb{R}^+$, and $h_f : \mathbb{R}^n \rightarrow \mathbb{R}^+$ are continuous. For every $t \in [0, t_f]$, the function $g(p, t)$ is convex about p .

(E11) There exists a constant $d_1 > 0$ with $g(p, t) \geq d_1 |p|_2^2$ for all $(p, t) \in P \times [0, t_f]$.

Assumptions (E9)–(E11) are generally met in applications with real vehicles. Assumption (E9) is satisfied when the values of admissible guidance vary along a continuum. The continuity requirement in assumption (E10) on the cost functions h , g , and h_f is typically satisfied. And the convexity requirement in assumption (E10) and quadratic boundedness from below in assumption (E11) can be met if g

is quadratic in p , e.g., $g(p, t) = p^\top(t)\gamma(t)p(t)$ for a symmetric and positive definite matrix $\gamma(t)$ (which is continuous with respect to t) such that d_1 can be chosen as the minimum eigenvalue of $\gamma(t)$ for $t \in [0, t_f]$ (see [6, Corollary VI.1.6]).

Theorem 4.1. *Consider problem (Pe) and let assumptions (E1)–(E4) and (E9)–(E11) hold. Then problem (Pe) has a solution.*

Proof. See Appendix A.9. □

We use Pontryagin’s minimum principle to characterize an optimal solution of (Pe). Consider the Hamiltonian

$$H(\zeta(t), p(t), \lambda(t), t) = \text{Tr}(\Pi(\zeta, t)) + h(\zeta(t), t) + g(p(t), t) + \lambda^\top(t)(\alpha\zeta(t) + \beta p(t)), \quad (4.2)$$

where $\lambda(t) \in \mathbb{R}^n$ is the costate associated with $\zeta(t)$. The necessary conditions of (local) optimality are as follows:

$$\dot{\zeta}^*(t) = \alpha\zeta^*(t) + \beta p^*(t), \quad (4.3a)$$

$$\zeta^*(0) = \zeta_0, \quad (4.3b)$$

$$\dot{\lambda}^*(t) = -\alpha^\top \lambda^*(t) - \nabla_\zeta h(\zeta^*(t), t) - \nabla_\zeta \text{Tr}(\Pi^*(\zeta^*, t)), \quad (4.3c)$$

$$\lambda^*(t_f) = \nabla_\zeta h_f(\zeta^*(t_f)), \quad (4.3d)$$

$$0 = \nabla_p g(p^*(t), t) + \beta^\top \lambda^*(t), \quad (4.3e)$$

where $\Pi^*(\cdot)$ is evaluated along the optimal system state $\zeta^*(\cdot)$ and we use the first-order necessary condition $\nabla_p H(\zeta^*(t), p^*(t), \lambda^*(t), t) = 0$ in (4.3e) for H to attain its

minimum at $p^*(t)$. The necessary condition (4.3) essentially requires the solution to a two-point boundary value problem, which further requires the derivation of $\nabla_{\zeta}\text{Tr}(\Pi^*(t))$. We refer to a similar derivation in [12], where the gradient of the covariance operator's trace with respect to sensor's guidance is taken. The i th row of $\nabla_{\zeta}\text{Tr}(\Pi^*(t))$, denoted by $[\nabla_{\zeta}\text{Tr}(\Pi^*(t))]_i$, is the partial derivative of $\text{Tr}(\Pi^*(t))$ with respect to the i th element of the state $\zeta^*(t)$ for $i \in \{1, 2, \dots, n\}$. Since trace is a linear operator, we have

$$[\nabla_{\zeta}\text{Tr}(\Pi^*(t))]_i = \frac{\partial\text{Tr}(\Pi^*(t))}{\partial[\zeta(t)]_i} = \text{Tr}\left(\frac{\partial\Pi^*(t)}{\partial[\zeta(t)]_i}\right). \quad (4.4)$$

By the chain rule, (4.4) becomes

$$\text{Tr}\left(\frac{\partial\Pi^*(t)}{\partial[\zeta(t)]_i}\right) = \text{Tr}(D_{\bar{\mathcal{C}}\bar{\mathcal{C}}^*(t)}\Pi^*(t) \circ D_{[\zeta(t)]_i}\bar{\mathcal{C}}\bar{\mathcal{C}}^*(t)), \quad (4.5)$$

where $D_{\bar{\mathcal{C}}\bar{\mathcal{C}}^*(t)}\Pi(t)$ is the Fréchet derivative of the Riccati operator with respect to the composite output operator $\bar{\mathcal{C}}\bar{\mathcal{C}}^*(t)$ and $D_{[\zeta(t)]_i}\bar{\mathcal{C}}\bar{\mathcal{C}}^*(t)$ is the Fréchet derivative of $\bar{\mathcal{C}}\bar{\mathcal{C}}^*(t)$ with respect to $[\zeta(t)]_i$. Denote $D_{\bar{\mathcal{C}}\bar{\mathcal{C}}^*(t)}\Pi^*(t)$ by $\Lambda(t)$ and, by [12, Theorem 5.5], $\Lambda(t)$ is the unique solution to

$$\begin{aligned} \Lambda h(t) = & - \int_0^t \mathcal{S}(t-s)((\Lambda h)(s)\bar{\mathcal{C}}\bar{\mathcal{C}}^*(s)\Pi(s) + \Pi(s)\bar{\mathcal{C}}\bar{\mathcal{C}}^*(s)(\Lambda h)(s) \\ & + \Pi(s)h(s)\Pi(s))\mathcal{S}^*(t-s)ds, \end{aligned} \quad (4.6)$$

$$\Lambda(0) = 0, \quad (4.7)$$

for all $h \in C([0, t_f], \mathcal{J}_1(\mathcal{H}))$ and all $t \in [0, t_f]$. The approximated version of problem (Pe) and the two-point boundary value problem (4.3) will be applied to solve for optimal guidance in Section 4.2.

4.2 Solving optimal guidance using approximation

Since the infinite-dimensional terms in (Pe) have to be approximated for computation as introduced in Section 2.5, we arrive at the approximated problem:

$$\begin{aligned} & \underset{p_N \in \mathcal{P}}{\text{minimize}} && \int_0^{t_f} \text{Tr}(\Pi_N(t)) + h(\zeta(t), t) + g(p_N(t), t) dt + h_f(\zeta(t_f)) \\ & \text{subject to} && \dot{\zeta}(t) = \alpha\zeta(t) + \beta p_N(t), \quad \zeta(0) = \zeta_0, \end{aligned} \tag{APe}$$

where $\Pi_N(t)$ is obtained through (2.38). It suffices to search for guidance p_N , because both the sensor state ζ and the approximated estimation covariance Π_N are fully determined by the guidance and initial conditions. The existence of a solution of problem (APe) is guaranteed in Theorem 4.2.

Theorem 4.2. *Consider problem (APe) and let assumptions (E5)–(E11) hold. Then (APe) has a solution.*

Proof. See Appendix A.10. □

Solving problem (APe) provides a candidate solution, denoted by p_N^* , where N is the dimension of the approximation. The candidate p_N^* may not equal the exact optimal solution, denoted by p^* , of the original problem (Pe). However, as we show in the following theorem, the candidate p_N^* yields the optimal value of (APe)

arbitrarily close to the one of (Pe), as the dimension N goes to infinity. Moreover, when p_N^* is evaluated in the original problem (Pe), the resulting cost is arbitrarily close to the optimal cost of (Pe).

Before we state this convergence result, we introduce an assumption on the set of admissible guidance functions.

(E12) There exist $p_{\max} > 0$ and $a_{\max} > 0$ such that the set of admissible guidance is $\mathcal{P}(p_{\max}, a_{\max}) = \{p \in C([0, t_f]; P) : |p(t)| \text{ is uniformly bounded by } p_{\max} \text{ and } |p(t_1) - p(t_2)| \leq a_{\max}|t_1 - t_2|, \forall t_1, t_2 \in [0, t_f]\}$.

Notice that the set $\mathcal{P}(p_{\max}, a_{\max})$ is sequentially compact, due to the Arzelà-Ascoli Theorem [67], since the guidance functions in $\mathcal{P}(p_{\max}, a_{\max})$ are uniformly equicontinuous and uniformly bounded. The parameters p_{\max} and a_{\max} may be determined by the vehicles carrying sensors. For example, p_{\max} and a_{\max} refer to the maximum speed and maximum acceleration, respectively, in the case of single integrator dynamics where p is the velocity command.

Theorem 4.3. *Consider problem (Pe) and its finite-dimensional approximation (APe). Let assumptions (E4)–(E12) hold and let p^* and p_N^* denote the optimal guidance of (Pe) and (APe), respectively. Then*

$$\lim_{N \rightarrow \infty} |J_{(\text{APe})}^*(p_N^*) - J_{(\text{Pe})}^*(p^*)| = 0. \quad (4.8)$$

Furthermore, the cost function of (Pe) evaluated at the guidance p_N^ converges to*

the optimal cost of (Pe)

$$\lim_{N \rightarrow \infty} |J_{(\text{Pe})}(p_N^*) - J_{(\text{Pe})}^*(p^*)| = 0. \quad (4.9)$$

Proof. See Appendix A.11. □

Remark 4.1. *Two implications follow from the convergence result in Theorem 4.3. First, the convergence in (4.8) affirms the usage of approximation since the optimal cost of the approximate problem (APe) gets arbitrarily close to that of the exact problem (Pe) as the approximation gets finer. Second, the convergence in (4.9) affirms the optimal guidance computed using approximation. When the approximate optimal guidance is evaluated by the cost function of the original problem (Pe), the resulting value is arbitrarily close to the optimal cost of (Pe) as the approximation gets finer. In other words, the approximate optimal guidance is a sufficiently accurate proxy for the exact optimal guidance.*

Remark 4.2. *Assumptions are made for the existence of a solution to problem (Pe) ((E9)–(E11)), well-posedness of the Riccati operators ((E1)–(E4)), and the convergence of the approximated solution ((E5)–(E8) and (E12)). Assumptions (E9)–(E11) are regarding the mobility cost and the set of admissible guidance, which are generally satisfied in engineering applications (see the discussion before Theorem 3.1). The rest of the assumptions are typically satisfied with the diffusion-advection equation and Galerkin approximation (using eigenfunctions of the Laplacian operator). Details of how to check similar assumptions for the dual control problem can be found in Section 3.2.1.*

The convergence stated in Theorem 4.3 is established based on several earlier stated results, including

1. the output operator's continuity with respect to location (assumption (E4)), which leads to the continuity of the uncertainty cost with respect to sensor state (Lemma 2.5);
2. existence of the Riccati operator (Lemma 2.4) and convergence of its approximation (Lemma 2.8); and
3. sequential compactness of the set of admissible guidance functions (assumption (E12)), which leads to the continuity of the cost function with respect to guidance (Lemma A.2 in the Appendix).

Notice that these key results, in an analogous manner, are also required in [96] when establishing the convergence to the exact optimal sensor locations of the approximate optimal locations [96, Theorem 4.3], i.e.,

1. continuity with respect to location and compactness of the output operator (dual of [57, Theorem 2.10]), which lead to continuity of the Riccati operator with respect to sensor locations [96, Theorem 4.1];
2. existence of the Riccati operator [96, Theorem 2.5] and the convergence of its approximation [96, Theorem 4.2]; and
3. sequential compactness of the set of admissible locations, which is inherited from the setting that the spatial domain is closed and bounded in a finite-dimensional space.

To compute an optimal solution to problem (A_{Pe}), we use Pontryagin’s minimum principle, which introduces a Hamiltonian function that has the same form as (4.2) except that the covariance operator $\Pi(t)$ in (4.2) is replaced by its approximation $\Pi_N(t)$. And correspondingly, the resulting two-point boundary value problem has the same form as (4.3) except for $\Pi(t)$ being replaced by $\Pi_N(t)$.

Remark 4.3. *The optimal sensor trajectory ζ^* steered by the optimal guidance p^* may be used as the reference trajectory tracked by the vehicle’s lower-level control. Although collision avoidance among the sensors is not discussed in this chapter, it can be incorporated into the lower-level control using numerous methods in the existing literature, e.g., [87] and the references therein.*

4.3 Simulation results

This section shows the simulation results obtained using the solution method proposed in Section 4.2. Comparison and analysis are made regarding the performance of the mobile sensor(s) under optimal guidance for the case of a single sensor, a team of homogeneous sensors, and a team of heterogeneous sensors.

We use the Galerkin scheme to approximate the infinite-dimensional terms. The orthonormal set of eigenfunctions of the Laplacian operator ∇^2 (with zero Dirichlet boundary condition) over the spatial domain $\Omega = [0, 1] \times [0, 1]$ is $\phi_{i,j}(x, y) = 2 \sin(\pi i x) \sin(\pi j y)$. With a single index $k = (i - 1)N + j$ such that $\phi_k = \phi_{i,j}$, the set of eigenfunctions $\{\phi_k\}_{k=1}^{N^2}$ spans an N^2 -dimensional space that is previously denoted by \mathcal{H}_N . For the orthogonal projection $P_N : \mathcal{H} \rightarrow \mathcal{H}_N$, it follows that $P_N^* = P_N$ and

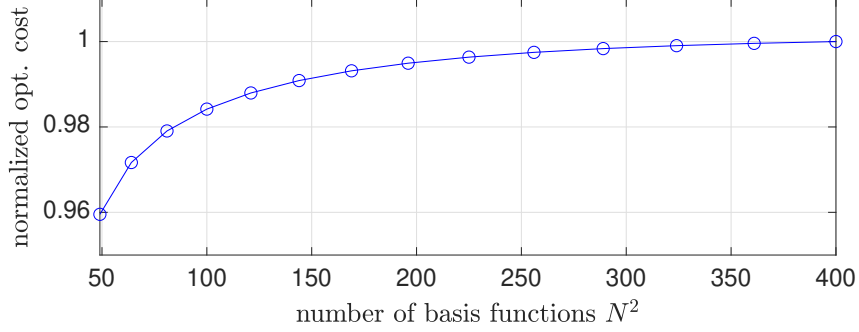


Figure 4.1: Approximate optimal costs $J_{(\text{APe})}^*(p_N^*)$ normalized with respect to the optimal cost for $N^2 = 400$.

$P_N^* P_N \rightarrow I$ strongly. And the assumption (2.42) in Theorem 4.2 holds uniformly for all $t \in [0, t_f]$ as $N \rightarrow \infty$ [11]. We set p_{\max} and a_{\max} to be sufficiently large so that the solution is in the set $\mathcal{P}(p_{\max}, a_{\max})$. We plot the optimal cost $J_{(\text{APe})}^*(p_N^*)$ for N from 7 to 20, as shown in Fig. 4.1. The optimal cost shows a tendency of exponential convergence as we increase the number of basis functions. And we choose $N = 12$ in the rest of the simulations since it is the smallest dimension with the optimal cost within 1% of the optimal cost evaluated with the maximum dimension $N = 20$ in the trials.

The parameters in the simulation are $t_f = 2$ and $a = 0.01$. We use single integrator dynamics for each sensor. The state ζ is the 2D location of the sensors and guidance p is the 2D velocity command. In some applications, the flow field \mathbf{v} of the diffusion-advection process can affect the mobile sensors. For example, surface vehicles that measure the concentration of certain chemical substances or biological entities in a water body are subject to the movement of the water. Considering this realistic condition, we append the flow field $\mathbf{v} = [0.1, -0.1]^\top$ of advection to the right-hand side of the single integrator dynamics, which means the sensors will

drift along the flow when zero guidance is implemented. The previous statements and results on the existence of solution and convergence of the approximate solution still hold within this setting. The optimization will find optimal guidance subject to (or possibly taking advantage of) this flow field. The sensor has the square-shaped average output kernel (see (2.20)) with $r_i = 0.05$, in which case its footprint only covers 1% of the domain in area. We set $g(p(t)) = \gamma p^\top(t)p(t)/2$ and $h(\zeta(t), t) = h_f(\zeta(t_f)) = 0$ as the mobility cost, which is simply the quadratic guidance effort for $\gamma > 0$.

Assumption (E4) holds for the choice of output operator (see Remark 2.1). With the Galerkin approximation using the orthonormal eigenfunctions $\{\phi_k\}_{k=1}^{N^2}$, it can be shown that assumption (E8) holds for $l_N(\cdot) = N^2 l(\cdot)$. Assumptions (E5)–(E7) hold with $q = 1$ under the Galerkin approximation with aforementioned basis functions $\{\phi\}_{k=1}^{N^2}$ [11]. Assumptions (E9)–(E11) and (E12) hold for the choice of functions in the mobility cost and parameters of the set of admissible guidance functions, respectively.

To evaluate the performance of the optimal guidance in simulation, we set the deterministic portion of the initial condition of the PDE to zero, i.e., $\hat{Z}_0 = 0$, which excludes the bias from choosing a particular non-zero one. The stochastic portion of the initial condition w_0 is chosen as a zero-mean Gaussian process with non-stationary kernel function $k_0 : \Omega \times \Omega \rightarrow \mathbb{R}^+$ such that

$$k_0(x_1, x_2) = 9 \exp\left(-\frac{|x_1 - x_2|_2^2}{200} - \frac{|x_1 - x_0|_2^2}{10} - \frac{|x_2 - x_0|_2^2}{10}\right), \quad (4.10)$$

where $x_0 \in \Omega$ represents the peak of the uncertainty in the domain and we set $x_0 = [0.75, 0.25]^\top$. For the state noise $w(t)$, we use a zero-mean Gaussian process with a homogeneous kernel function $k : \Omega \times \Omega \rightarrow \mathbb{R}^+$ such that

$$k(x_1, x_2) = \exp\left(-\frac{|x_1 - x_2|_2^2}{2000}\right). \quad (4.11)$$

We use the forward-backward sweep method [53] to solve the two-point boundary problem (4.3) (with Π replaced by Π_N) and subsequently compute the optimal guidance. A fixed-step length of 0.01 and a relative tolerance of 1×10^{-6} are applied in the iterative procedure. The forward propagation of (4.3a) and (2.38) and the backward propagation of (4.3c) are computed via the Runge-Kutta method.

4.3.1 Single sensor results

Two important parameters in the problem setting are the sensor noise variance R and mobility penalty γ . Smaller R yields higher sensor quality, whereas smaller γ yields better mobility of the vehicle. For example, if γ is the mass of the vehicle, then the guidance effort is the kinetic energy of the vehicle. These parameters affect the performance of the estimation as shown next. In this simulation, the sensor is initiated at $\zeta_0 = [0.3, 0.1]^\top$. Monte Carlo simulations of 100 trials compare the optimal guidance with three naive guidance policies whose corresponding sensor trajectories are as follows:

1. Naive 1: crossing the domain by reaching the opposite of the initial location within domain at $[0.7, 0.9]^\top$ at a constant speed.

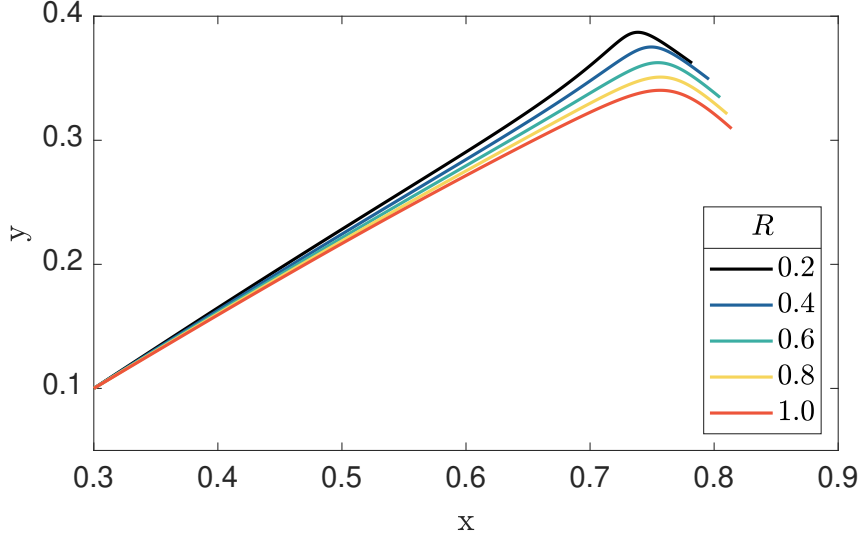


Figure 4.2: Optimal trajectories for various values of the sensor noise variance R

2. Naive 2: reaching the peak of the initial uncertainty x_0 at a constant speed.
3. Naive 3: circulating the domain in the clockwise direction with center $[0.5, 0.5]^\top$, radius $1/\sqrt{5}$, and angular speed π rad/s.

A stationary sensor is also included for comparison whose guidance, named null guidance, merely compensates for the flow field \mathbf{v} .

First, hold either R or γ fixed and vary the other to observe the variation of the optimal trajectory. Fig. 4.2 displays the trajectories when $\gamma = 0.5$ and R varies from 0.2 to 1. The sensor maneuvers less as R increases, which indicates the optimal guidance's compensation for deteriorating sensor quality by moving it closer to the peak of the initial uncertainty at $x_0 = [0.75, 0.25]^\top$.

For the Monte Carlo trials, the mean and standard deviation of the terminal estimation error's norm are shown in Fig. 4.3. The optimal guidance exhibits smaller mean and variance of terminal estimation error over the naive guidance policies and the null guidance at each evaluated R . Notice that the advantage is preserved when

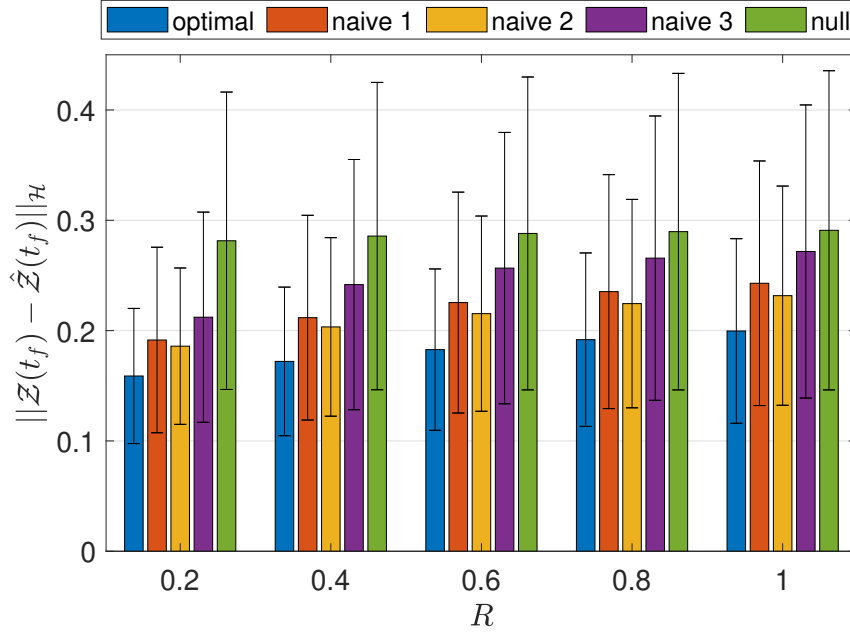


Figure 4.3: Norm of the terminal estimation error for various values of sensor noise variance R . The color bar shows the mean value; the error bar shows the standard deviation. The value of mobility penalty γ is fixed at 0.5, whereas the sensor noise’s variance R takes values in the set $\{0.2, 0.4, 0.6, 0.8, 1\}$.

the sensor quality deteriorates as R increases.

Fig. 4.4 displays the trajectories when $R = 0.2$ and γ varies from 0.5 to 2.5. A bigger value of γ suppresses the guidance effort and hence reduces the range of the sensor’s motion. The results of Monte Carlo trials when γ varies are shown in Fig. 4.5. Notice that the mean and standard deviation are invariant for each naive guidance policy and the null guidance among the varying γ since the sensor trajectory steered by each of these guidance policies is independent of γ . The optimal guidance shows its advantage over the other guidance policies at a relatively smaller values of γ , e.g., at 0.5 and 1. This advantage is gradually lost as γ takes relatively bigger values, e.g., 2 and 2.5. This comparison suggests that the optimal guidance may not be the best option for vehicles with large γ (e.g., when the vehicle is heavy),

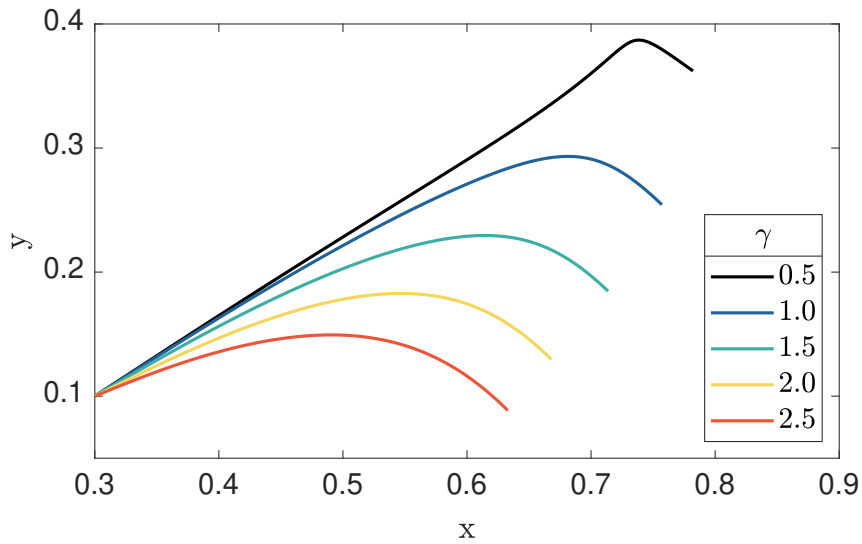


Figure 4.4: Optimal trajectories for various values of the mobility penalty γ

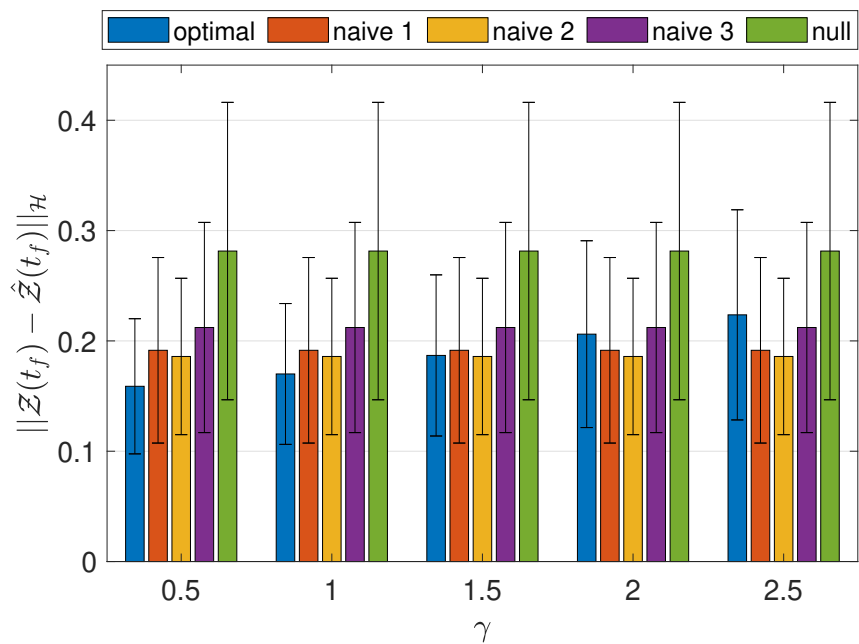


Figure 4.5: Norm of the terminal estimation error for various values of the mobility penalty γ . The color bar shows the mean value; the error bar shows the standard deviation. The value of sensor noise's variance R is fixed at 0.2, whereas the mobility penalty γ takes values in the set $\{0.5, 1, 1.5, 2, 2.5\}$.

despite the fact that the guidance is still optimal for the chosen cost function in simulation.

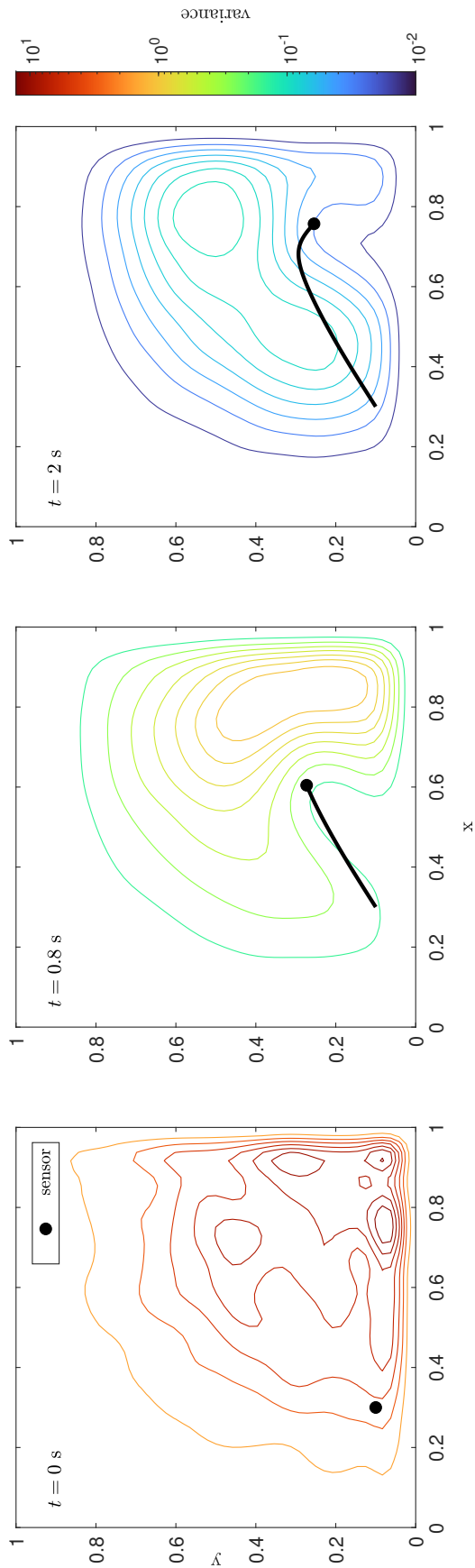


Figure 4.6: Trajectory of the sensor following the optimal guidance. The contours represent the level curves of pointwise variance of the estimation error on a uniform grid within the domain, computed from the Monte Carlo simulations.

Fig. 4.6 shows the snapshots of the sensor trajectory under the optimal guidance and contour plot of the pointwise variance of the estimation error among the Monte Carlo trials with $\gamma = 1$ and $R = 0.2$. The pointwise variance is computed at each point in a uniform grid of 144×144 sampling points in the domain Ω . The sensor is steered quickly towards the area with higher uncertainty near $[0.75, 0.25]^\top$ (see the snapshot at $t = 0.8$ s). Eventually, the sensor starts to drift along the flow field $\mathbf{v} = [0.1, -0.1]^\top$ (see the snapshot at $t = 2$ s). That sensor can effectively reduce the uncertainty of the estimation error as can be observed from the drop in the pointwise variance in the sensor's footprint. Note that the zero Dirichlet boundary condition also contributes to reducing the uncertainty of the estimation error via diffusion and advection.

4.3.2 Team of homogeneous sensors

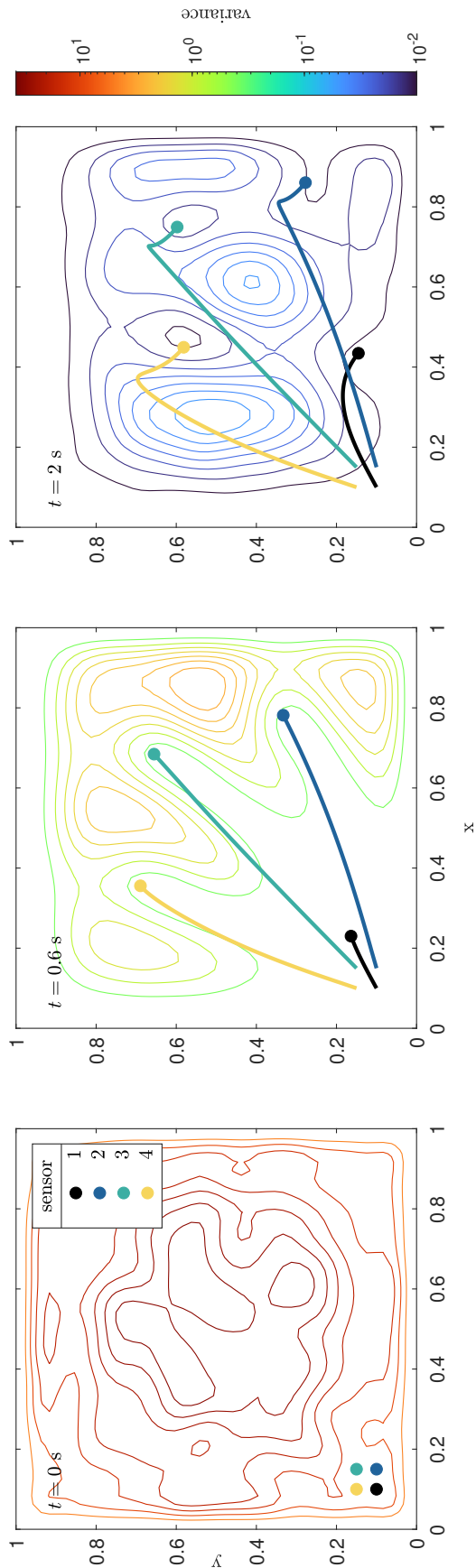


Figure 4.7: Trajectories of multiple homogeneous sensors following the optimal guidance. The contours represent the level curves of pointwise variance of the estimation error on a uniform grid within the domain.

To demonstrate the framework’s capability in guiding a team of multiple sensors, we simulate four homogeneous sensors ($R = 0.2$, $\gamma = 0.5$). To adapt to a total of four sensors, the kernel functions for w_0 and w are enlarged four times in (4.10) and (4.11), respectively, and the peak of the initial uncertainty is set to the center $[0.5, 0.5]^\top$. The other settings are identical to those in Section 4.3.1. Fig. 4.7 shows the snapshots of the sensors’ trajectories under the optimal guidance and contour plot of the pointwise variance of the estimation error among the Monte Carlo trials. Similar to the case of a single sensor in Fig. 4.6, the sensors quickly sweep the peak of the initial uncertainty in the center and expand to cover the domain (see the snapshot at $t = 0.6$ s). The pointwise variance drops along sensors’ footprints. The sensors essentially drift along the flow to reduce the guidance effort (see the snapshot at $t = 2$ s).

4.3.3 Team of heterogeneous sensors

The parameters R and γ essentially relate to operational planning: one may invest more for better sensor quality or a swifter vehicle. Consequently, one would necessarily invest more for a team of superior mobile sensors (e.g., $R = 0.2$ and $\gamma = 0.5$) than a team of poor mobile sensors (e.g., $R = 1$ and $\gamma = 2.5$). The latter has five times as much sensor noise (in terms of standard deviation) and five times the mobility penalty as the former. One may balance the conflicting needs of performance and investment by deploying a team of heterogeneous sensors, i.e., a mixed team of superior and poor sensors.

The following simulation compares the performance of a team of heterogeneous sensors (including m_p poor sensors and $8 - m_p$ superior sensors, for m_p in the range of $\{1, 2, \dots, 7\}$) with that of homogeneous teams ($m_p = 0$ for superior sensors only and $m_p = 8$ for poor sensors only). The sensors are introduced in the lower left corner of the domain and the coordinates are shown in Table 4.1. To adapt to a total of eight sensors, the kernel functions for w_0 and w are enlarged eight times in (4.10) and (4.11), respectively, and the peak of the initial uncertainty is set to the center of the domain at $[0.5, 0.5]^\top$. Fig. 4.8 shows the normalized optimal total cost and uncertainty cost for the heterogeneous team compared with homogeneous teams of superior and poor sensors. The performance deteriorates judged by the rising costs as the number of poor sensors increases in team. However, the degradation of the heterogeneous team (when $m_p \leq 5$) is maintained within 20% of the superior team in both the total cost and uncertainty cost, which indicates the cost effectiveness of the heterogeneous team since the investment reduces linearly as m_p increases.

sensor	1	2	3	4	5	6	7	8
x	0.1	0.15	0.2	0.1	0.15	0.2	0.1	0.15
y	0.1	0.1	0.1	0.15	0.15	0.15	0.2	0.2

Table 4.1: Coordinates of initial sensor locations

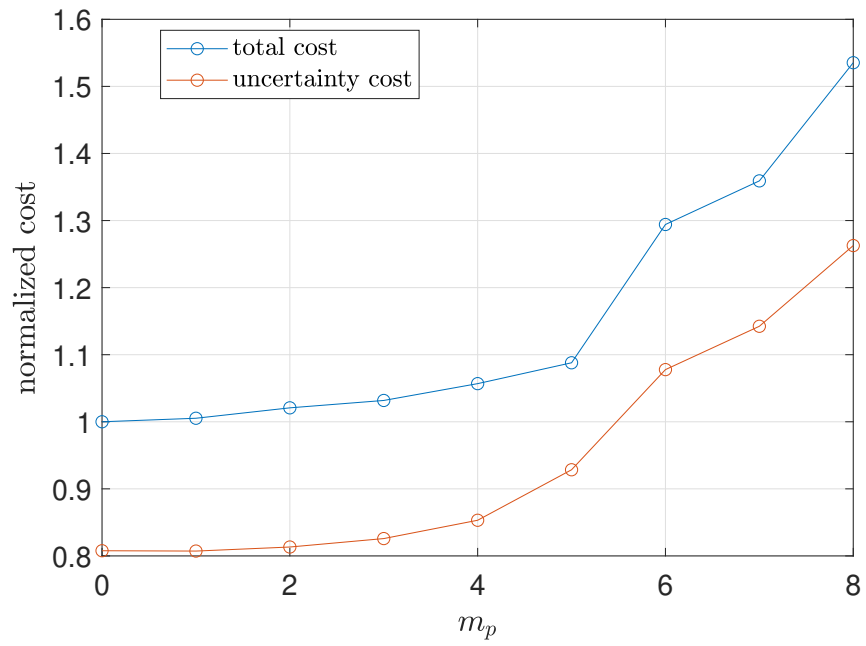


Figure 4.8: Normalized optimal total cost and uncertainty cost of a heterogeneous team with m_p poor sensors and $8 - m_p$ superior sensors.

Chapter 5: Cooperative estimation and control: simulations and experiments

In this chapter, we propose a framework for controlling a 2D diffusion process with mobile collocated sensors and actuators. The framework has been demonstrated in experiments on an outdoor multi-quadrotor testbed.

We start with a quick review of the background and notation for this chapter. Consider a team of m mobile agents in a 2D domain $\Omega = [0, l] \times [0, l]$, where each agent carries an actuator and a sensor. The words vehicle, actuator, and sensor all refer to a mobile agent in this chapter although their appearance depends on the context. We model each agent's motion by a single integrator, i.e.,

$$\dot{\xi}_i(t) = v_i(t), \tag{5.1}$$

where $\xi_i(t) \in \Omega$ and $v_i(t) \in V \subseteq \mathbb{R}^2$ contain the 2D position and velocity of agent i for all t . The variable v_i serves as the guidance that steers the agent. Concatenating ξ_i and v_i vertically for $i \in \{1, 2, \dots, m\}$ to get $\xi \in \Omega^m$ and $v \in V^m$, respectively, we have

$$\dot{\xi}(t) = v(t). \tag{5.2}$$

With a slight abuse of notation, we use V to denote the feasible set of velocity for all agents, i.e., $v(t) \in V \subseteq \mathbb{R}^{2m}$. The single integrator model is taken for its simple form although complicated agent dynamics can be applied. The optimal trajectory associated with the dynamics (5.2) can serve the reference signal for tracking by lower-level control of the vehicles if it does not match the vehicles' exact dynamics.

We use a 2D diffusion equation to model the spatiotemporal processes that is controlled by the mobile actuators

$$\frac{\partial z(x, y, t)}{\partial t} = a \nabla^2 z(x, y, t) + \sum_{i=1}^m \mathcal{B}_i(x, y) u_i(t) + w(x, y, t), \quad (5.3)$$

$$z(\cdot, \cdot, t)|_{\partial\Omega} = 0, \quad (5.4)$$

$$z(x, y, 0) = \hat{z}_0(x, y) + \omega_0(x, y), \quad (5.5)$$

where $z(\cdot, \cdot, t)$ is the state at time t and u_i is the control implemented by actuator i with its actuation characterized spatially by $\mathcal{B}_i(\cdot, \cdot)$. The initial state $z(\cdot, \cdot, 0)$ has nominal value \hat{z}_0 with initial uncertainty ω_0 . The term w characterizes the state noise and model uncertainties. The parameter a is the diffusivity, which characterizes how fast the state z diffuses. The state z lives in the state space $L^2(\Omega)$. The Dirichlet boundary condition (BC) is considered in (5.4), where the boundary of the domain serves the role of (passive) actuation and will eventually draw the state to zero when the actuators implement zero control. The Neumann BC is also considered in this chapter, where

$$\frac{\partial z(\cdot, \cdot, t)}{\partial \mathbf{n}}|_{\partial\Omega} = 0. \quad (5.6)$$

In reality, the Dirichlet and Neumann boundary conditions correspond to actuation and insulation at the boundary. In the case of oil spills, filters and booms at the boundary of the domain can be modelled by these two types of boundary conditions, respectively.

Depending on the model's preciseness, the input operator \mathcal{B}_i can have different shapes. For example, a Gaussian function with its center at actuator i 's location (x_i, y_i) with a bounded support is a natural way to modeling the effect that the actuation concentrates at the location of release and spreads to its surroundings with exponentially decaying magnitude:

$$\mathcal{B}_i(x, y) = \begin{cases} \frac{1}{2\pi\sigma_i^2} \exp\left(-\frac{(x-x_i)^2}{\sigma_i^2} - \frac{(y-y_i)^2}{\sigma_i^2}\right), & \text{if } |x-x_i| \leq \sigma_i \text{ and } |y-y_i| \leq \sigma_i \\ 0, & \text{otherwise.} \end{cases} \quad (5.7)$$

A simplification of the Gaussian function assumes that the actuation distributes uniformly in a square (or, more generally, a rectangle)

$$\mathcal{B}_i(x, y) = \begin{cases} \frac{1}{4\sigma_i^2}, & \text{if } |x-x_i| \leq \sigma_i \text{ and } |y-y_i| \leq \sigma_i \\ 0, & \text{otherwise.} \end{cases} \quad (5.8)$$

In this case the input operator can approximate the point actuation when $\sigma_i \rightarrow 0$ [85, Remark 3], that is, a Dirac delta function that is nonzero at the location of the actuator i .

Recall that the each pair of sensor and actuator are collocated. The measure-

ment by sensor i depends on its location such that

$$y_i(t) = \iint_{\Omega} \mathcal{C}_i(x, y) z(x, y, t) dx dy + \nu_i(t), \quad (5.9)$$

where \mathcal{C}_i is the measurement kernel of sensor i and ν_i is the sensor noise. The kernel may have various shapes, e.g., an interval average kernel that corresponds to a camera-type sensor, where the average measurement over a $2r_i \times 2r_i$ area is taken

$$\mathcal{C}_i(x, y) = \begin{cases} \frac{1}{4r_i^2}, & \text{if } |x - x_i| \leq r_i \text{ and } |y - y_i| \leq r_i \\ 0, & \text{otherwise;} \end{cases} \quad (5.10)$$

or a pointwise kernel that corresponds to a single-pixel sensor

$$\mathcal{C}_i(x, y) = \delta(x - x_i) \delta(y - y_i). \quad (5.11)$$

The sensors could be mobile by themselves, in which case separately designed guidance strategy can be implemented, e.g., the guidance design in Chapter 4.

We denote by $y(t)$ the collection of all sensors' measurements at time t , i.e.,

$$y(t) = [y_1(t), \dots, y_m(t)]^\top. \quad (5.12)$$

The dynamics of PDE (5.3)–(5.5) and the observation equation (5.12) can be

conveniently characterized by the abstract linear system:

$$\dot{\mathcal{Z}}(t) = \mathcal{A}\mathcal{Z}(t) + \mathcal{B}(\xi(t))u(t) + \omega(t), \quad (5.13)$$

$$\mathcal{Z}(0) = \hat{\mathcal{Z}}_0 + \omega_0, \quad (5.14)$$

$$y(t) = \mathcal{C}^*(\xi(t))\mathcal{Z}(t) + \nu(t), \quad (5.15)$$

where $\mathcal{Z}(\cdot)$ is the state within state space $\mathcal{H} = L^2(\Omega)$ and $u(\cdot)$ is the control within the control space $u(t) \in U \subseteq \mathbb{R}^m$ for $t \in [0, t_f]$. In the case of diffusion process (5.3), for $\phi \in \mathcal{H}$, $(\mathcal{A}\phi)(x, y) = a\nabla^2\phi(x, y)$, where the operator \mathcal{A} has domain $\text{Dom}(\mathcal{A}) = H^2(\Omega) \cap H_0^1(\Omega)$ (see Chapter 3). For any $\xi(t) \in \Omega^m$ and all t , the input operator $\mathcal{B}(\xi(t)) \in \mathcal{L}(U; \mathcal{H})$ is a function of the actuator locations such that $\mathcal{B}(\xi(t)) = [\mathcal{B}_1(\xi_1(t)), \dots, \mathcal{B}_m(\xi_m(t))]^\top$, where $\mathcal{B}_i(\xi_i(t)) \in L^2(\Omega)$ for all $i \in \{1, 2, \dots, m\}$. The noise ω_0 , $\omega(t)$, and $\nu(t)$ are zero-mean Gaussian with appropriate dimensions and covariance Π_0° , \mathcal{Q} , and R , respectively. Moreover, they are mutually independent for all t .

The output operator $\mathcal{C}^*(\xi(t)) \in \mathcal{L}(\mathcal{H}; \mathbb{R}^m)$ is defined by

$$\mathcal{C}^*(\xi(t))\phi = [\mathcal{C}_1^*(\xi_1(t))\phi, \dots, \mathcal{C}_m^*(\xi_m(t))\phi] \quad (5.16)$$

for $\phi \in L^2(\Omega)$, where \mathcal{C}_i^* is the adjoint of \mathcal{C}_i such that

$$\mathcal{C}_i^*\phi = \iint_{\Omega} \mathcal{C}_i(x, y)\phi(x, y)dx dy, \quad i \in \{1, 2, \dots, m\}. \quad (5.17)$$

Due to the infinite-dimensional nature of (5.13), approximations to (5.13) and (5.15) permit numerical computation. Consider a finite-dimensional subspace $\mathcal{H}_N \subset \mathcal{H}$ with dimension N . The inner product and norm of \mathcal{H}_N are inherited from that of \mathcal{H} . Let $P_N : \mathcal{H} \rightarrow \mathcal{H}_N$ denote the orthogonal projection of \mathcal{H} onto \mathcal{H}_N . We use the Galerkin scheme with the \mathcal{H}_N spanned by the eigenfunctions $\phi_{ij}(x, y) = 2 \sin(\pi ix/l) \sin(\pi jy/l)/l$ of the Laplacian operator ∇^2 with Dirichlet BC for $i, j \in \{1, 2, \dots, N\}$ (for Neumann BC, the eigenfunctions for approximation are $\psi_{i,j}(x, y) = 2 \cos(\pi ix/l) \cos(\pi jy/l)/l$ for $i, j \in \{0, 1, \dots, N - 1\}$). Let $Z_N(t) = P_N \mathcal{Z}(t)$ denote the finite-dimensional approximation of $\mathcal{Z}(t)$. The finite-dimensional approximations of (5.13)–(5.15) are

$$\dot{Z}_N(t) = A_N Z_N(t) + B_N(\xi(t))u(t) + \omega_N(t), \quad (5.18)$$

$$Z_N(0) = P_N(\hat{\mathcal{Z}}_0 + \omega_0), \quad (5.19)$$

$$y_N(t) = C_N^*(\xi(t))Z_N(t) + \nu(t), \quad (5.20)$$

where $A_N \in \mathcal{L}(\mathcal{H}_N)$, $B_N(\xi(t)) \in \mathcal{L}(U; \mathcal{H}_N)$, and $C_N^*(\xi(t))$ are approximations of \mathcal{A} , $\mathcal{B}(\xi(t))$, and $\mathcal{C}^*(\xi(t))$, respectively, for all $\xi(t) \in \Omega^m$ and all t . Note that the measurement $y_N \in \mathbb{R}^m$. The noise $\omega_N(t)$ and its covariance Q_N are the finite-dimensional approximations of $\omega(t)$ and \mathcal{Q} , respectively. Since the actuator state $\xi(t)$ is a function of time t , we sometimes use $B_N(t)$ and $C_N^*(t)$ for brevity.

Our formulation will be based on the finite-dimensional system (5.18)–(5.20). This is known as early-lumping [56], where the infinite-dimensional system is approximated, and subsequently the controller is designed. The opposite is late-lumping,

where the controller design refers to the original system, and approximations only happen at the stage of computation, e.g., see Chapter 3.

We use the Kalman filter to reconstruct the state Z_N using sensor measurements y_N :

$$\dot{\hat{Z}}_N(t) = A_N \hat{Z}_N(t) + \Pi_N^e(t) C_N(t) R^{-1} (y(t) - \hat{y}_N(t)), \quad (5.21)$$

$$\hat{Z}_N(0) = \hat{Z}_{N,0}, \quad (5.22)$$

$$\hat{y}_N(t) = C_N^*(t) \hat{Z}_N(t), \quad (5.23)$$

where \hat{Z}_N is the estimated state with initial value $\hat{Z}_{N,0} = P_N \hat{Z}_0$, and $\Pi_N^e \in \mathcal{L}(\mathcal{H}_N)$ is the covariance of the estimate \hat{Z}_N which follows the Riccati equation

$$\dot{\Pi}_N^e(t) = A_N \Pi_N^e(t) + \Pi_N^e(t) A_N^* + Q_N(t) - \Pi_N^e(t) C_N(t) R^{-1} C_N^*(t) \Pi_N^e(t). \quad (5.24)$$

The initial value of $\Pi_N^e(0)$ is the approximated covariance $\Pi^e(0)$ of the initial state noise ω_0 .

5.1 Cooperative estimation and control framework

We propose a framework for a team of collocated mobile sensors and actuators to estimate and control a 2D diffusion process. We use the Kalman filter to reconstruct the state information using sensor measurements. The reconstructed state is fed into an optimization problem that solves the actuation and guidance of the actuators. We first introduce the optimization problem below and then show how

it is incorporated into the framework.

The goal of optimization is to plan the actuator guidance and actuation so that the magnitude of the PDE state reduces more quickly than by diffusion alone. First, define the admissible set of guidance and actuation functions such that $v(\cdot) \in \mathcal{V} = L^2([0, t_f]; V)$ and $u(\cdot) \in \mathcal{U} = L^2([0, t_f]; U)$. The cost of controlling the PDE state, named PDE cost, is the sum of quadratic costs of the state and actuation:

$$\int_0^{t_f} \langle Z_N(t), \kappa Z_N(t) \rangle + u(t)^\top \gamma u(t) dt + \langle Z_N(t_f), \kappa_f Z_N(t_f) \rangle. \quad (5.25)$$

Here, $\langle \cdot, \cdot \rangle$ denotes the inner product on \mathcal{H}_N ; κ and $\kappa_f \in \mathcal{L}(\mathcal{H}_N)$ are nonnegative and self-adjoint and $\gamma \in \mathbb{R}^{m \times m}$ is symmetric and positive definite. The PDE cost penalizes the magnitude of the state while restricting the total weighted quadratic actuation. Another term we consider in the cost function is the mobility cost:

$$\int_0^{t_f} v(t)^\top q v(t) dt, \quad (5.26)$$

where $q \in \mathbb{R}^{2m \times 2m}$ is symmetric and positive definite. The mobility cost is a weighted quadratic function of the guidance; it may be interpreted as the guidance effort.

The constraints for planning include the deterministic dynamics of the PDE and the dynamics of the mobile actuators. The two dynamics are coupled by the input operator $B_N(\xi(\cdot))$, which is a function of the actuator state ξ . The constraints also include physical limitations of the actuators and their carrying vehicles, i.e.,

each actuator has its actuation limited to an interval

$$-u_{\max} \leq u_i(t) \leq 0, \quad (5.27)$$

and the speed of each vehicle is bounded

$$\|v_i(t)\|_2 \leq v_{\max} \quad (5.28)$$

for $i \in \{1, 2, \dots, m\}$, where u_{\max} and v_{\max} are positive and correspond to the maximum actuation and maximum speed, respectively. Summarizing (5.25)–(5.28), we obtain the following problem formulation:

$$\begin{aligned} & \underset{u \in \mathcal{U}, v \in \mathcal{V}}{\text{minimize}} && \int_0^{t_f} \langle Z_N(t), \kappa Z_N(t) \rangle + u(t)^\top \gamma u(t) + v(t)^\top q v(t) dt + \langle Z_N(t_f), \kappa_f Z_N(t_f) \rangle \\ & \text{subject to} && \dot{Z}_N(t) = A_N Z_N(t) + B_N(\xi(t)) u(t), \quad Z_N(0) = Z_{0,N}, \\ & && \dot{\xi}(t) = v(t), \quad \xi(0) = \xi_0, \\ & && -u_{\max} \leq u_i(t) \leq 0, \\ & && \|v_i(t)\|_2 \leq v_{\max}, \quad i \in \{1, 2, \dots, m\}. \end{aligned} \quad (\text{Pexp})$$

The inputs to problem (Pexp) are the PDE's initial state $Z_{0,N}$ and the actuators' initial locations ξ_0 . Subsequently, problem (Pexp) simultaneously solves for the optimal guidance v^* and optimal actuation u^* , which are treated as outputs. When the exact state $Z_{0,N}$ is not available to be fed into (Pexp), the estimate $\hat{Z}_{0,N}$ is the input to (Pexp) in practice, and the state's propagation follows the deterministic

PDE dynamics applied in (Pexp) as the constraint. We use a nonlinear optimal control solver ICLOCS2 [63] to compute a solution to (Pexp).

An alternative approach would be to detach the sensors from the actuators. In such a scenario, the sensors could be stationary or mobile. For the latter case, sensors' guidance can be designed for reducing the uncertainty of the estimation, e.g., minimizing the covariance of the Kalman filter (see Chapter 4). Such a scheme is not applied here due to its heavy computational load (which includes a N^4 -dimensional Riccati equation in the constraints). Also, the sensors collocated with the actuators can provide sufficient state estimation for planning actuation and guidance when solving problem (Pexp).

The framework is implemented in the following manner: at each planning moment, the state estimation \hat{Z}_N and the location of the vehicles ξ are fed into (Pexp) for the optimal guidance v^* and actuation u^* for the planning horizon of t_f . Once v^* and u^* are solved, the former steers the vehicles along the new trajectories while the system's state Z_N is propagated subject to the optimal actuation u^* . At the same time, the sensors' measurements are collected to propagate the state estimation \hat{Z}_N . The procedure repeats until the terminal time or other likely terminal conditions (e.g., the norm of state Z_N is sufficiently close to zero).

5.2 Numerical studies

This section analyzes and evaluates the performance of the proposed framework in simulation. We first show an example of the optimal solution to problem

(Pexp). We then analyze problem (Pexp)’s solution by examining how its performance depends on model parameters. Finally, we evaluate the entire framework using Monte Carlo simulations with comparison to naive guidance and actuation strategies.

5.2.1 An example of optimal guidance and actuation

Consider the following example for problem (Pexp): For simplicity, only one vehicle $m = 1$ is deployed in the domain Ω with length $l = 30$ m and is initialized at $\xi_0 = [1, 3]^\top$ m. The models in (5.8) and (5.10) are used for the input and output of the PDE, respectively, with $r_1 = \sigma_1 = 0.1$. The initial PDE is $\hat{Z}_0(x, y) = (30x - x^2)(30y - y^2)/50625$ and is approximated using $N^2 = 13^2$ basis functions $\{\phi_{i,j}\}_{i,j=1}^N$ for Dirichlet BC and $\{\psi_{i,j}\}_{i,j=0}^{N-1}$ for Neumann BC to obtain $Z_N(0)$. Other parameters in this simulation are as follows: $u_{\max} = 11$ kg/m²s, $v_{\max} = 6$ m/s, and $t_f = 60$ s. The matrices $\kappa = \kappa_f = I_{13^2}$, $\gamma = 0.1$, and $q = 0.1I_2$. We use ICLOCS2 as the solver for problem (Pexp) using trapezoidal discretization and 10^{-2} tolerance (for local absolute error). The resulting snapshots of the optimal trajectory are shown in Figs. 5.1(a) and 5.1(b) with Dirichlet BC and Neumann BC, respectively. In both cases, the actuator moves towards the central region of the domain where the initial distribution concentrates (0–10 s). For the Dirichlet BC, the actuator then stays near the same area to reduce the remaining spots with relatively big magnitude (10–30 s) and essentially ceases moving as the process is controlled close to zero (30–60 s). For the Neumann BC, the actuator covers a bigger area (10–60 s) than

with the Dirichlet BC due to the boundary insulation effect of Neumann BC. The Dirichlet BC serves as a passive actuation that reduces the process magnitude by diffusion; Fig. 5.2 shows that the reduction in state norm $\|Z_N\|$ with Dirichlet BC is faster than that with Neumann BC, and Fig. 5.3 shows that the actuation and speed of the actuator with Dirichlet BC lasts shorter than those with Neumann BC. Also note that initial actuation and speed with both BCs are u_{\max} and v_{\max} , respectively, indicating the actuator's best effort to control the process by reaching its actuation and speed limits.

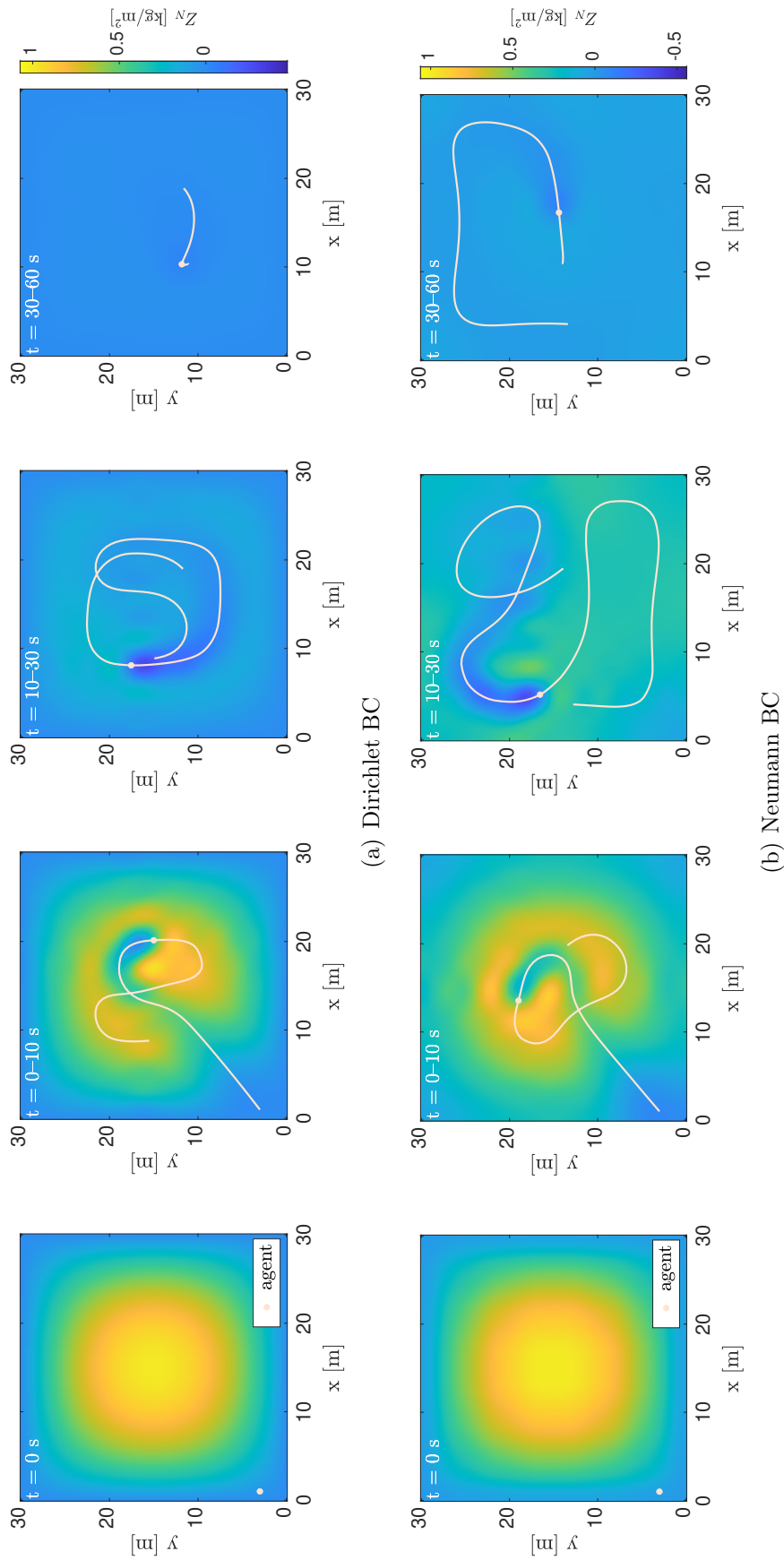


Figure 5.1: Snapshots of a diffusion process and the trajectories of the mobile agent with Dirichlet BC and Neumann BC. The process and agent location (dot) are depicted at the middle of the interval shown on top left.

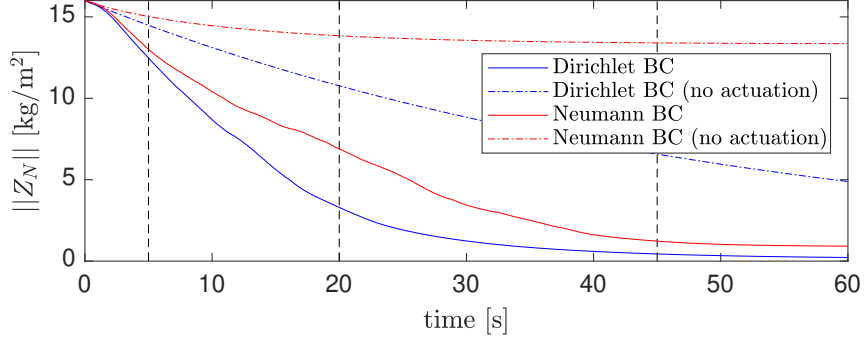


Figure 5.2: Reduction of the state norm. The vertical dashed lines correspond to the time of snapshots in Fig. 5.1.

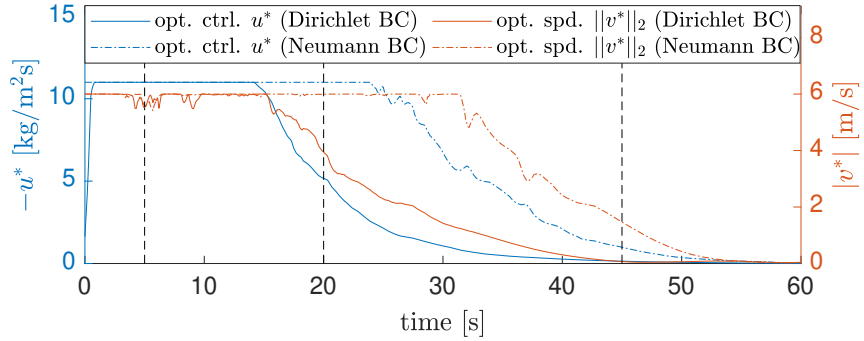


Figure 5.3: Optimal control and speed solved from (Pexp). The vertical dashed lines correspond to the time of snapshots in Fig. 5.1.

5.2.2 Nondimensional analysis of the parameter space

For the ease of analysis in various applications where the values of model parameters are at different scales, we conduct a nondimensional analysis of selected parameters. The nondimensional analysis uses the Buckingham π Theorem [7] to compute sets of $n_{\text{ND}} = n_{\text{D}} - n_{\text{U}}$ dimensionless parameters from n_{D} parameters that are expressed in terms of n_{U} independent physical units. We choose the following $n_{\text{D}} = 6$ parameters and display their physical units in Table 5.1: the initial process state norm $\|Z_N(0)\|$ (kg/m^2), maximum speed v_{max} (m/s), maximum actuation u_{max}

(kg/m²/s), diffusivity a (m²/s), domain size l^2 (m²), and total time t_f (s). Note that the process state could have other units, e.g., temperature (°C) for forest fires.

Unit	$\ Z_N(0)\ $	v_{\max}	u_{\max}	a	l^2	t_f
kg	1		1			
s		-1	-1	-1		1
m	-2	1	-2	2	2	

Table 5.1: Model parameters and their physical units

Since there are $n_U = 3$ independent physical units in Table 5.1, there are $n_{ND} = 3$ nondimensional parameters [7]. We introduce the following domain-independent parameters: relative speed \bar{v}_{\max} and relative diffusivity \bar{a} . These parameters scale v_{\max} and a to a unit-sized domain as follows:

$$\bar{v}_{\max} = \frac{v_{\max}}{l}, \quad \bar{a} = \frac{a}{l^2}. \quad (5.29)$$

Using the scaled parameters in (5.29), we define the three nondimensional parameters: *nondimensional speed* \bar{v}_{\max}/\bar{a} , *actuation effectiveness* $(u_{\max}/\|Z_N(0)\|)/\bar{a}$, and *total diffusion* $\bar{a}t_f$. Although these are not the only nondimensional terms (e.g., $\bar{v}_{\max}t_f$ is also dimensionless), we choose these three terms for their meaningful physical interpretations below.

The *nondimensional speed* (NS) has a clear interpretation in terms of the vehicle speed relative to the process diffusivity. When NS is significantly greater than one, the mobile actuators are dominant in shaping the distribution of the state. Moreover, the impact of the actuation is mainly local because the relative diffusion rate is low. Contrarily, when NS is significantly smaller than one, diffusion is domi-

nant in shaping the distribution of the state. The large diffusivity can propagate the impact of actuation to its surroundings faster than the actuator motion, in which case the actuators may be treated as essentially stationary.

The *actuation effectiveness* (AE) characterizes the relation between actuation and diffusion. The numerator $u_{\max}/\|Z_N(0)\|$ is the ratio of the maximum possible actuation to the initial state's norm, which characterizes roughly how fast the actuation can affect the state. The denominator indicates how fast the diffusion smooths process. In the case of zero Dirichlet BC, AE characterizes the in-domain actuation compared to the boundary actuation.

The *total diffusion* (TD) simply characterizes the total particle transportation caused by diffusion in a unit-sized domain for a duration of t_f . Increasing the relative diffusivity \bar{a} or the terminal time t_f increases the total diffusion.

The effect of the nondimensional parameters is quantitatively analyzed in simulation. Since the parameters may vary at different scales, for example, the diffusivity a could range from 10^{-5} m²/s (molecular diffusion) to 500 m²/s (horizontal eddy diffusivity in the ocean) [2], while the maximum speed of an unmanned vehicle may vary from 0.1 m/s to 20 m/s, it could be burdensome to cover all the parameters in their entire range on a fine grid. We first use a coarse grid, where the diffusivity $a \in \{10^{-5}, 10^{-4}, 10^{-3}, 10^{-2}\}$ m²/s, to see the overall tendency of performance change

evaluated by the following three metrics:

$$Z_{\text{rate}} = \frac{\|Z_N(0)\| - \|Z_N(t_f)\|}{t_f}, \quad (5.30)$$

$$u_{\text{avg}} = \frac{\int_0^{t_f} |u(t)| dt}{t_f}, \quad (5.31)$$

$$v_{\text{avg}} = \frac{\int_0^{t_f} \|v(t)\|_2 dt}{t_f}, \quad (5.32)$$

which stand for *reduction rate of the state norm*, *average actuation*, and *average speed*, respectively. The parameters for problem (Pexp) are identical to those in Section 5.2.1 except for the initial condition $\hat{Z}_0(x, y) = (30x - x^2)(30y - y^2)/10125$.

The results are shown in Fig. 5.4 with both the Dirichlet BC and Neumann BC. The reduction rate of the state norm Z_{rate} rises in the former and maintains a constant value in the latter as the diffusivity a increases. This is true because the Dirichlet BC serves as (passive) actuation whose efficiency is proportional to diffusivity, whereas Neumann BC serves as insulation and does not impact the state. For the same reason, the average actuation u_{avg} drops for the Dirichlet BC and maintains a constant value for the Neumann BC since the boundary's actuation becomes dominant in the former case as diffusivity increases, which relieves the actuator from implementing actuation. The average speed v_{avg} drops as diffusivity increases for both types of BCs because greater diffusivity contributes more to the spreading of the actuation to the surroundings of the actuators, which relieves the actuator from travelling at the maximum speed. Note that the average speed for the Dirichlet BC is smaller than that for the Neumann BC as diffusivity increases

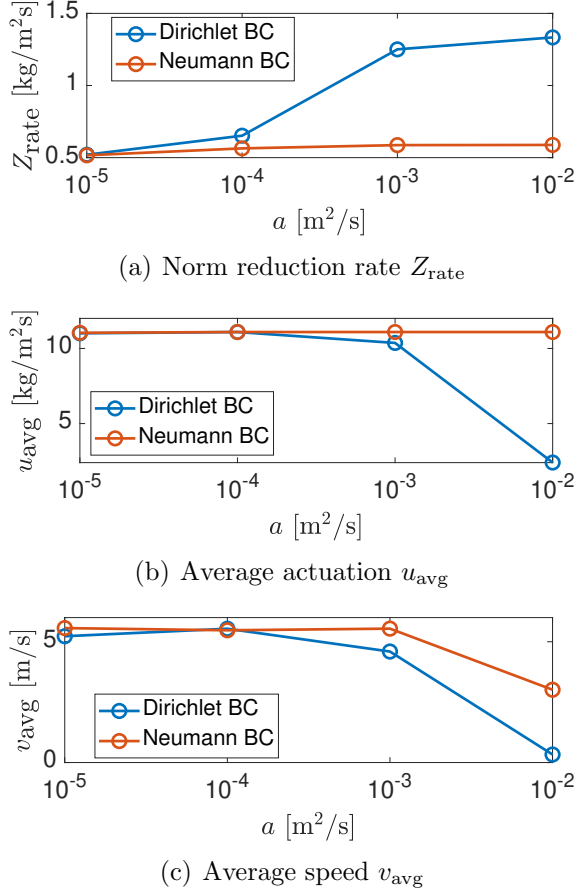


Figure 5.4: Performance of the optimal solution to problem (Pexp) for diffusivity a in the range of 10^{-5} to 10^{-2} m²/s.

due to the former's increasingly dominant boundary actuation.

The result at a coarse parameter grid provide an overall tendency of performance when the diffusivity changes. We proceed to evaluate the performance on a finer grid with a fixed diffusivity $a = 10^{-3}$ m²/s. We vary the values of v_{max} , u_{max} , and t_f , where each results in the variation of one nondimensional term independently. Specifically, we apply the following set of values: $v_{\text{max}} \in \{1, 2, \dots, 10\}$ m/s, $u_{\text{max}} \in \{6, 7, \dots, 15\}$ kg/m²/s, and $t_f \in \{60, 90, 120\}$ s. The other parameters for the simulations are identical to those in the case of the coarse grid.

Fig. 5.5 shows the results on the fine grid with Dirichlet BC. In Fig. 5.5(a), we

display the variation of state norm's reduction rate Z_{rate} when NS and AE vary with TD fixed (top) and when AE and TD vary with NS fixed (bottom). A clear tendency of greater state reduction rate can be observed when NS and AE increase, which is expected since actuators with higher maximum speed and maximum actuation can reduce the state norm more efficiently. The reduction rate drops as TD increases because bigger terminal time t_f yields a bigger denominator in the reduction rate Z_{rate} and the numerator is almost constant (due to the zero Dirichlet BC's eventual zero state norm). The reduction rate is not sensitive to NS when AE is fixed, which we do not show. In Fig. 5.5(b), we plot the average actuation u_{avg} when NS and AE vary with TD fixed (top) and when AE and TD vary with NS fixed (bottom). Similar tendencies can be observed as in Fig. 5.5(a). Additionally, the average actuation is capped by the maximum actuation u_{max} (which is proportional to AE in the plot). The average actuation is not sensitive to NS when AE is fixed, which we do not show. In Fig. 5.5(c), we display the average speed v_{avg} when NS and AE vary with TD fixed (top) and when NS and TD vary with AE fixed (bottom). The overall tendency is that the average speed v_{avg} increases when NS and AE increase or TD decreases. Also, the average speed is capped by the maximum speed v_{max} (which is proportional to NS in the figure) when v_{max} is relatively small.

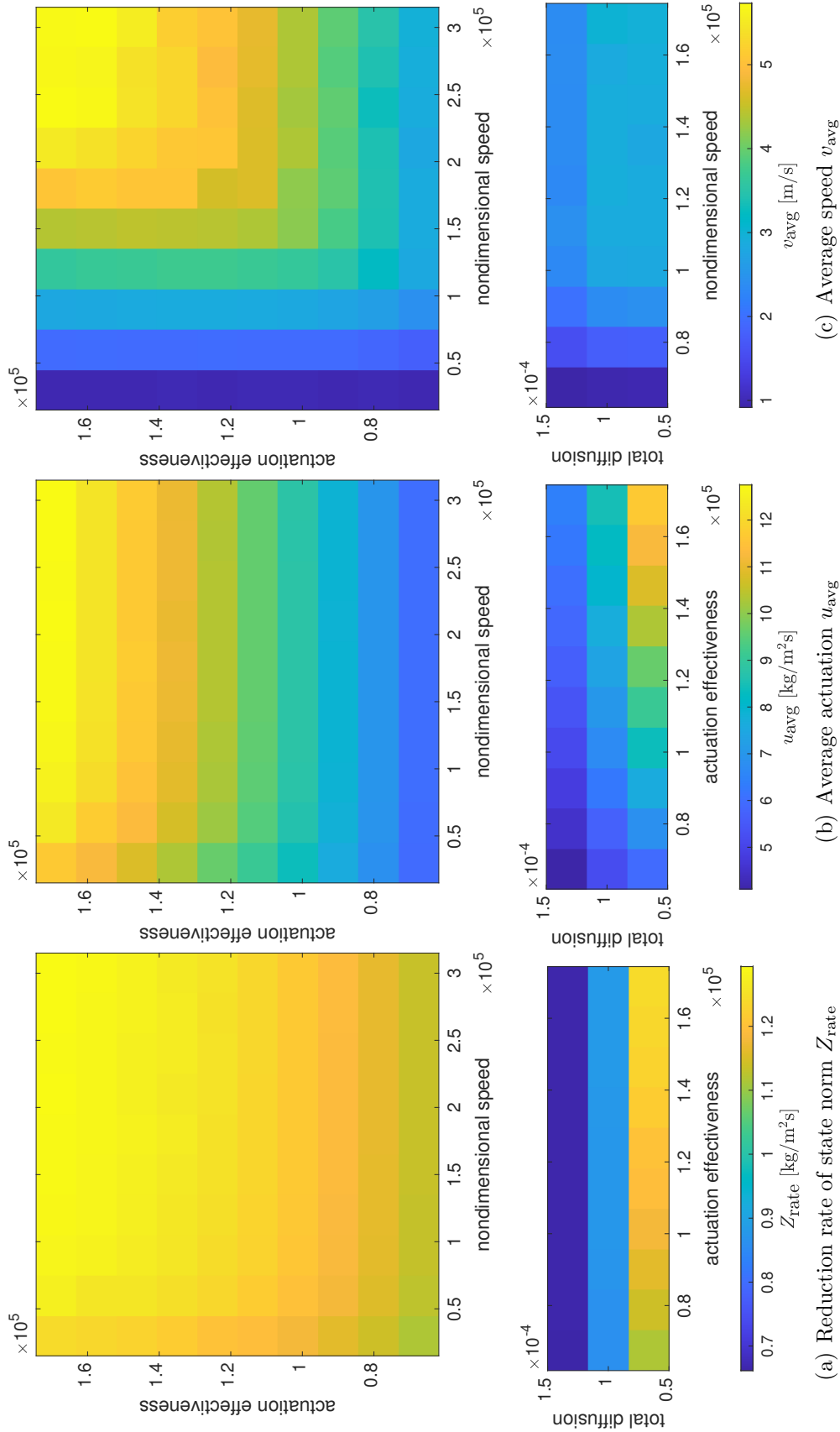


Figure 5.5: Performance of problem (Pexp)'s optimal solution as bivariate heat maps of the nondimensional parameters (Dirichlet BC).

The plots for the Neumann BC with the same values of nondimensional parameters and the same metrics as for the Dirichlet BC are shown in Fig. 5.6. The tendency therein are consistent with the Dirichlet BC in Fig 5.5. Hence, we do not expand the descriptions. But observe the scale of the reduction rate Z_{rate} with Neumann BC in Fig. 5.6(a) is almost half of that with Dirichlet BC in Fig. 5.5(a) due to the (passive) actuation implemented by the boundary actuation of the latter.

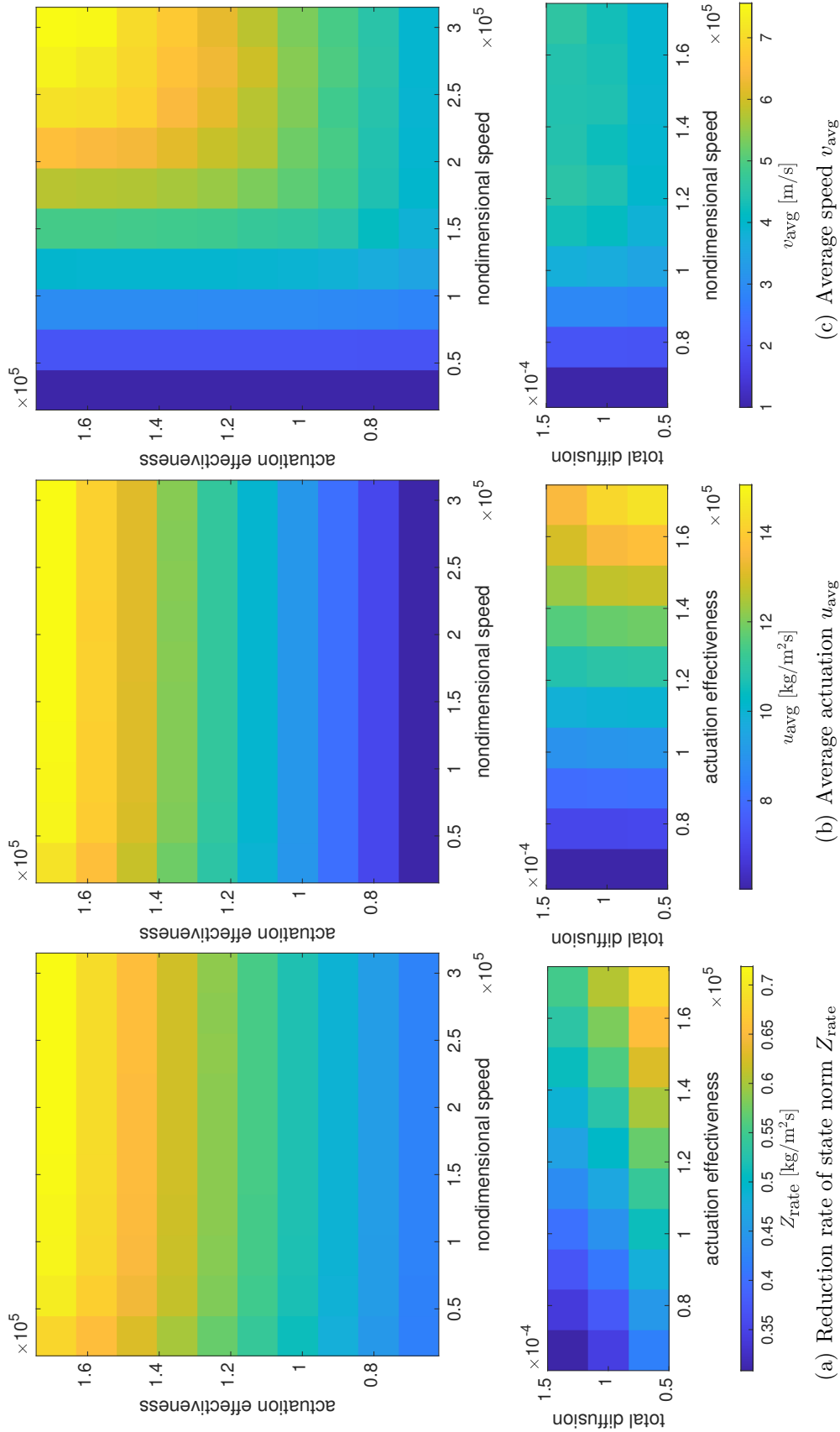


Figure 5.6: Performance of problem (Pexp)'s optimal solution as bivariate heat maps of the nondimensional parameters (Neumann BC).

5.2.3 Monte Carlo simulations

To evaluate the performance of the overall framework, we conduct Monte Carlo simulations with two comparison guidance and actuation strategies. Both strategies use random walk as the guidance policy, whereas one applies linear-quadratic-Gaussian (LQG) feedback as the actuation and the other applies constant actuation $u_{\text{const}} = -2 \text{ kg/m}^2\text{s}$, named the *semi-naive* and *naive* strategies, respectively. For the LQG actuation in the semi-naive strategy, the gain for the estimation-based feedback control is solved from minimizing an infinite-horizon quadratic cost $\int_t^\infty \langle Z_N(\tau), \kappa Z_N(\tau) \rangle + u(\tau)^\top \gamma u(\tau) d\tau$ at each decision time t . The same parameters for the noise model, Kalman filter, and bounds on speed and actuation are applied to all strategies for a fair comparison. The framework is implemented with a planning horizon of 15 s, which is set to be the terminal time t_f of problem (Pexp). The simulations for all strategies run in discrete-time with 0.5 s sample/decision time. The approximation has dimension $N^2 = 13^2$, and the matrices for the cost function are $\kappa = \kappa_f = I_{13^2}$, $\gamma = 0.1I_4$, and $q = 0.1I_8$. The total time T is 150 (300) s for the simulations with Dirichlet (Neumann) BC. The diffusivity a is taken in the range $\{10^{-5}, 10^{-4}, 10^{-3}\} \text{ m}^2/\text{s}$. The initial conditions $\mathcal{Z}_0(x, y)$ with Dirichlet and Neumann BC are $(30x - x^2)(30y - y^2)/1875$ and $(30x - x^2)(30y - y^2)/5625$, respectively. The kernel functions K_0 and K for the Gaussian-process-modelled initial noise ω_0

and state noise $\omega(\cdot)$, respectively, are

$$K_0(x_1, x_2) = 9 \exp \left(-\frac{\|x_{12}\|_2^2}{20} - \frac{\|x_{10}\|_2^2}{400} - \frac{\|x_{20}\|_2^2}{400} \right), \quad (5.33)$$

$$K(x_1, x_2) = 0.1 \exp(-500 \|x_{12}\|_2^2), \quad (5.34)$$

where $x_{ij} = x_i - x_j$ for $i, j \in \{0, 1, 2\}$, $x_1, x_2 \in \Omega$, and $x_0 = [l/2, l/2]^\top$. The measurement noise on each sensor follows the standard normal distribution. The bounds on the speed and actuation are $v_{\max} = 1$ m²/s and $u_{\max} = 5$ kg/m²s. Four agents are deployed with their initial locations randomly assigned in the domain Ω by a uniform distribution. 100 trials are conducted for each value of diffusivity and each type of BC.

Two metrics are evaluated: the norm of the state $\|Z_N(T)\|$ and the average norm reduction per unit actuation (RPA), $(\|Z_N(0)\| - \|Z_N(T)\|) / \int_0^T \|u(t)\|_2 dt$, both computed at the total time T . These two metrics evaluate the ability of reducing the state norm and the efficiency of actuation, respectively. The results are shown in Fig. 5.7. The optimal policy can reduce the state norm to the lowest among the three strategies, for both the Dirichlet and Neumann BCs and for all values of diffusivity. The semi-naive is slightly better than the naive strategy due to the feedback control in the former (compared to the open-loop control in the latter). In terms of actuation efficiency, the optimal policy has the greatest RPA at all values of diffusivity for the Neumann BC, which suggests the highest actuation efficiency. For the Dirichlet BC, the optimal strategy's RPA is the highest among all strategies at $a = 10^{-5}$ m²/s. At relatively greater values of diffusivity (10^{-4} and 10^{-3} m²/s),

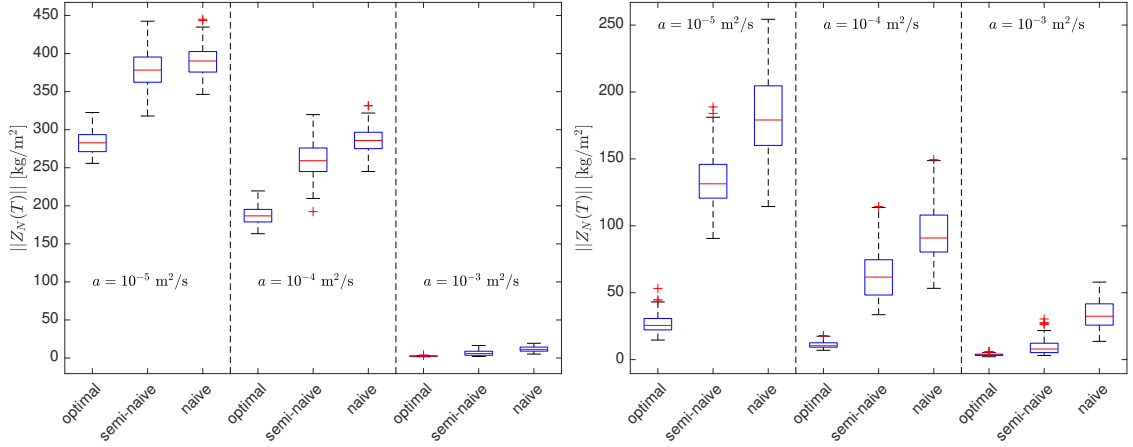
the naive strategy has the highest RPA. But the naive strategy's RPA is subject to the change in u_{const} . In other words, its RPA may not be the highest should u_{const} takes other values. Note that when diffusivity is relatively small ($a = 10^{-5} \text{ m}^2/\text{s}$) with Neumann BC, some trials with the semi-naive and naive strategies cause the accumulation of negative actuation such that the state $Z_N(t)$ turns negative and $\|Z_N(T)\| > \|Z_N(0)\|$. The negative values of the RPA in Fig. 5.7(d) indicate the such accumulation, which results in inefficiency and waste of actuation.

5.3 Experimental demonstration of the framework

This section shows the experimental results for the demonstration of the cooperative estimation and control framework on an outdoor multi-quadrotor testbed. We first review the multi-quadrotor testbed in the literature.

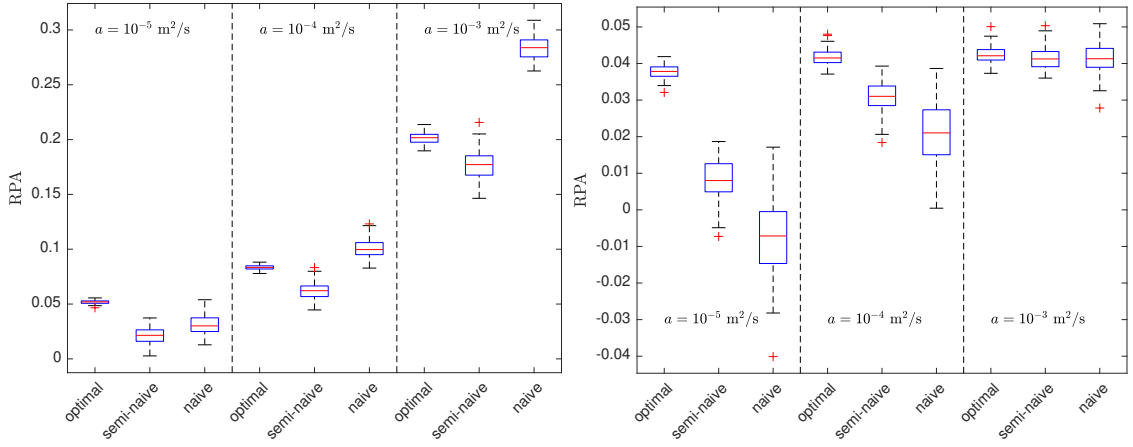
5.3.1 Survey of multi-quadrotor testbed in the literature

The quadrotor is a type of aircraft that is propelled and lifted by four rotors. The simple structure yields straightforward dynamics and a vast number of research on controller design for both the maneuver of a single quadrotor and the collective motion of multiple quadrotors. A recent review [70] introduces existing multi-quadrotor testbeds developed for research, industry, or entertainment purposes. One theoretical research topic that applies to multiple quadrotors is formation control, where position-, displacement-, and distance-based control have been studied for different sensing capability and interaction topology of agents [64]. Exemplary re-



(a) Terminal state norm with Dirichlet BC

(b) Terminal state norm with Neumann BC



(c) Average norm reduction per unit actuation with Dirichlet BC

(d) Average norm reduction per unit actuation with Neumann BC

Figure 5.7: Results for Monte Carlo simulations. Smaller values of the state norm $\|Z_N(T)\|$ in (a) and (b) indicate more effective actuation, whereas bigger values of the RPA in (c) and (d) indicate more efficient actuation.

sults with experimental validation can be found in [38, 52, 55]. Another research topic that applies to multiple quadrotors is the autonomous swarm, which refers to a team of agents who can respond to the tasks that require cooperation based on individual autonomy. No rigid formation is required in this case. Representative applications of the autonomous swarm includes surveillance, search, and tracking, for example, [77, 90, 94].

5.3.2 Multi-quadrotor testbed in this work

Our testbed contains a ground station and six custom-built quadrotors: two use the DJI F450 frame while the other four use the Tarot 650 frame (see Fig. 5.8). Each quadrotor is equipped with a Pixhawk 2 onboard flight controller for lower-level control, a real-time kinematic (RTK) GPS for improved positioning, and a downward-facing lidar for fine altitude reading. Each quadrotor communicates its status and receives commands from the ground station over 915 MHz telemetry radio. We assign a unique frequency band to each quadrotor within the range of 902–928 MHz to suppress interference between the radio modules.

On the ground station, the quadrotors’ high-level trajectory planning is computed in MATLAB. The open-source software OpenMACE [37] (developed by Heron Systems Inc.) interfaces between the quadrotors and the ground station. OpenMACE broadcasts the quadrotors key status (GPS coordinates, altitude, attitude angles, and battery voltage) and listens to commands (waypoint, velocity, and take-off/land) via the Robot Operating System (ROS), which allows users to compute and



Figure 5.8: Quadrotors in the testbed with the DJI F450 frame (left) and the Tarot 650 frame (right)

send control commands to quadrotors in MATLAB through its interface with ROS. OpenMACE provides a graphical display that shows the locations of the quadrotors on a satellite map with key status information and enables the toggling of flight modes. The testbed supports virtual quadrotors that are controlled by ArduCopter in the software in the loop (SITL) simulator. The software architecture of the testbed is summarized in Fig. 5.9. The quadrotors are constrained to fly in a $90 \times 30 \times 10 \text{ m}^3$ area within the Fearless Flight Facility (F3), an outdoor netted flight test site at the University of Maryland.

5.3.3 Setup and procedure of the experiments

The experiments were conducted at F3 within a $30 \times 30 \times 10 \text{ m}^3$ area. Four quadrotors were deployed in the experiments, and each represents a pair of collocated sensor and actuator. The spatiotemporal field and its interactions with the sensors and actuators were virtual: the simulated process was computed on the ground station, and the measurement/actuation by the sensors/actuators was syn-

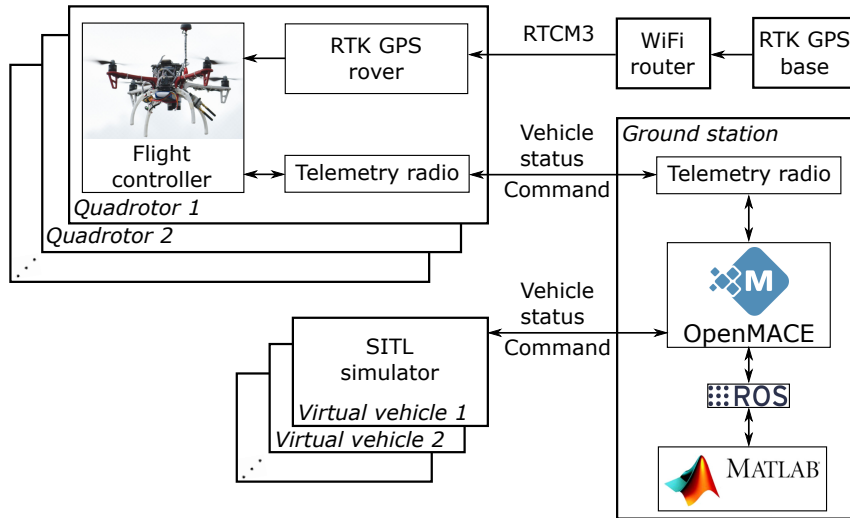


Figure 5.9: Block diagram of hardware and software architecture of the multi-quadrotor testbed

thesized based on the quadrotors' real-time locations. The software architecture that supports the experiments is shown in Fig. 5.10. Due to software incompatibility across operating systems (OS), two laptops were used for the experiments: one with Ubuntu 16.04 OS and the other with Windows 10 OS (both with Intel i7-8650U processor). The Ubuntu computer runs OpenMACE to send waypoint commands to and receive real-time locations from the quadrotors. Based on the quadrotors' locations, the same computer propagates the simulated process with the optimal actuation and maintains an estimation of the process in MATLAB. The optimal actuation and guidance are computed on the Windows computer using ICLOCS2 with the (estimated) state and vehicles' locations passed from the Ubuntu computer at the start of each planning horizon via TCP/IP. Once the solution is computed, the optimal trajectories that are propagated using the single integrator dynamics (5.2) are passed back to the Ubuntu computer along with the optimal actuation. Both the simulated process and the estimated process are paused during the time

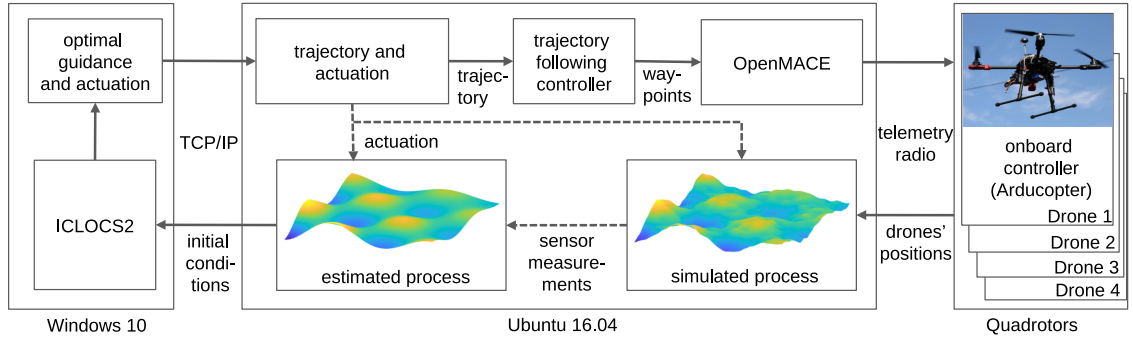


Figure 5.10: Software architecture for the experiments. Dashed arrows indicate synthetic values.

when ICLOCS2 computes the optimal solution.

The MATLAB script on the Ubuntu computer uses a timer that updates the simulated process and estimated process at 0.5 s. This is the minimum interval that the MATLAB script can handle all tasks, including sending waypoints to and updating real-time locations of the quadrotors, updating real-time display of quadrotors' locations, and propagating the simulated and estimated processes. For the quadrotors to follow the optimal trajectory, we command each quadrotor to the waypoint three steps (1.5 s) ahead of the current time along its optimal trajectory. This look-ahead waypoint control is implemented due to 0.5–1 s delay between the MATLAB script sending a waypoint command till the quadrotors starting to move towards this waypoint. Collision avoidance of the quadrotors is implemented by separating the altitudes of quadrotors by 1.5 m (which is chosen to reduce downwash effects).

We conducted two experiments: Experiment 1 has Dirichlet BC and Experiment 2 has Neumann BC. Both experiments have 0.5 s sample/decision time, 15 s planning time (t_f), and 180 s total time (T). To reduce the computational load for solving the optimal actuation and guidance, we relax the quadratic constraint

$|v_i|_2 \leq v_{\max}$ to a linear constraint $|v_i|_\infty \leq v_{\max}$ for $i \in \{1, 2, 3, 4\}$ such that each vehicle's speeds along the horizontal and vertical axis are bounded by v_{\max} . In the experiments, we set $v_{\max} = 1$ m/s, and each quadrotor's onboard controller (ArduCopter) is set to have maximum speed for reaching a waypoint at $\sqrt{2} \approx 1.41$ m/s to approximately enforce the speed constraint. We also reduce the number of basis functions to $N^2 = 9^2$ for approximations to relieve the computation load. Other parameters used in the experiments are as follows: $a = 10^{-3}$ m²/s (Experiment 1), $a = 10^{-4}$ m²/s (Experiment 2), $u_{\max} = 5$ kg/m²s, $\mathcal{Z}_0(x, y) = 10|\sin(2\pi x/30)\sin(2\pi y/30)|$ (Experiment 1), $\mathcal{Z}_0(x, y) = 2(30x - x^2)(30y - y^2)/16875$ (Experiment 2), quadrotors' initial locations $\{[5, 5]^\top, [25, 25]^\top, [5, 25]^\top, [25, 5]^\top\}$, and matrices $\kappa = \kappa_f = I_{9^2}$, $\gamma = 0.1I_4$, and $q = 0.01I_8$ for cost functions in problem (Pexp). The spatial correlation for the initial and state noise and the measurement noise model are identical to the settings in the Monte Carlo simulations in section 5.2.3.

5.3.4 Results and discussion

The evolution of the diffusion process and trajectories of the quadrotors are shown in Figs. 5.11 and 5.12 for Experiments 1 and 2, respectively. For the first 30 (60) seconds in Experiment 1 (2), the quadrotors are moving around the peaks in of the initial state with actuation at full level u_{\max} (as seen in Fig. 5.13). The full level actuation lasts longer in Experiment 2 than in Experiment 1 (with Dirichlet BC) due to the boundary's passive actuation in the latter case, where actuation from the actuators is saved. Subsequently, the quadrotors spread out to the domain to

implement actuation to the regions that have a relatively large magnitude of the process. During this time, the actuation is not conducted at full level u_{\max} . The norm reduction is shown in Fig 5.14. The comparison to the cases with no actuation indicates the capability of the proposed framework for controlling a 2D diffusion process subject to state and measurement noise and delays in implementation. A video recording of Experiment 1 from 60 s to 105 s is available at <https://youtu.be/kv5ist9zD3w>.

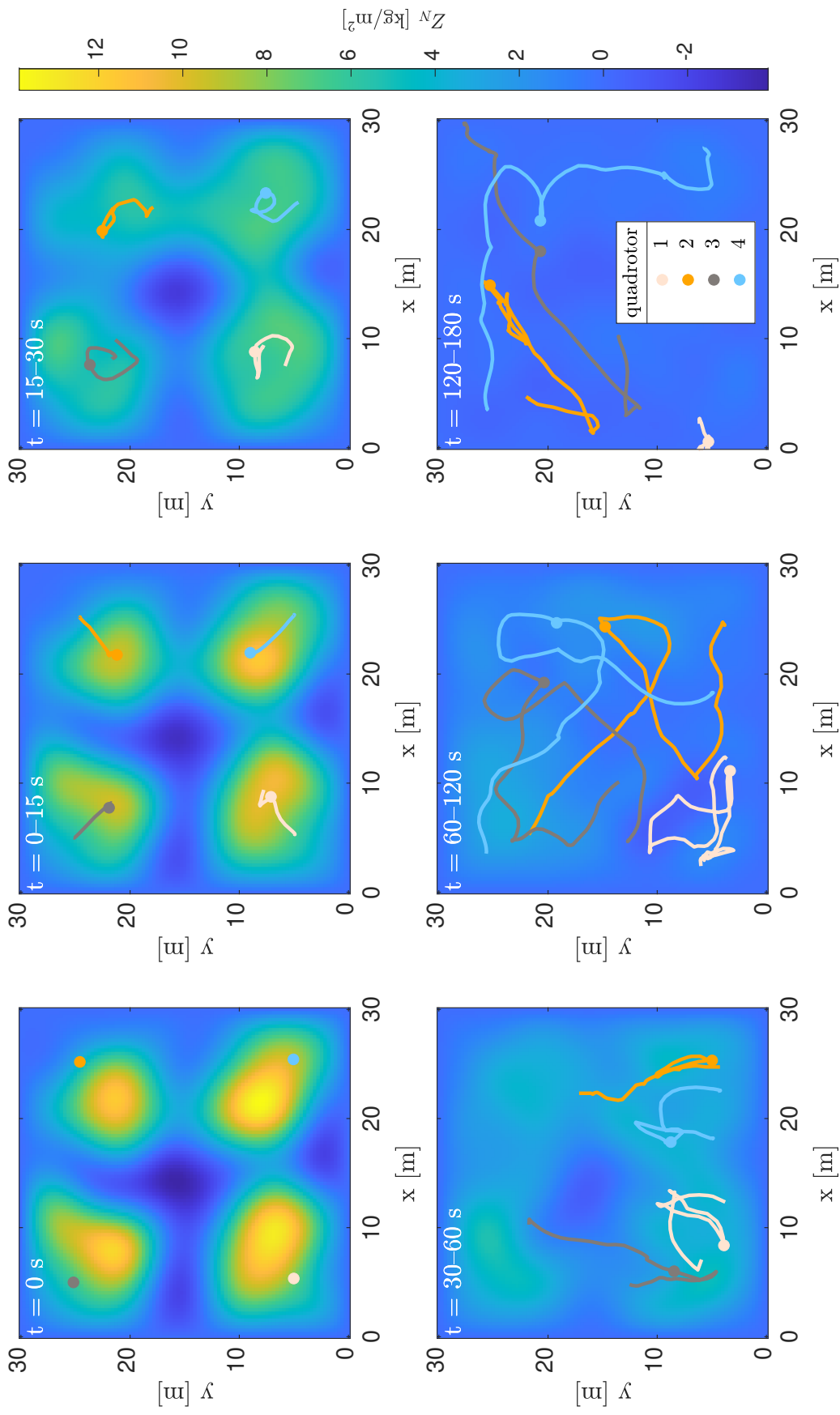


Figure 5.11: Snapshots of a virtual diffusion process and the trajectories of the actual quadrotors in Experiment 1. The process and the quadrotor locations (dots) are taken at the middle of the interval shown on top left.

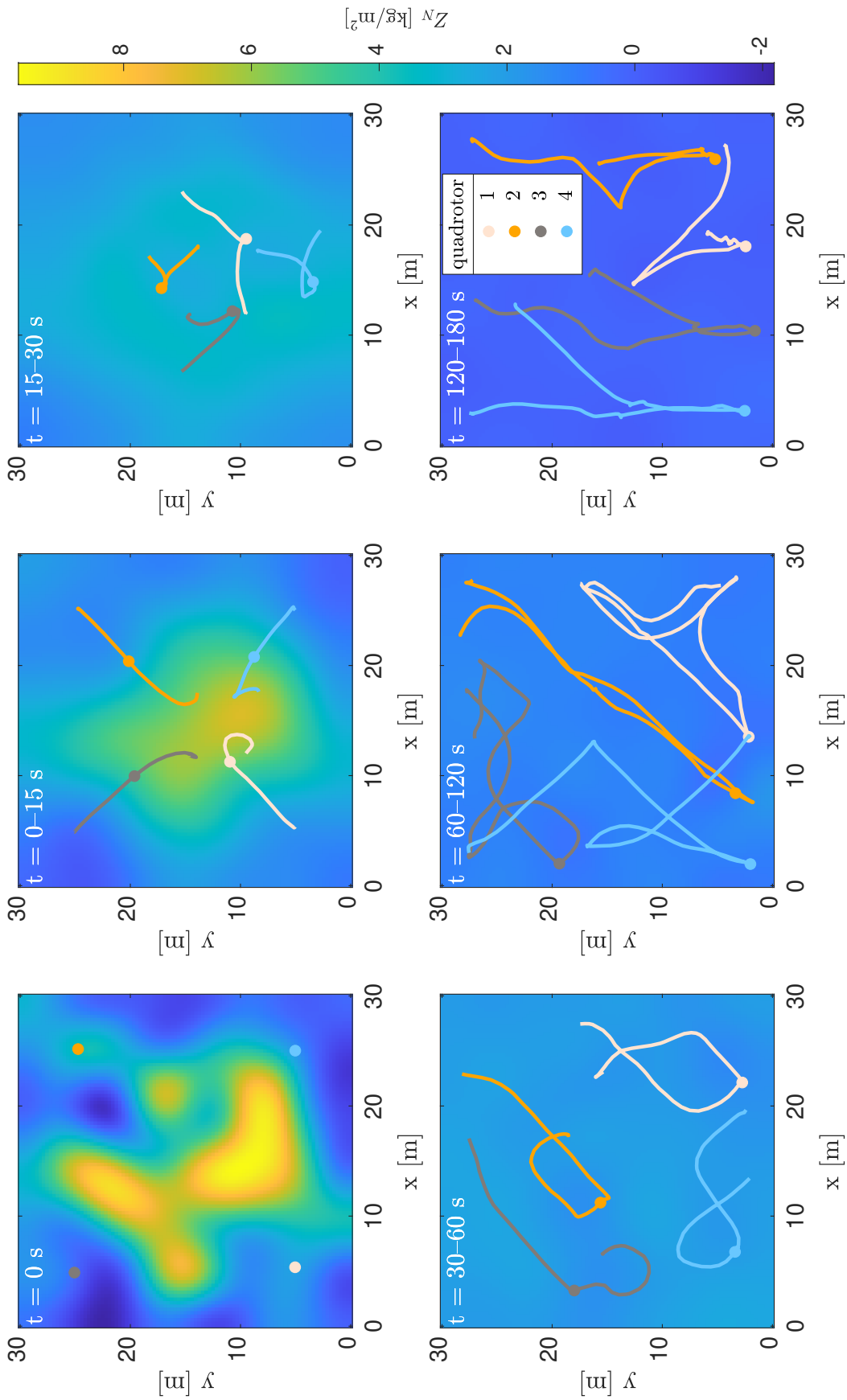


Figure 5.12: Snapshots of a virtual diffusion process and the trajectories of the actual quadrotors in Experiment 2. The process and the quadrotor locations (dots) are taken at the middle of the interval shown on top left.

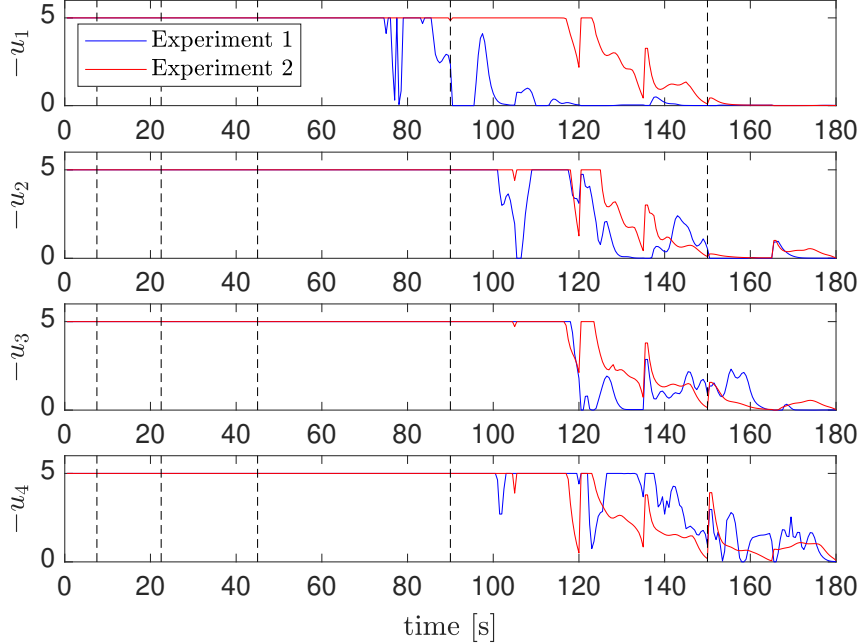


Figure 5.13: Optimal actuation in experiments. The unit for the vertical axes is $\text{kg}/\text{m}^2\text{s}$. The vertical dashed lines correspond to the time of snapshots in Figs. 5.11 and 5.12.

Despite the results above, we also realized the framework’s limitations in its current stage from the experimental demonstration. Below we discuss lessons learned from the demonstration, which suggest potential improvements for the framework’s implementation with real spatiotemporal processes.

1. The major time consumption of the framework is on the computation of the optimal guidance and actuation, where the average computation time for the planning horizon (15 s) is 27.8 s and 41.7 s for Experiments 1 and 2, respectively. Although ICLOCS2 provides efficient computation of the solution, for practical applications of the framework, the computation time needs to be reduced to a level at which the spatiotemporal process does not significantly change during the time of solving the optimization problem. One approach to reducing the computation time is to reduce the order of the model. For example, one may apply the domain-

decomposition method [24] which only keeps relatively higher-order approximation near the actuators (where finer characterization of the process is needed) and applies relatively lower-order approximation to the other area.

2. The proposed framework supports the usage of surface or ground vehicles as long as their lower-level controller can track the optimal trajectories, and the speed limit of such vehicles can be incorporated by v_{\max} . Furthermore, they are more suitable than aerial vehicles when planning takes significant time since almost no fuel or energy is needed to maintain their working status, unlike quadrotors that need the power to maintain the hovering state.

3. We use a look-ahead waypoint-following scheme to steer the quadrotors to travel along the designated trajectories, which updates waypoints at 2 Hz. This scheme is simple to implement. With the lower-level waypoint control of the onboard controller (Pixhawk 2), the trajectory-following is acceptable (not shown). For trajectory-following with better precision, an onboard computer may be used that samples and corrects the vehicles' motion at a higher rate ($\gg 2$ Hz).

4. We only consider the diffusion process in this chapter. However, advection caused by a velocity field could be incorporated, which leads to a diffusion-advection process. The latter is not considered here for the significantly increased computation time when solving problem (P_{exp}) with the advection term. Nevertheless, the diffusion-advection process extends the framework to more application scenarios. Simulations results in Chapter 3 suggest that the actuators can take advantage of the velocity field to conserve energy, where the formation therein is similar to problem (P_{exp}) in this chapter.

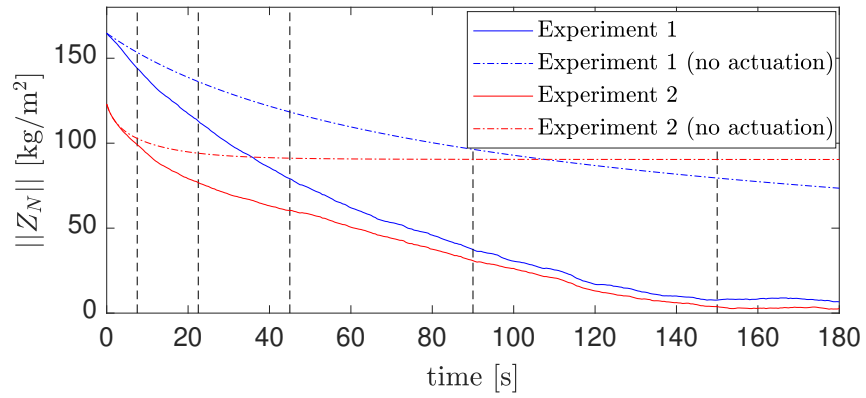


Figure 5.14: Reduction of the state norm in experiments. The vertical dashed lines correspond to the time of snapshots in Figs. 5.11 and 5.12.

Chapter 6: Conclusion

This dissertation develops several frameworks for estimation and control of a partial differential equation modeled spatiotemporal process using a team of mobile sensors and actuators. The proposed methods utilize tools from infinite-dimensional systems, optimization, Galerkin approximation, and nonlinear programming. Moreover, an outdoor multi-quadrotor testbed is set up for demonstrations of the proposed framework.

6.1 Summary of contributions

This dissertation addresses the problem of deploying mobile sensors and actuators to estimate and control a spatiotemporal process. From the theoretical perspective, we use optimization to formulate the problems of study that unifies the goal of reducing estimation uncertainty or controlling the PDE state and the limitations of the vehicles that carry the sensors or actuators. Conditions for the existence of solution and convergence of the approximate optimal solution within each formulation are proved. From the experimental perspective, we introduce a cooperative estimation and control framework to demonstrate the practical feasibility of the proposed formulations after adaptations to practical applications. Results

from both numerical studies and experimental demonstration confirm the value of the proposed framework.

Chapter 3 proposes an optimization framework that steers a team of mobile actuators to control a DPS modeled by a 2D diffusion-advection process. Specifically, jointly optimal control of the DPS and guidance of the mobile actuators are solved such that the sum of a quadratic PDE cost and a generic mobility cost is minimized subject to the dynamics of the DPS and of the mobile actuators. We obtain an equivalent problem using LQR of an abstract linear system, which reduces the problem to search for optimal guidance only. The optimal control can be synthesized once the optimal guidance is obtained. Conditions on the existence of a solution are established based on the equivalent problem. We use the Galerkin approximation scheme to reduce the problem to a finite-dimensional one and apply a gradient-descent method to compute optimal guidance and control numerically. We prove conditions under which the approximate optimal guidance converges to that of the exact optimal guidance in the sense that when evaluating these two solutions by the original cost function, the difference becomes arbitrarily small as the dimension of approximation increases. The convergence justifies the appropriateness of both the approximate problem and its solution. The performance of the proposed optimal control and guidance is illustrated with two numerical examples, where exponential convergence of the approximate optimal cost is observed.

Chapter 4 proposes a guidance design method for a team of mobile sensors to estimate a spatiotemporal process modeled by a 2D diffusion-advection process. We formulate an optimization problem that minimizes the sum of the trace of the covari-

ance operator of the Kalman-Bucy filter and a generic mobility cost of the sensors subject to the dynamics of the sensor platforms. Conditions for the existence of a solution to the proposed problem are established, where a fundamental assumption is that the output kernel is continuous with respect to location. The approximation of the infinite-dimensional terms permits the computation of the optimal guidance. And we prove that the approximated problem's optimal cost converges to that of the exact problem. Moreover, we prove that the optimal guidance obtained from an approximate problem yields the cost evaluated by the exact problem's cost function arbitrarily close to the exact optimal cost. We use Pontryagin's minimum principle to compute optimal guidance numerically. The numerical solutions are evaluated in simulations. We study how the optimal trajectory and terminal estimation error change subject to the varying values of sensor noise variance and the mobility penalty for a single sensor. Trajectories of the sensors and the evolution of the pointwise variance are shown for a single sensor and a homogeneous team of sensors in a flow field. We also study the cost-effectiveness of a heterogeneous team of mixed sensors with superior and poor qualities by comparing the performance degradation to that of the homogeneous team of superior sensors.

Chapter 5 proposes a framework of cooperative estimation and control of a 2D diffusion process using collocated mobile sensors and actuators. The actuators' guidance and actuation are solved from an optimization problem that minimizes the magnitude of the process with penalties on guidance and actuation effort. The sensors' measurement is fed to a Kalman filter to estimate state subject to Gaussian state and measurement noise. The estimation is periodically fed to the optimization

problem to plan for optimal guidance and actuation. Extensive numerical studies have been conducted to analyze and evaluate the performance of the proposed framework with both parameter sweep on the nondimensional parameters of the optimization problem and Monte Carlo simulations of the entire framework. Comparisons to naive strategies suggest the proposed framework’s advantage in controlling the spatiotemporal process and efficiency of actuation. The framework is demonstrated on an outdoor multi-quadrotor testbed at the Fearless Flight Facility of the University of Maryland. The quadrotors carry the virtual sensors and actuators that interact with a simulated spatiotemporal process via synthesized actuation and sensor measurement, which are generated based on the quadrotors’ real-time locations. Experimental results demonstrate the framework’s capability in controlling the spatiotemporal process and suggest potential improvement towards application to real spatiotemporal processes.

6.2 Ongoing and future work

Ongoing and future work include establishing the convergence rate of the approximate optimal cost in Chapters 3 and 4, which will provide reference to the number of basis functions in approximations for practical applications. Problems with other types of PDE cost may be considered, such as the operator norm of the Riccati operator [57] to characterize unknown initial conditions and H_2 - or H_∞ -performance criteria for different types of perturbation [43, 58]. Applications with other types of PDE-modelled systems may be considered, e.g., monitoring deforma-

tion of large infrastructures (bridges) or controlling congested traffic [93].

On the sensor/actuator side, decentralized guidance design may be incorporated in future work to enable more autonomy of the team than a centralized implementation. The decentralized scheme will make the team's performance less dependent on a central node (or server), although it poses another level of complexity to the problem. Sensors and actuators that travel along the boundary of a 2D or 3D domain may be considered as well, which would result in boundary controller and observer design, respectively.

For practical feasibility, computational methods that require less power or time will be pursued, such as domain-decomposition methods or data-driven methods. Finite-element methods for a bigger domain with possibly irregular shapes will be incorporated into the current framework to broaden the potential applications. The integration of a heterogeneous team of mobile independent sensors and actuators may be considered to exploit the sensing and actuation capabilities. Moreover, the cooperative estimation and control framework could be validated with real spatiotemporal processes, e.g., monitoring and mitigating harmful algal blooms with unmanned aerial and surface vehicles.

Chapter A: Proofs

A.1 Proof of Lemma 2.3

Proof. Without loss of generality, consider the case of one mobile actuator, i.e., $m_a = 1$. The case of multiple actuators follows naturally. We first show a consequence of the input operator \mathcal{B} being continuous with respect to location. Consider two actuator states, ξ_1 and $\xi_2 \in C([0, t_f]; \mathbb{R}^n)$. For any $\phi \in \mathcal{H} = L^2(\Omega)$ and all $t \in [0, t_f]$,

$$\begin{aligned} |\mathcal{B}^*(M\xi_1(t), t)\phi - \mathcal{B}^*(M\xi_2(t), t)\phi| &\leq \|\mathcal{B}(M\xi_1(t), t) - \mathcal{B}(M\xi_2(t), t)\|_{L^2(\Omega)} \|\phi\|_{L^2(\Omega)} \\ &\leq l (|M(\xi_1(t) - \xi_2(t))|_2) \|\phi\|_{L^2(\Omega)}, \end{aligned} \quad (\text{A.1})$$

where we use the fact that $\mathcal{B}(\cdot, \cdot)$ is the integral kernel of $\mathcal{B}^*(\cdot, \cdot)$. Hence,

$$\|\mathcal{B}^*(M\xi_1(t), t) - \mathcal{B}^*(M\xi_2(t), t)\|_{\mathcal{L}(\mathcal{H}; \mathbb{R})} \leq l (|M(\xi_1(t) - \xi_2(t))|_2). \quad (\text{A.2})$$

Since \mathbb{R} is finite-dimensional, there exists $c_1 > 0$ such that [10, Proof of Lemma 4.3]

$$\|\mathcal{B}^*(M\xi_1(t), t) - \mathcal{B}^*(M\xi_2(t), t)\|_{\mathcal{J}_1(\mathcal{H};\mathbb{R})} \leq c_1 \|\mathcal{B}^*(M\xi_1(t), t) - \mathcal{B}^*(M\xi_2(t), t)\|_{\mathcal{L}(\mathcal{H};\mathbb{R})} \quad (\text{A.3})$$

For brevity, we shall use $\mathcal{B}_1(t)$ for $\mathcal{B}(M\xi_1(t), t)$ and $\mathcal{B}_2(t)$ for $\mathcal{B}(M\xi_2(t), t)$. Now,

$$\begin{aligned} & \|\mathcal{B}_1(t)R^{-1}\mathcal{B}_1^*(t) - \mathcal{B}_2(t)R^{-1}\mathcal{B}_2^*(t)\|_{\mathcal{J}_1(\mathcal{H})} \\ & \leq \|\mathcal{B}_1(t)R^{-1}\|_{\mathcal{J}_1(\mathbb{R};\mathcal{H})} \|\mathcal{B}_1^*(t) - \mathcal{B}_2^*(t)\|_{\mathcal{J}_1(\mathcal{H};\mathbb{R})} \\ & \quad + \|R^{-1}\mathcal{B}_2^*(t)\|_{\mathcal{J}_1(\mathcal{H};\mathbb{R})} \|\mathcal{B}_1(t) - \mathcal{B}_2(t)\|_{\mathcal{J}_1(\mathbb{R};\mathcal{H})} \\ & = (\|\mathcal{B}_1(t)R^{-1}\|_{\mathcal{J}_1(\mathbb{R};\mathcal{H})} + \|R^{-1}\mathcal{B}_2^*(t)\|_{\mathcal{J}_1(\mathcal{H};\mathbb{R})}) \|\mathcal{B}_1^*(t) - \mathcal{B}_2^*(t)\|_{\mathcal{J}_1(\mathcal{H};\mathbb{R})} \\ & \leq c_2 \|\mathcal{B}_1^*(t) - \mathcal{B}_2^*(t)\|_{\mathcal{J}_1(\mathcal{H};\mathbb{R})} \\ & \leq c_2 c_1 l(|M(\xi_1(t) - \xi_2(t))|_2) \end{aligned} \quad (\text{A.4})$$

for some $c_2 > 0$ where the last inequality follows from (A.2) and (A.3).

We now continue to prove that $K^c : C([0, t_f]; \mathbb{R}^n) \rightarrow \mathbb{R}$ is a continuous mapping. For brevity, we use $\Pi_1^c(0)$ and $\Pi_2^c(0)$ for the Riccati operator associated with trajectory ξ_1 and ξ_2 , respectively. We also suppress the usage of the time argument of the integrand in the following derivation. We start with $K^c(\xi_1) - K^c(\xi_2)$:

$$\begin{aligned} K^c(\xi_1) - K^c(\xi_2) &= \langle \mathcal{Z}_0, \int_0^{t_f} \mathcal{S}^* \Pi_1^c \mathcal{B}_1 R^{-1} (\mathcal{B}_1^* \Pi_1^c - \mathcal{B}_2^* \Pi_2^c) \mathcal{S} d\tau \mathcal{Z}_0 \rangle \\ & \quad + \langle \mathcal{Z}_0, \int_0^{t_f} \mathcal{S}^* (\Pi_1^c \mathcal{B}_1 - \Pi_2^c \mathcal{B}_2) R^{-1} \mathcal{B}_2^* \Pi_2^c \mathcal{S} d\tau \mathcal{Z}_0 \rangle. \end{aligned}$$

Our analysis continues with the first term on the right-hand side, because the second term can be analyzed similarly using the following derivation:

$$\begin{aligned}
& \langle \mathcal{Z}_0, \int_0^{t_f} \mathcal{S}^* \Pi_1^c \mathcal{B}_1 R^{-1} (\mathcal{B}_1^* \Pi_1^c - \mathcal{B}_2^* \Pi_2^c) \mathcal{S} d\tau \mathcal{Z}_0 \rangle \\
&= \langle \mathcal{Z}_0, \int_0^{t_f} \mathcal{S}^* \Pi_1^c \mathcal{B}_1 R^{-1} \mathcal{B}_1^* (\Pi_1^c - \Pi_2^c) \mathcal{S} d\tau \mathcal{Z}_0 \rangle \\
&+ \langle \mathcal{Z}_0, \int_0^{t_f} \mathcal{S}^* \Pi_1^c \mathcal{B}_1 R^{-1} (\mathcal{B}_1^* - \mathcal{B}_2^*) \Pi_2^c \mathcal{S} d\tau \mathcal{Z}_0 \rangle. \tag{A.5}
\end{aligned}$$

Take absolute values on both sides, we get

$$\begin{aligned}
& |\langle \mathcal{Z}_0, \int_0^{t_f} \mathcal{S}^* \Pi_1^c \mathcal{B}_1 R^{-1} (\mathcal{B}_1^* \Pi_1^c - \mathcal{B}_2^* \Pi_2^c) \mathcal{S} d\tau \mathcal{Z}_0 \rangle| \\
&\leq \|\mathcal{Z}_0\|_{\mathcal{H}}^2 \int_0^{t_f} (\|\mathcal{S}^*\|_{\mathcal{L}(\mathcal{H})} \|\Pi_1^c \mathcal{B}_1 R^{-1} \mathcal{B}_1^*\|_{\mathcal{L}(\mathcal{H})} \|\Pi_1^c - \Pi_2^c\|_{\mathcal{L}(\mathcal{H})} \|\mathcal{S}\|_{\mathcal{L}(\mathcal{H})}) d\tau \\
&+ \|\mathcal{Z}_0\|_{\mathcal{H}}^2 \int_0^{t_f} (\|\mathcal{S}^*\|_{\mathcal{L}(\mathcal{H})} \|\Pi_1^c \mathcal{B}_1 R^{-1}\|_{\mathcal{L}(\mathbb{R}; \mathcal{H})} \|\Pi_2^c\|_{\mathcal{L}(\mathcal{H})} \|\mathcal{B}_1^* - \mathcal{B}_2^*\|_{\mathcal{L}(\mathcal{H}; \mathbb{R})} \|\mathcal{S}\|_{\mathcal{L}(\mathcal{H})}) d\tau.
\end{aligned}$$

Since there exists c_{t_f} such that $\|\mathcal{S}(t)\|_{\mathcal{L}(\mathcal{H})} \leq c_{t_f}$ and $\|\mathcal{S}^*(t)\|_{\mathcal{L}(\mathcal{H})} \leq c_{t_f}$ for all $t \in [0, t_f]$, it follows that

$$\begin{aligned}
& |\langle \mathcal{Z}_0, \int_0^{t_f} \mathcal{S}^* \Pi_1^c \mathcal{B}_1 R^{-1} (\mathcal{B}_1^* \Pi_1^c - \mathcal{B}_2^* \Pi_2^c) \mathcal{S} d\tau \mathcal{Z}_0 \rangle| \\
&\leq \|\mathcal{Z}_0\|_{\mathcal{H}}^2 c_{t_f}^2 \int_0^{t_f} (\|\Pi_1^c \mathcal{B}_1 R^{-1} \mathcal{B}_1^*\|_{\mathcal{L}(\mathcal{H})} \|\Pi_1^c - \Pi_2^c\|_{\mathcal{L}(\mathcal{H})} \\
&+ \|\Pi_1^c \mathcal{B}_1 R^{-1}\|_{\mathcal{L}(\mathbb{R}; \mathcal{H})} \|\Pi_2^c\|_{\mathcal{L}(\mathcal{H})} \|\mathcal{B}_1^* - \mathcal{B}_2^*\|_{\mathcal{L}(\mathcal{H}; \mathbb{R})}) d\tau.
\end{aligned}$$

Since $\mathcal{J}_q(\mathcal{H}) \hookrightarrow \mathcal{L}(\mathcal{H})$ [11], there exists $c_3 > 0$ such that $\|\Pi_1^c(\tau) - \Pi_2^c(\tau)\|_{\mathcal{L}(\mathcal{H})} \leq c_3 \|\Pi_1^c(\tau) - \Pi_2^c(\tau)\|_{\mathcal{J}_q(\mathcal{H})}$ for $1 \leq q < \infty$. Hence, the following inequality holds for

$q = 1$:

$$\begin{aligned}
& |\langle \mathcal{Z}_0, \int_0^{t_f} \mathcal{S}^* \Pi_1^c \mathcal{B}_1 R^{-1} (\mathcal{B}_1^* \Pi_1^c - \mathcal{B}_2^* \Pi_2^c) \mathcal{S} d\tau \mathcal{Z}_0 \rangle | \\
& \leq \|\mathcal{Z}_0\|_{\mathcal{H}}^2 c_{t_f}^2 \int_0^{t_f} (c_3 \|\Pi_1^c \mathcal{B}_1 R^{-1} \mathcal{B}_1^*\|_{\mathcal{L}(\mathcal{H})} \|\Pi_1^c - \Pi_2^c\|_{\mathcal{J}_1(\mathcal{H})} \\
& \quad + \|\Pi_1^c \mathcal{B}_1 R^{-1}\|_{\mathcal{L}(\mathbb{R}; \mathcal{H})} \|\Pi_2^c\|_{\mathcal{L}(\mathcal{H})} \|\mathcal{B}_1^* - \mathcal{B}_2^*\|_{\mathcal{L}(\mathcal{H}; \mathbb{R})}) d\tau \\
& \leq \|\mathcal{Z}_0\|_{\mathcal{H}}^2 c_{t_f}^2 \left(c_3 \int_0^{t_f} \|\Pi_1^c \mathcal{B}_1 R^{-1} \mathcal{B}_1^*\|_{\mathcal{L}(\mathcal{H})} d\tau \operatorname{ess\,sup}_{t \in [0, t_f]} \|\Pi_1^c(t) - \Pi_2^c(t)\|_{\mathcal{J}_1(\mathcal{H})} \right. \\
& \quad \left. + \int_0^{t_f} \|\Pi_1^c \mathcal{B}_1 R^{-1}\|_{\mathcal{L}(\mathbb{R}; \mathcal{H})} \|\Pi_2^c\|_{\mathcal{L}(\mathcal{H})} d\tau \operatorname{ess\,sup}_{t \in [0, t_f]} \|\mathcal{B}_1^*(t) - \mathcal{B}_2^*(t)\|_{\mathcal{L}(\mathcal{H}; \mathbb{R})} \right). \tag{A.6}
\end{aligned}$$

We now wish to bound

$$\operatorname{ess\,sup}_{t \in [0, t_f]} \|\Pi_1^c(t) - \Pi_2^c(t)\|_{\mathcal{J}_1(\mathcal{H})} \quad \text{and} \quad \operatorname{ess\,sup}_{t \in [0, t_f]} \|\mathcal{B}_1^*(t) - \mathcal{B}_2^*(t)\|_{\mathcal{L}(\mathcal{H}; \mathbb{R})}. \tag{A.7}$$

Notice that $\Pi^c(\cdot)$ is continuous on $[0, t_f]$ into $\mathcal{J}_1(\mathcal{H})$ (Lemma 2.1). Hence,

$$\operatorname{ess\,sup}_{t \in [0, t_f]} \|\Pi_1^c(t) - \Pi_2^c(t)\|_{\mathcal{J}_1(\mathcal{H})} = \sup_{t \in [0, t_f]} \|\Pi_1^c(t) - \Pi_2^c(t)\|_{\mathcal{J}_1(\mathcal{H})}. \tag{A.8}$$

By (2.14), the mapping $\Pi^c : [0, t_f] \rightarrow \mathcal{J}_1(\mathcal{H})$ varies continuously with respect to $\bar{\mathcal{B}}\bar{\mathcal{B}}^*(\cdot)$ [11] in $\sup_{t \in [0, t_f]} \|\cdot\|_{\mathcal{J}_1(\mathcal{H})}$ -norm. Hence, there exists $c_4 > 0$ such that

$$\sup_{t \in [0, t_f]} \|\Pi_1^c(t) - \Pi_2^c(t)\|_{\mathcal{J}_1(\mathcal{H})} \leq \sup_{t \in [0, t_f]} c_4 \|\bar{\mathcal{B}}_1 \bar{\mathcal{B}}_1^*(t) - \bar{\mathcal{B}}_2 \bar{\mathcal{B}}_2^*(t)\|_{\mathcal{J}_1(\mathcal{H})}. \tag{A.9}$$

Recall $\mathcal{B}(\cdot)R^{-1}\mathcal{B}^*(\cdot) = \bar{\mathcal{B}}\bar{\mathcal{B}}^*(\cdot)$ and combine (A.4), (A.8), and (A.9):

$$\operatorname{ess\,sup}_{t \in [0, t_f]} \|\Pi_1^c(t) - \Pi_2^c(t)\|_{\mathcal{J}_1(\mathcal{H})} \leq \sup_{t \in [0, t_f]} c_4 c_1 c_2 l (|M(\xi_1(t) - \xi_2(t))|_2). \quad (\text{A.10})$$

It remains to bound $\operatorname{ess\,sup}_{t \in [0, t_f]} \|\mathcal{B}_1^*(t) - \mathcal{B}_2^*(t)\|_{\mathcal{L}(\mathcal{H}; \mathbb{R})}$. By (A.2),

$$\operatorname{ess\,sup}_{t \in [0, t_f]} \|\mathcal{B}_1^*(t) - \mathcal{B}_2^*(t)\|_{\mathcal{L}(\mathcal{H}; \mathbb{R})} \leq \operatorname{ess\,sup}_{t \in [0, t_f]} l (|M(\xi_1(t) - \xi_2(t))|_2). \quad (\text{A.11})$$

Finally, plugging (A.10) and (A.11) into (A.6), it follows that $|K^c(\xi_1) - K^c(\xi_2)| \rightarrow 0$ as $\sup_{t \in [0, t_f]} |\xi_1(t) - \xi_2(t)| \rightarrow 0$, which concludes the continuity of the mapping $K^c(\cdot)$. \square

A.2 Proof of Lemma 2.5

Proof. Without loss of generality, consider the case of one mobile sensor, i.e., $m_s = 1$. The case of multiple sensors follows naturally. We first show a consequence of the output operator \mathcal{C}^* being continuous with respect to location. Consider two sensor states $\zeta_1, \zeta_2 \in C([0, t_f]; \mathbb{R}^n)$. For any $\phi \in \mathcal{H} = L^2(\Omega)$ and all $t \in [0, t_f]$,

$$\begin{aligned} |\mathcal{C}^*(M\zeta_1(t), t)\phi - \mathcal{C}^*(M\zeta_2(t), t)\phi| &\leq \|\mathcal{C}(M\zeta_1(t), t) - \mathcal{C}(M\zeta_2(t), t)\|_{L^2(\Omega)} \|\phi\|_{L^2(\Omega)} \\ &\leq l (|M(\zeta_1(t) - \zeta_2(t))|_2) \|\phi\|_{L^2(\Omega)}, \end{aligned} \quad (\text{A.12})$$

where we use the fact that $\mathcal{C}(\cdot, \cdot)$ is the integral kernel of $\mathcal{C}^*(\cdot, \cdot)$. Hence,

$$\|\mathcal{C}^*(M\zeta_1(t), t) - \mathcal{C}^*(M\zeta_2(t), t)\|_{\mathcal{L}(\mathcal{H}; \mathbb{R})} \leq l(|M(\zeta_1(t) - \zeta_2(t))|_2). \quad (\text{A.13})$$

Since \mathbb{R} is finite-dimensional, there exists $c_5 > 0$ such that [12, proof of Lemma 4.3]

$$\|\mathcal{C}^*(M\zeta_1(t), t) - \mathcal{C}^*(M\zeta_2(t), t)\|_{\mathcal{J}_1(\mathcal{H}; \mathbb{R})} \leq c_5 \|\mathcal{C}^*(M\zeta_1(t), t) - \mathcal{C}^*(M\zeta_2(t), t)\|_{\mathcal{L}(\mathcal{H}; \mathbb{R})}. \quad (\text{A.14})$$

For brevity, we shall use $\mathcal{C}_1(t)$ for $\mathcal{C}(M\zeta_1(t), t)$ and $\mathcal{C}_2(t)$ for $\mathcal{C}(M\zeta_2(t), t)$. Now,

$$\begin{aligned} & \|\mathcal{C}_1(t)R^{-1}\mathcal{C}_1^*(t) - \mathcal{C}_2(t)R^{-1}\mathcal{C}_2^*(t)\|_{\mathcal{J}_1(\mathcal{H})} \\ & \leq \|\mathcal{C}_1(t)R^{-1}\|_{\mathcal{J}_1(\mathbb{R}; \mathcal{H})} \|\mathcal{C}_1^*(t) - \mathcal{C}_2^*(t)\|_{\mathcal{J}_1(\mathcal{H}; \mathbb{R})} + \|R^{-1}\mathcal{C}_2^*(t)\|_{\mathcal{J}_1(\mathcal{H}; \mathbb{R})} \|\mathcal{C}_1(t) - \mathcal{C}_2(t)\|_{\mathcal{J}_1(\mathbb{R}; \mathcal{H})} \\ & = \left(\|\mathcal{C}_1(t)R^{-1}\|_{\mathcal{J}_1(\mathbb{R}; \mathcal{H})} + \|R^{-1}\mathcal{C}_2^*(t)\|_{\mathcal{J}_1(\mathcal{H}; \mathbb{R})} \right) \|\mathcal{C}_1^*(t) - \mathcal{C}_2^*(t)\|_{\mathcal{J}_1(\mathcal{H}; \mathbb{R})} \\ & \leq c_6 \|\mathcal{C}_1^*(t) - \mathcal{C}_2^*(t)\|_{\mathcal{J}_1(\mathcal{H}; \mathbb{R})} \\ & \leq c_6 c_5 l(|M(\zeta_1(t) - \zeta_2(t))|_2) \end{aligned} \quad (\text{A.15})$$

for some $c_6 > 0$, where the last inequality follows from (A.13) and (A.14).

By (2.25), the mapping $\Pi^e : [0, t_f] \rightarrow \mathcal{J}_1(\mathcal{H})$ varies continuously with respect to $\bar{\mathcal{C}}\bar{\mathcal{C}}^*(\cdot)$ [12] in $\sup_{t \in [0, t_f]} \|\cdot\|_{\mathcal{J}_1(\mathcal{H})}$ -norm. Hence, there exists $c_7 > 0$ such that

$$\sup_{t \in [0, t_f]} \|\Pi_1^e(t) - \Pi_2^e(t)\|_{\mathcal{J}_1(\mathcal{H})} \leq \sup_{t \in [0, t_f]} c_7 \|\bar{\mathcal{C}}_1\bar{\mathcal{C}}_1^*(t) - \bar{\mathcal{C}}_2\bar{\mathcal{C}}_2^*(t)\|_{\mathcal{J}_1(\mathcal{H})}. \quad (\text{A.16})$$

Now, we have

$$\begin{aligned}
|K^e(\zeta_1) - K^e(\zeta_2)| &= \left| \int_0^{t_f} \text{Tr}(\Pi_1^e(t)) - \text{Tr}(\Pi_2^e(t)) dt \right| \\
&= \left| \int_0^{t_f} \|\Pi_1^e(t)\|_{\mathcal{J}_1(\mathcal{H})} - \|\Pi_2^e(t)\|_{\mathcal{J}_1(\mathcal{H})} dt \right| \\
&\leq \int_0^{t_f} \|\Pi_1^e(t) - \Pi_2^e(t)\|_{\mathcal{J}_1(\mathcal{H})} dt \\
&\leq \sup_{t \in [0, t_f]} \|\Pi_1^e(t) - \Pi_2^e(t)\|_{\mathcal{J}_1(\mathcal{H})} t_f. \tag{A.17}
\end{aligned}$$

It follows from (A.15)–(A.17) that

$$|K^e(\zeta_1) - K^e(\zeta_2)| \leq c_5 c_6 c_7 t_f \sup_{t \in [0, t_f]} l(|M(\zeta_1(t) - \zeta_2(t))|_2),$$

and we conclude the continuity of $K^e(\cdot)$. \square

A.3 Proof of Lemma 2.7

Proof. Since the norm defined on \mathcal{H}_N is inherited from that of \mathcal{H} , the proof follows from the same derivation of Lemma 2.3. \square

A.4 Proof of Lemma 2.9

Proof. Since the norm defined on \mathcal{H}_N is inherited from that of \mathcal{H} , the proof follows from the same derivation of Lemma 2.5's proof. \square

A.5 Proof of Theorem 3.1

The proof of Theorem 3.1 uses Definition A.1 and Theorem A.1 (stated below) to establish the existence of an optimal solution of (Pc1).

Definition A.1. *Suppose $(X, \|\cdot\|)$ is a normed linear space.*

1. *A sequence $\{x_k\} \subset X$ is weakly convergent to an $x \in X$, denoted by $x_k \rightharpoonup x$, if $\lim_{k \rightarrow \infty} (x^*, x_k) = (x^*, x)$ for all x^* belonging to the dual space X^* .*
2. *A subset $A \subset X$ is weakly sequentially closed if $\{x_k\} \subset A$ and $x_k \rightharpoonup x$ implies $x \in A$.*
3. *A subset $A \subset X$ is weakly sequentially compact if for every sequence $\{x_k\} \subset A$ there exists a subsequence $\{x_{k_i}\} \subset \{x_k\}$ and an $x \in A$ with $x_{k_i} \rightharpoonup x$.*
4. *Suppose $A \subset X$ and $f : A \rightarrow \mathbb{R}$. The mapping f is weakly sequentially lower semicontinuous on A if $\{x_k\} \subset A$ and $x_k \rightharpoonup x \in A$ implies $f(x) \leq \liminf_{k \rightarrow \infty} f(x_k)$.*

Theorem A.1. *[88, Theorem 6.1.4] Suppose $(X, \|\cdot\|)$ is a normed linear space, $M_0 \subset X$ is weakly sequentially compact and $f : M_0 \rightarrow \mathbb{R}$ is weakly sequentially lower semicontinuous on M_0 . Then there exists an $\bar{x} \in M_0$ such that $f(\bar{x}) = \inf\{f(x) : x \in M_0\}$.*

Proof of Theorem 3.1. Without loss of generality, we consider the case of one mobile actuator, i.e., $m_a = 1$. The case of $m_a \geq 2$ follows naturally.

We want to apply Theorem [A.1](#) to prove that the minimum of the cost function of [\(Pc1\)](#) is achieved on a subset \mathcal{P}_0 (defined below) of the admissible set in which the cost of guidance is upper bounded. Consider problem [\(Pc1\)](#)'s admissible set of guidance functions $\mathcal{P} = \{p \in L^2([0, t_f]; \mathbb{R}^m) : p(t) \in P, t \in [0, t_f]\}$. Since there exists $p_0 \in \mathcal{P}$ such that $J_{(\text{Pc1})}(p_0) < \infty$ (e.g., a zero guidance function that yields a stationary sensor), we define $\mathcal{P}_0 = \{p \in \mathcal{P} : J_{(\text{Pc1})}(p) \leq J_{(\text{Pc1})}(p_0)\}$. We wish to prove [Condition-1](#), [Condition-2](#), and [Condition-3](#) stated below:

[Condition-1](#): The set \mathcal{P}_0 is bounded.

[Condition-2](#): The set \mathcal{P}_0 is weakly sequentially closed.

[Condition-3](#): The mapping $J_{(\text{Pc1})}(\cdot) : \mathcal{P} \rightarrow \mathbb{R}$ is weakly sequentially lower semicontinuous on \mathcal{P}_0 .

[Condition-1](#) and [Condition-2](#) imply that \mathcal{P}_0 is weakly sequentially compact.

By Theorem [A.1](#), problem [\(Pc1\)](#) has a solution when [Condition-1](#)–[Condition-3](#) hold.

Before proving these three conditions, we define a mapping $T : L^2([0, t_f]; \mathbb{R}^m) \rightarrow C([0, t_f]; \mathbb{R}^n)$ by $(Tp)(t) = \xi(t) = e^{\alpha t} \xi_0 + \int_0^t e^{\alpha(t-\tau)} \beta p(\tau) d\tau$ for $t \in [0, t_f]$. The continuity of the map T is straightforward [[88](#)], i.e., there exists $c_8 > 0$ such that $\|Tp\|_{C([0, t_f]; \mathbb{R}^n)} \leq c_8 \|p\|_{C([0, t_f]; \mathbb{R}^m)}$.

Proof of Condition-1: Suppose $p \in \mathcal{P}_0$, then

$$\begin{aligned}
J_{(\mathbf{Pc1})}(p_0) &\geq J_{(\mathbf{Pc1})}(p) \\
&= h_f(Tp(t_f)) + \int_0^{t_f} h(Tp(t), t) + g(p(t), t) dt \\
&\quad + \langle \mathcal{Z}_0, \Pi(0)\mathcal{Z}_0 \rangle \\
&\geq \int_0^{t_f} d_1 |p(t)|_2^2 dt \\
&= d_1 \|p\|_{L^2([0, t_f]; \mathbb{R}^m)}^2, \tag{A.18}
\end{aligned}$$

where the second inequality follows from the nonnegativity of $h_f(\cdot)$, $h(\cdot, \cdot)$, and $\langle \mathcal{Z}_0, \Pi(0)\mathcal{Z}_0 \rangle$. Since $d_1 > 0$, the boundedness of \mathcal{P}_0 follows.

Proof of Condition-2: Suppose $\{p_k\} \subset \mathcal{P}_0$ and $\{p_k\}$ converges weakly to p (denoted by $p_k \rightharpoonup p$). We want to show $p \in \mathcal{P}_0$. We start with proving that \mathcal{P} is weakly sequentially closed and, hence, $p \in \mathcal{P}$. Subsequently, we show $J_{(\mathbf{Pc1})}(p) \leq J_{(\mathbf{Pc1})}(p_0)$ to conclude Condition-2.

To show that the set \mathcal{P} is weakly sequentially closed, by [80, Theorem 2.11], it suffices to show that \mathcal{P} is closed and convex. Let $\{q_k\} \subset \mathcal{P}$ and $q_k \rightarrow q$. We want to show $q \in \mathcal{P}$, i.e., $q \in L^2([0, t_f]; \mathbb{R}^m)$ and $q(t) \in P$ for $t \in [0, t_f]$. Since $L^2([0, t_f]; \mathbb{R}^m)$ is complete, we can choose a subsequence $\{q_{k_j}\} \subset \mathcal{P}$ that converges to q pointwise almost everywhere on $[0, t_f]$ [92, p. 53]. Since P is closed (assumption (C9)), $q(t) \in P$ for almost all $t \in [0, t_f]$. Hence, \mathcal{P} is closed. The convexity of \mathcal{P} follows from that of P (assumption (C9)), i.e., if $p_1, p_2 \in \mathcal{P}$, then $\lambda p_1 + (1 - \lambda)p_2 \in L^2([0, t_f]; \mathbb{R}^m)$ and $\lambda p_1(t) + (1 - \lambda)p_2(t) \in P$ for $t \in [0, t_f]$ and $\lambda \in [0, 1]$.

What remain to be shown is $J_{(\mathbf{Pc1})}(p) \leq J_{(\mathbf{Pc1})}(p_0)$. Since $p_k \rightharpoonup p$, by definition, we have $Tp_k \rightarrow Tp$. We now show that the sequence $\{Tp_k\}$ contains a uniformly convergent subsequence in $C([0, t_f]; \mathbb{R}^n)$. The sequence $\{Tp_k\} \subset C([0, t_f]; \mathbb{R}^n)$ is uniformly bounded and uniformly equicontinuous for the following reasons: Since $\|Tp_k\|_{C([0, t_f]; \mathbb{R}^n)} \leq c_8 \|p_k\|_{L^2([0, t_f]; \mathbb{R}^m)}$, it follows that $\|Tp_k\|_{C([0, t_f]; \mathbb{R}^n)}$ is uniformly bounded, because $\{p_k\} \subset \mathcal{P}_0$ which is a bounded set. For $s, t \in [0, t_f]$, we have

$$\begin{aligned} |Tp_k(t) - Tp_k(s)|_1 &= \left| \int_s^t \alpha Tp_k(\tau) + \beta p_k(\tau) d\tau \right|_1 \\ &\leq |t - s| |\alpha|_1 \|Tp_k\|_{C([0, t_f]; \mathbb{R}^n)} + |t - s|^{1/2} |\beta|_2 \|p_k\|_{L^2([0, t_f]; \mathbb{R}^m)}. \end{aligned}$$

Since $\{\|p_k\|_{L^2([0, t_f]; \mathbb{R}^m)}\}$ and $\{\|Tp_k\|_{C([0, t_f]; \mathbb{R}^n)}\}$ both are uniformly bounded for all $p_k \in \mathcal{P}_0$, $\{Tp_k\}$ is uniformly equicontinuous. By the Arzelà-Ascoli Theorem [67], there is a uniformly convergent subsequence $\{Tp_{k_j}\} \subset \{Tp_k\}$.

Without loss of generality, we assume $p_k \rightharpoonup p$ and $Tp_k \rightarrow Tp$ uniformly on $[0, t_f]$, and $J_{(\mathbf{Pc1})}(p_k) \leq J_{(\mathbf{Pc1})}(p_0)$. We have $J_{(\mathbf{Pc1})}(p_0) - J_{(\mathbf{Pc1})}(p) = J_{(\mathbf{Pc1})}(p_0) - J_{(\mathbf{Pc1})}(p_k) + J_{(\mathbf{Pc1})}(p_k) - J_{(\mathbf{Pc1})}(p) \geq J_{(\mathbf{Pc1})}(p_k) - J_{(\mathbf{Pc1})}(p)$, by which, to show $J_{(\mathbf{Pc1})}(p) \leq J_{(\mathbf{Pc1})}(p_0)$, it suffices to show $J_{(\mathbf{Pc1})}(p) \leq \liminf_{k \rightarrow \infty} J_{(\mathbf{Pc1})}(p_k)$, which is to show

$$\begin{aligned} &h_f(Tp(t_f)) + \int_0^{t_f} h(Tp(t), t) + g(p(t), t) dt + \langle \mathcal{Z}_0, \Pi(0) \mathcal{Z}_0 \rangle \\ &\leq \liminf_{k \rightarrow \infty} h_f(Tp_k(t_f)) + \int_0^{t_f} h(Tp_k(t), t) + g(p_k(t), t) dt + \langle \mathcal{Z}_0, \Pi^k(0) \mathcal{Z}_0 \rangle, \quad (\text{A.19}) \end{aligned}$$

where $\Pi^k(0)$ is the solution of (2.14) associated with actuator state Tp_k . Since

$\{Tp_k\}$ converges to Tp uniformly on $[0, t_f]$, the continuity of $h_f(\cdot)$ implies

$$h_f(Tp(t_f)) = \liminf_{k \rightarrow \infty} h_f(Tp_k(t_f)); \quad (\text{A.20})$$

Fatou's lemma [67] implies

$$\int_0^{t_f} h(Tp(t), t) dt \leq \liminf_{k \rightarrow \infty} \int_0^{t_f} h(Tp_k(t), t) dt; \quad (\text{A.21})$$

and Lemma 2.3 implies

$$\langle \mathcal{Z}_0, \Pi(0)\mathcal{Z}_0 \rangle = \liminf_{k \rightarrow \infty} \langle \mathcal{Z}_0, \Pi^k(0)\mathcal{Z}_0 \rangle. \quad (\text{A.22})$$

To prove (A.19), based on (A.20)–(A.22), it suffices to show

$$\int_0^{t_f} g(p(t), t) dt \leq \liminf_{k \rightarrow \infty} \int_0^{t_f} g(p_k(t), t) dt. \quad (\text{A.23})$$

By contradiction, assume there is $\lambda > 0$ such that

$$\liminf_{k \rightarrow \infty} \int_0^{t_f} g(p_k(t), t) dt < \lambda < \int_0^{t_f} g(p(t), t) dt. \quad (\text{A.24})$$

There exists a subsequence $\{p_{k_j}\} \subset \{p_k\}$ such that $O_\lambda = \{q \in L^2([0, t_f]; \mathbb{R}^m) : \int_0^{t_f} g(q(t), t) dt \leq \lambda\}$ and $\{p_{k_j}\} \subset O_\lambda$. We wish to show that O_λ is weakly sequentially closed. By [80, Theorem 2.11], it suffices to show that O_λ is convex and closed. Since $g(\cdot, t) : \mathbb{R}^m \rightarrow \mathbb{R}$ is convex for all $t \in [0, t_f]$, it follows that O_λ is convex.

Let $\{q_k\} \subset O_\lambda$ and $\|q_k - q\|_{L^2([0, t_f]; \mathbb{R}^m)}$ converges to 0 as $k \rightarrow \infty$. We can choose a subsequence $\{q_{k_j}\} \subset \{q_k\}$ such that q_{k_j} converges to q pointwise almost everywhere on $[0, t_f]$ [92, p. 53]. Now we have

- (1) $g(q_{k_j}(t), t) \geq 0$ for all $t \in [0, t_f]$ (assumption (C11));
- (2) $\lim_{j \rightarrow \infty} g(q_{k_j}(t), t) = g(q(t), t)$ almost everywhere on $[0, t_f]$.

By Fatou's lemma [67],

$$\int_0^{t_f} g(q(t), t) dt \leq \liminf_{k \rightarrow \infty} \int_0^{t_f} g(q_{k_j}(t), t) dt \leq \lambda,$$

where the last inequality holds due to $\{q_{k_j}\} \subset O_\lambda$. Hence, $q \in O_\lambda$ and O_λ is closed.

Since O_λ is weakly sequentially closed, $p_{k_j} \rightharpoonup p$ implies that $p \in O_\lambda$, which contradicts (A.24). Hence, $J_{(\text{Pc1})}(p) \leq J_{(\text{Pc1})}(p_0)$ is proved, and we conclude Condition-2.

Proof of Condition-3: We now show that the mapping $J_{(\text{Pc1})}(\cdot) : \mathcal{P} \rightarrow \mathbb{R}$ is weakly sequentially lower semicontinuous on \mathcal{P}_0 . Suppose $\{p_k\} \subset \mathcal{P}_0$ and $p_k \rightharpoonup p \in \mathcal{P}_0$. We wish to show $J_{(\text{Pc1})}(p) \leq \liminf_{k \rightarrow \infty} J_{(\text{Pc1})}(p_k)$, which has been established when we proved $J_{(\text{Pc1})}(p) \leq J_{(\text{Pc1})}(p_0)$ in Condition-2 (starting from (A.19)).

So we conclude that the existence of a solution of problem (Pc1). □

A.6 Proof of Theorem 3.2

Proof. By contradiction, assume there are p_0^* and u_0^* minimizing (Pc) and $p_0^* \neq p^*$ and $u_0^* \neq u^*$ such that $J_{(\text{Pc})}^*(u_0^*, p_0^*) < J_{(\text{Pc})}(u^*, p^*) = J_{(\text{Pc1})}(p^*)$. Denote \bar{u}_0^* the optimal control (2.12) associated with actuator trajectory steered by p_0^* . It follows that $J_{(\text{Pc})}^*(u_0^*, p_0^*) = J_{(\text{Pc})}(\bar{u}_0^*, p_0^*)$, because $J_{(\text{Pc})}^*(u_0^*, p_0^*) > J_{(\text{Pc})}(\bar{u}_0^*, p_0^*)$ violates the opti-

mality of u_0^* and $J_{(\text{Pc})}^*(u_0^*, p_0^*) < J_{(\text{Pc})}(\bar{u}_0^*, p_0^*)$ contradicts the fact that \bar{u}_0^* minimizes the quadratic cost $J(\mathcal{Z}, u)$ (see Lemma 2.2). Since $J_{(\text{Pc})}(\bar{u}_0^*, p_0^*) = \langle \mathcal{Z}_0, \Pi_0^*(0)\mathcal{Z}_0 \rangle + J_m(\xi_0^*, p_0^*) = J_{(\text{Pc1})}(p_0^*) < J_{(\text{Pc1})}^*(p^*)$, where $\Pi_0^*(0)$ associates with trajectory ξ_0^* steered by p_0^* , it follows that p^* is not an optimal solution of (Pc1), which contradicts the optimality of p^* for (Pc1). \square

A.7 Proof of Theorem 3.3

Proof. Since $\langle Z_{0,N}, \Pi_N(0)Z_{0,N} \rangle \geq 0$ and the mapping $K_N^c : C([0, t_f]; \mathbb{R}^n) \rightarrow \mathbb{R}^+$ is continuous (see Lemma 2.7), the proof is analogous to that of Theorem 3.1, where we use $\langle Z_{0,N}, \Pi_N(0)Z_{0,N} \rangle$ to substitute $\langle \mathcal{Z}_0, \Pi(0)\mathcal{Z}_0 \rangle$. The proof that u_N^* and p_N^* minimize problem (APc) follows from the same logic as the proof of Theorem 3.2. \square

A.8 Proof of Theorem 3.4

Before we prove Theorem 3.4, we first establish two intermediate results in Lemma A.1.

Lemma A.1. *Consider problem (Pc1) and its approximation (APc1). If assumptions (C4)–(C7) and (C9)–(C12) hold, then the following two implications hold:*

1. *For $p \in C([0, t_f]; P)$, $\lim_{N \rightarrow \infty} |J_{(\text{APc1})}(p) - J_{(\text{Pc1})}(p)| = 0$, where N is the dimension of approximation applied in (APc1).*
2. *The mapping $J_{(\text{Pc1})} : C([0, t_f]; P) \rightarrow \mathbb{R}^+$ is continuous, where $J_{(\text{Pc1})}(p) = \langle \mathcal{Z}_0, \Pi(0)\mathcal{Z}_0 \rangle + J_m(\xi, p)$. Here, the actuator state ξ follows the dynamics (2.2) steered by the guidance p , and $\Pi(0)$ follows (2.13) with the actuator state ξ .*

Proof. 1. We first prove for $p \in C([0, t_f]; P)$,

$$\lim_{N \rightarrow \infty} |J_{(\text{APc1})}(p) - J_{(\text{Pc1})}(p)| = 0. \quad (\text{A.25})$$

The limit (A.25) is established for the following reason: By Lemma 2.6,

$$\lim_{N \rightarrow \infty} \|\Pi(0) - \Pi_N(0)\|_{\mathcal{J}_q(\mathcal{H})} = 0. \quad (\text{A.26})$$

Since $\mathcal{J}_q(\mathcal{H}) \hookrightarrow \mathcal{L}(\mathcal{H})$ [11], it follows that

$$\lim_{N \rightarrow \infty} \|\Pi(0) - \Pi_N(0)\|_{\mathcal{L}(\mathcal{H})} = 0. \quad (\text{A.27})$$

The convergence (A.27) and the fact

$$\lim_{N \rightarrow \infty} \|Z_{0,N} - Z_0\|_{\mathcal{H}} = 0 \quad (\text{A.28})$$

imply that

$$\lim_{N \rightarrow \infty} |\langle Z_{0,N}, \Pi_N(0)Z_{0,N} \rangle - \langle Z_0, \Pi(0)Z_0 \rangle| = 0. \quad (\text{A.29})$$

The limit in (A.25) follows naturally since $J_{(\text{APc1})}(p) - J_{(\text{Pc1})}(p) = \langle Z_{0,N}, \Pi_N(0)Z_{0,N} \rangle - \langle Z_0, \Pi(0)Z_0 \rangle$.

2. Consider the continuous mapping $T : L^2([0, t_f]; \mathbb{R}^m) \rightarrow C([0, t_f]; \mathbb{R}^n)$ as defined in the proof of Theorem 3.1 such that $(Tp)(t) = \xi(t) = e^{\alpha t} \xi_0 + \int_0^t e^{\alpha(t-\tau)} \beta p(\tau) d\tau$ for $t \in [0, t_f]$. Since the admissible guidance is in $C([0, t_f]; \mathbb{R}^m) \subset L^2([0, t_f]; \mathbb{R}^m)$,

the continuity of T is preserved, i.e., there exists $d_2 > 0$ such that for $p_1, p_2 \in C([0, t_f]; \mathbb{R}^m)$

$$\|Tp_1 - Tp_2\|_{C([0, t_f]; \mathbb{R}^n)} \leq d_2 \|p_1 - p_2\|_{C([0, t_f]; \mathbb{R}^m)}. \quad (\text{A.30})$$

Furthermore, define the mapping $\bar{J}_m : C([0, t_f]; \mathbb{R}^m) \rightarrow \mathbb{R}^+$ by

$$\bar{J}_m(p) = J_m(Tp, p). \quad (\text{A.31})$$

Define mappings $G : C([0, t_f]; \mathbb{R}^m) \rightarrow \mathbb{R}^+$, $H : C([0, t_f]; \mathbb{R}^n) \rightarrow \mathbb{R}^+$, and $H_f : C([0, t_f]; \mathbb{R}^n) \rightarrow \mathbb{R}^+$ such that

$$G(p) = \int_0^{t_f} g(p(t), t) dt, \quad (\text{A.32})$$

$$H(p) = \int_0^{t_f} h(Tp(t), t) dt, \quad (\text{A.33})$$

$$H_f(p) = h_f(Tp(t_f)). \quad (\text{A.34})$$

We first show the mapping \bar{J}_m is continuous by showing that the mappings G , H , and H_f are continuous since $\bar{J}_m(p) = G(p) + H(p) + H_f(p)$.

Let $p_1, p_2 \in \mathcal{P}(p_{\max}, a_{\max})$. Both the set of admissible guidance's values $P_0 = \cup_{t \in [0, t_f]} \{p(t) : p \in \mathcal{P}(p_{\max}, a_{\max})\}$ and the interval $[0, t_f]$ are closed and bounded (hence compact). Since $g : P_0 \times [0, t_f] \rightarrow \mathbb{R}^+$ is continuous, by the Heine-Cantor Theorem [76, Proposition 5.8.2], g is uniformly continuous, i.e., for all $\epsilon > 0$ there

exists $\delta > 0$ such that for all $t \in [0, t_f]$

$$|p_1(t) - p_2(t)| < \delta \Rightarrow |g(p_1(t), t) - g(p_2(t), t)| < \epsilon. \quad (\text{A.35})$$

Hence, it follows that

$$\begin{aligned} \|p_1 - p_2\|_{C([0, t_f]; \mathbb{R}^m)} &= \sup_{t \in [0, t_f]} |p_1(t) - p_2(t)| < \delta, \\ \Rightarrow |g(p_1(t), t) - g(p_2(t), t)| &< \epsilon, \quad \forall t \in [0, t_f]. \end{aligned} \quad (\text{A.36})$$

Therefore, for all $\epsilon > 0$ there exists $\delta > 0$ such that $\|p_1 - p_2\|_{C([0, t_f]; \mathbb{R}^m)} < \delta$ implies

$$\int_0^{t_f} |g(p_1(t), t) - g(p_2(t), t)| dt < \epsilon t_f, \quad (\text{A.37})$$

which concludes the continuity of the mapping G .

Since the continuous image of a compact set is compact [76, Proposition 5.5.1], the image set $T(\mathcal{P}(p_{\max}, a_{\max}))$ is compact, i.e., the set $\Xi = \{\xi \in C([0, t_f]; \mathbb{R}^n) : \xi = Tp, p \in \mathcal{P}(p_{\max}, a_{\max})\}$ is compact. The compactness of Ξ implies that the set of actuator state's values $\xi(t)$, $\Xi_0 = \cup_{t \in [0, t_f]} \{\xi(t) | \xi \in \Xi\}$, is closed. Furthermore, since $\|Tp\|_{C([0, t_f]; \mathbb{R}^n)}$ is bounded (see (A.30)) and Ξ_0 is finite-dimensional, the set Ξ_0 is compact. The compactness of Ξ_0 and continuity of the function $h : \Xi_0 \times [0, t_f] \rightarrow \mathbb{R}^+$ implies that h is uniformly continuous by the Heine-Cantor Theorem [76, Proposition 5.8.2]. Hence, for all $\epsilon > 0$ there exists $\delta > 0$ such that if

$\|p_1 - p_2\|_{C([0,t_f];\mathbb{R}^m)} < \delta/d_2$, which implies $\|Tp_1 - Tp_2\|_{C([0,t_f];\mathbb{R}^n)} < \delta$, then

$$\int_0^{t_f} |h(Tp_1(t), t) - h(Tp_2(t), t)| dt \leq \epsilon t_f, \quad (\text{A.38})$$

which concludes the continuity of the mapping H .

The mapping H_f is continuous because for all $\epsilon > 0$ there exists $\delta > 0$ such that if $\|p_1 - p_2\|_{C([0,t_f];\mathbb{R}^m)} < \delta/d$, which implies $\sup_{t \in [0,t_f]} |Tp_1(t) - Tp_2(t)| < \delta$, then

$$|Tp_1(t_f) - Tp_2(t_f)| < \delta, \quad (\text{A.39})$$

and, furthermore, $|H_f(p_1) - H_f(p_2)| = |h_f(Tp_1(t_f)) - h_f(Tp_2(t_f))| < \epsilon$ due to the continuity of h_f . Hence, we conclude the continuity of \bar{J}_m .

The cost function of **(Pc1)** is the sum of two parts: the PDE cost $\langle \mathcal{Z}_0, \Pi(0)\mathcal{Z}_0 \rangle$, cast as a continuous mapping $K^c : C([0, t_f]; \mathbb{R}^n) \rightarrow \mathbb{R}^+$ (see Lemma 2.3) and the mobility cost $J_m(\xi, p)$, cast as a continuous mapping $\bar{J}_m : C([0, t_f]; \mathbb{R}^m) \rightarrow \mathbb{R}^+$. Due to the continuity of the mapping T (see (A.30)), there exists $d_3 > 0$ such that

$$|K^c(Tp_1) - K^c(Tp_2)|_1 \leq d_3 \|p_1 - p_2\|_{C([0,t_f];\mathbb{R}^m)}. \quad (\text{A.40})$$

The continuity of the mapping $J_{(\text{Pc1})}$ follows from (A.40) and the continuity of \bar{J}_m . \square

We now prove Theorem 3.4.

Proof of Theorem 3.4. In the notation $J_{(\text{APc1})}(p_N^*)$, the dimension of approximation

in (APc1), which is N in this case, is indicated by its solution p_N^* . We append a subscript to indicate the dimension when it is not explicitly reflected by the argument, e.g., $J_{(\text{APc1})_N}(p)$.

We first show (3.2), i.e., $|J_{(\text{APc1})}^*(p_N^*) - J_{(\text{Pc1})}^*(p^*)| \rightarrow 0$ as $N \rightarrow \infty$. First,

$$\begin{aligned} J_{(\text{APc1})}^*(p_N^*) &= \min_{p \in \mathcal{P}(p_{\max}, a_{\max})} J_{(\text{APc1})}(p) \\ &\leq J_{(\text{APc1})}(p^*) \\ &\leq |J_{(\text{APc1})}(p^*) - J_{(\text{Pc1})}^*(p^*)| + J_{(\text{Pc1})}^*(p^*). \end{aligned}$$

Since $|J_{(\text{APc1})}(p^*) - J_{(\text{Pc1})}^*(p^*)| \rightarrow 0$ as $N \rightarrow \infty$ (see Lemma A.1-1), it follows that

$$\limsup_{N \rightarrow \infty} J_{(\text{APc1})}^*(p_N^*) \leq J_{(\text{Pc1})}^*(p^*). \quad (\text{A.41})$$

To proceed with proving (3.2), in addition to (A.41), we shall show

$$\liminf_{N \rightarrow \infty} J_{(\text{APc1})}^*(p_N^*) \geq J_{(\text{Pc1})}^*(p^*). \quad (\text{A.42})$$

Choose a convergent subsequence $\{J_{(\text{APc1})}^*(p_{N_k}^*)\}_{k=1}^{\infty}$ such that $\lim_{k \rightarrow \infty} J_{(\text{APc1})}^*(p_{N_k}^*) = \liminf_{N \rightarrow \infty} J_{(\text{APc1})}^*(p_N^*)$. Since the guidance functions defined in the set $\mathcal{P}(p_{\max}, a_{\max})$ are uniformly equicontinuous and uniformly bounded, by the Arzelà-Ascoli Theorem [67], there is a uniformly convergent subsequence of $\{p_{N_k}^*\}_{k=1}^{\infty}$ which we use the

same index $\{N_k\}_{k=1}^\infty$ to simplify notation and let the limit of $\{p_{N_k}^*\}_{k=1}^\infty$ be p_{inf}^* , i.e.,

$$\lim_{k \rightarrow \infty} \|p_{N_k}^* - p_{\text{inf}}^*\|_{C([0, t_f]; \mathbb{R}^n)} = 0. \quad (\text{A.43})$$

Now, $|J_{(\text{APc1})}^*(p_{N_k}^*) - J_{(\text{Pc1})}(p_{\text{inf}}^*)| \leq |J_{(\text{APc1})}^*(p_{N_k}^*) - J_{(\text{Pc1})}(p_{N_k}^*)| + |J_{(\text{Pc1})}(p_{N_k}^*) - J_{(\text{Pc1})}(p_{\text{inf}}^*)|$,

which implies

$$\begin{aligned} \limsup_{k \rightarrow \infty} |J_{(\text{APc1})}^*(p_{N_k}^*) - J_{(\text{Pc1})}(p_{\text{inf}}^*)| &\leq \lim_{k \rightarrow \infty} |J_{(\text{APc1})}^*(p_{N_k}^*) - J_{(\text{Pc1})}(p_{N_k}^*)| \\ &+ \lim_{k \rightarrow \infty} |J_{(\text{Pc1})}(p_{N_k}^*) - J_{(\text{Pc1})}(p_{\text{inf}}^*)|. \end{aligned} \quad (\text{A.44})$$

The first limit on the right-hand side of (A.44) is zero for the following reason. For all $p \in \mathcal{P}(p_{\text{max}}, a_{\text{max}})$, $J_{(\text{APc1})_N}(p)$ converges to $J_{(\text{Pc1})}(p)$ pointwise as the dimension of approximation $N \rightarrow \infty$ (see Lemma A.1-1). Furthermore, since the sequence of approximated PDE cost $\{\langle Z_N(0), \Pi_N(0)Z_N(0) \rangle\}_{N=1}^\infty$ is a monotonically increasing sequence, the sequence $\{J_{(\text{APc1})_N}(p)\}_{N=1}^\infty$ is a monotonically increasing sequence for each p on the compact set $\mathcal{P}(p_{\text{max}}, a_{\text{max}})$. By Dini's Theorem [68, Theorem 7.13], $|J_{(\text{APc1})_N}(p) - J_{(\text{Pc1})}(p)| \rightarrow 0$ uniformly on $\mathcal{P}(p_{\text{max}}, a_{\text{max}})$ as $N \rightarrow \infty$. By Moore-Osgood Theorem [68, Theorem 7.11], this uniform convergence and the convergence $p_{N_k}^* \rightarrow p_{\text{inf}}^*$ as $k \rightarrow \infty$ (see (A.43)) imply that $\lim_{k \rightarrow \infty} J_{(\text{Pc1})}(p_{N_k}^*) = \lim_{j \rightarrow \infty} \lim_{k \rightarrow \infty} J_{(\text{APc1})_j}^*(p_{N_k}^*)$, in which the iterated limit equals the double limit [78, p. 140], i.e.,

$$\lim_{j \rightarrow \infty} \lim_{k \rightarrow \infty} J_{(\text{APc1})_j}^*(p_{N_k}^*) = \lim_{\substack{j \rightarrow \infty \\ k \rightarrow \infty}} J_{(\text{APc1})_j}^*(p_{N_k}^*) \lim_{k \rightarrow \infty} J_{(\text{APc1})}^*(p_{N_k}^*).$$

The second limit on the right-hand side of (A.44) is zero due to Lemma A.1-2.

Hence, it follows from (A.44) that $\lim_{k \rightarrow \infty} J_{(\text{APc1})}^*(p_{N_k}^*) = J_{(\text{Pc1})}(p_{\text{inf}}^*)$, which implies

$$\begin{aligned} \liminf_{N \rightarrow \infty} J_{(\text{APc1})}^*(p_N^*) &= \lim_{k \rightarrow \infty} J_{(\text{APc1})}^*(p_{N_k}^*) \\ &= J_{(\text{Pc1})}(p_{\text{inf}}^*) \\ &\geq J_{(\text{Pc1})}^*(p^*). \end{aligned} \tag{A.45}$$

Therefore, we conclude $\lim_{N \rightarrow \infty} J_{(\text{APc1})}^*(p_N^*) = J_{(\text{Pc1})}^*(p^*)$ from (A.41) and (A.45).

Next, we show (3.3), i.e., $|J_{(\text{Pc1})}(p_N^*) - J_{(\text{Pc1})}^*(p^*)| \rightarrow 0$ as $N \rightarrow \infty$. We start with $J_{(\text{Pc1})}^*(p^*) \leq J_{(\text{Pc1})}(p_N^*)$ for all N , which implies that

$$J_{(\text{Pc1})}^*(p^*) \leq \liminf_{N \rightarrow \infty} J_{(\text{Pc1})}(p_N^*). \tag{A.46}$$

To prove (3.3), what remains to be shown is $J_{(\text{Pc1})}^*(p^*) \geq \limsup_{N \rightarrow \infty} J_{(\text{Pc1})}(p_N^*)$. Choose a convergent subsequence $\{J_{(\text{Pc1})}(p_{N_j}^*)\}_{j=1}^\infty$ such that $\lim_{j \rightarrow \infty} J_{(\text{Pc1})}(p_{N_j}^*) = \limsup_{N \rightarrow \infty} J_{(\text{Pc1})}(p_N^*)$. Since $\{p_{N_j}^*\}_{j=1}^\infty \subset \mathcal{P}(p_{\text{max}}, a_{\text{max}})$ is uniformly equicontinuous and uniformly bounded, by Arzelà-Ascoli Theorem [67], the sequence has a (uniformly) convergent subsequence which we denote with the same indices N_j to simplify notation. Denote the limit of $\{p_{N_j}^*\}_{j=1}^\infty$ by p_{sup}^* such that

$$\lim_{j \rightarrow \infty} \left\| p_{N_j}^* - p_{\text{sup}}^* \right\|_{C([0, t_f]; \mathbb{R}^m)} = 0. \tag{A.47}$$

Due to the continuity of $J_{(\mathbf{Pc1})}(\cdot)$ (see Lemma A.1-1), we have

$$J_{(\mathbf{Pc1})}(p_{\text{sup}}^*) = \lim_{j \rightarrow \infty} J_{(\mathbf{Pc1})}(p_{N_j}^*) = \limsup_{N \rightarrow \infty} J_{(\mathbf{Pc1})}(p_N^*). \quad (\text{A.48})$$

It follows that

$$\begin{aligned} J_{(\mathbf{Pc1})}(p_{\text{sup}}^*) &\leq |J_{(\mathbf{Pc1})}(p_{\text{sup}}^*) - J_{(\mathbf{Pc1})}^*(p^*)| + J_{(\mathbf{Pc1})}^*(p^*) \\ &= |J_{(\mathbf{Pc1})}(p_{\text{sup}}^*) - \lim_{N \rightarrow \infty} J_{(\mathbf{APc1})}^*(p_N^*)| + J_{(\mathbf{Pc1})}^*(p^*) \\ &= |J_{(\mathbf{Pc1})}(p_{\text{sup}}^*) - \lim_{j \rightarrow \infty} J_{(\mathbf{APc1})}^*(p_{N_j}^*)| + J_{(\mathbf{Pc1})}^*(p^*). \end{aligned} \quad (\text{A.49})$$

Since the sequence of approximated PDE cost $\{\langle Z_N(0), \Pi_N(0)Z_N(0) \rangle\}_{N=1}^{\infty}$ is monotonically increasing, the sequence $\{J_{(\mathbf{APc1})_N}(p)\}_{N=1}^{\infty}$ is a monotonically increasing sequence for each p on the compact set $\mathcal{P}(p_{\text{max}}, a_{\text{max}})$. Since $\lim_{N \rightarrow \infty} J_{(\mathbf{APc1})_N}(p) = J_{(\mathbf{Pc1})}(p)$ for all $p \in \mathcal{P}(p_{\text{max}}, a_{\text{max}})$ (see Lemma A.1-1), by Dini's Theorem [68, Theorem 7.13], the limit holds uniformly on $\mathcal{P}(p_{\text{max}}, a_{\text{max}})$ as $N \rightarrow \infty$. By Moore-Osgood Theorem [68, Theorem 7.11], this uniform convergence and the convergence $p_{N_j}^* \rightarrow p_{\text{sup}}^*$ as $j \rightarrow \infty$ (see (A.47)) imply that

$$J_{(\mathbf{Pc1})}(p_{\text{sup}}^*) = \lim_{k \rightarrow \infty} \lim_{j \rightarrow \infty} J_{(\mathbf{APc1})_k}^*(p_{N_j}^*). \quad (\text{A.50})$$

Furthermore, the iterated limit equals the double limit [78, p. 140], i.e.,

$$\lim_{k \rightarrow \infty} \lim_{j \rightarrow \infty} J_{(\mathbf{APc1})_k}^*(p_{N_j}^*) = \lim_{j \rightarrow \infty} \lim_{k \rightarrow \infty} J_{(\mathbf{APc1})_k}^*(p_{N_j}^*) = \lim_{j \rightarrow \infty} J_{(\mathbf{APc1})}^*(p_{N_j}^*). \quad (\text{A.51})$$

Hence, combining (A.49)–(A.51), we have

$$J_{(\mathbf{Pcl})}^*(p^*) \geq J_{(\mathbf{Pcl})}(p_{\text{sup}}^*) = \limsup_{N \rightarrow \infty} J_{(\mathbf{Pcl})}(p_N^*), \quad (\text{A.52})$$

from which and (A.46) we conclude the desired convergence $\lim_{N \rightarrow \infty} J_{(\mathbf{Pcl})}(p_N^*) = J_{(\mathbf{Pcl})}^*(p^*)$. \square

A.9 Proof of Theorem 4.1

Proof. Since we have proved that the uncertainty cost $\int_0^{t_f} \text{Tr}(\Pi(t))dt$ is a continuous mapping $K^e(\cdot)$ of the sensor state ζ (see Lemma 2.5), the existence of optimal guidance of (Pe) can be proved using the techniques of proving existence of solution to an optimal control (guidance) problem, for which we refer to Theorem A.1.

Without loss of generality, we consider the case of one mobile sensor, i.e., $m_s = 1$. The case of $m_s \geq 2$ follows naturally.

Our proof follows the proof in [88, Chapter 6.2] which proves existence of a solution to an optimal control problem based on functional analytic theorems. Consider problem (Pe)'s admissible set of guidance functions $\mathcal{P} = \{p \in L^2([0, t_f]; \mathbb{R}^m) : p(t) \in P, t \in [0, t_f]\}$. Since there exists $p_0 \in \mathcal{P}$ such that $J_{(\mathbf{Pe})}(p_0) < \infty$ (e.g., $p_0 = 0$ that yields a stationary sensor at ζ_0), let $\mathcal{P}_0 = \{p \in \mathcal{P} : J_{(\mathbf{Pe})}(p) \leq J_{(\mathbf{Pe})}(p_0)\}$. We wish to prove Condition-1, Condition-2, and Condition-3 stated below:

Condition-1: The set \mathcal{P}_0 is bounded.

Condition-2: The set \mathcal{P}_0 is weakly sequentially closed.

Condition-3: The mapping $J_{(\mathbf{Pe})}(\cdot) : \mathcal{P} \rightarrow \mathbb{R}^+$ is weakly sequentially lower semicon-

tinuous on \mathcal{P}_0 .

Condition-1 and Condition-2 imply that \mathcal{P}_0 is weakly sequentially compact.

By Theorem A.1, problem (Pe) has a solution when Condition-1–Condition-3 hold.

We first define a mapping $T : L^2([0, t_f]; \mathbb{R}^m) \rightarrow C([0, t_f]; \mathbb{R}^n)$ by $(Tp)(t) = \zeta(t) = e^{\alpha t} \zeta_0 + \int_0^t e^{\alpha(t-\tau)} \beta p(\tau) d\tau$ for $t \in [0, t_f]$ before we show the above three conditions. The continuity of the map T is straightforward [88], i.e., there exists $c_9 > 0$ such that $\|Tp\|_{C([0, t_f]; \mathbb{R}^n)} \leq c_9 \|p\|_{L^2([0, t_f]; \mathbb{R}^m)}$.

Proof of Condition-1: Suppose $p \in \mathcal{P}_0$, then

$$\begin{aligned}
J_{(\mathbf{Pe})}(p_0) &\geq J_{(\mathbf{Pe})}(p) \\
&= \int_0^{t_f} h(Tp(t), t) + g(p(t), t) + \text{Tr}(\Pi(t)) dt + h_f(Tp(t_f)) \\
&\geq \int_0^{t_f} d_1 |p(t)|_2^2 dt \\
&= d_1 \|p\|_{L^2([0, t_f]; \mathbb{R}^m)}^2.
\end{aligned} \tag{A.53}$$

Since $d_1 > 0$, the boundedness of \mathcal{P}_0 follows.

Proof of Condition-2: Suppose $\{p_k\} \subset \mathcal{P}_0$ and $\{p_k\}$ converges to p weakly (denoted by $p_k \rightharpoonup p$). We wish to show $p \in \mathcal{P}_0$. We start with establishing that \mathcal{P} is weakly sequentially closed and, hence, $p \in \mathcal{P}$. Subsequently, we show $J_{(\mathbf{Pe})}(p) \leq J_{(\mathbf{Pe})}(p_0)$ to conclude Condition-2.

To show that the set \mathcal{P}_0 is weakly sequentially closed, by [80, Theorem 2.11], it suffices to show that \mathcal{P} is closed and convex. Let $\{q_k\} \subset \mathcal{P}$ and $q_k \rightarrow q$. We want to show $q \in \mathcal{P}$, i.e., $q \in L^2([0, t_f]; \mathbb{R}^m)$ and $q(t) \in P$ for $t \in [0, t_f]$. Since $L^2([0, t_f]; \mathbb{R}^m)$

is complete, we can choose a subsequence $\{q_{k_j}\} \subset \mathcal{P}$ that converges to q pointwise almost everywhere on $[0, t_f]$ [92, p. 53]. Since P is closed (assumption (E9)), $q(t) \in P$ for almost all $t \in [0, t_f]$. Hence, \mathcal{P} is closed. The convexity of \mathcal{P} follows from that of P (assumption (E9)), i.e., if $p_1, p_2 \in \mathcal{P}$, then $\lambda p_1 + (1 - \lambda)p_2 \in L^2([0, t_f]; \mathbb{R}^m)$ and $\lambda p_1(t) + (1 - \lambda)p_2(t) \in P$ for $t \in [0, t_f]$ and $\lambda \in [0, 1]$.

What remain to be shown is $J_{(\mathbf{p}_e)}(p) \leq J_{(\mathbf{p}_e)}(p_0)$. Since $p_k \rightharpoonup p$, by definition, we have $Tp_k \rightarrow Tp$. We now show that the sequence $\{Tp_k\}$ contains a uniformly convergent subsequence in $C([0, t_f]; \mathbb{R}^n)$. The sequence $\{Tp_k\} \subset C([0, t_f]; \mathbb{R}^n)$ is uniformly bounded and uniformly equicontinuous for the following reasons: Since $\|Tp_k\|_{C([0, t_f]; \mathbb{R}^n)} \leq c_4 c_5 \|p_k\|_{L^2([0, t_f]; \mathbb{R}^m)}$, it follows that $\|Tp_k\|_{C([0, t_f]; \mathbb{R}^n)}$ is uniformly bounded, because $\{p_k\} \subset \mathcal{P}_0$ which is a bounded set. For $s, t \in [0, t_f]$, we have

$$\begin{aligned} |Tp_k(s) - Tp_k(t)|_1 &= \left| \int_s^t \alpha Tp_k(\tau) + \beta p_k(\tau) d\tau \right|_1 \\ &\leq |t - s| |\alpha|_1 \|Tp_k\|_{C([0, t_f]; \mathbb{R}^n)} + |t - s|^{1/2} |\beta|_2 \|p_k\|_{L^2([0, t_f]; \mathbb{R}^m)}. \end{aligned}$$

Since $\{\|p_k\|_{L^2([0, t_f]; \mathbb{R}^m)}\}$ and $\{\|Tp_k\|_{C([0, t_f]; \mathbb{R}^n)}\}$ both are uniformly bounded for all $p_k \in \mathcal{P}_0$, $\{Tp_k\}$ is uniformly equicontinuous. By the Arzelà-Ascoli Theorem [67], there is a uniformly convergent subsequence $\{Tp_{k_j}\} \subset \{Tp_k\}$.

Without loss of generality, we assume $p_k \rightharpoonup p$ and $Tp_k \rightarrow Tp$ uniformly on

$[0, t_f]$, and $J_{(\mathbf{P}_e)}(p_k) \leq J_{(\mathbf{P}_e)}(p_0)$. We have

$$\begin{aligned} J_{(\mathbf{P}_e)}(p_0) - J_{(\mathbf{P}_e)}(p) &= J_{(\mathbf{P}_e)}(p_0) - J_{(\mathbf{P}_e)}(p_k) + J_{(\mathbf{P}_e)}(p_k) - J_{(\mathbf{P}_e)}(p) \\ &\geq J_{(\mathbf{P}_e)}(p_k) - J_{(\mathbf{P}_e)}(p). \end{aligned} \quad (\text{A.54})$$

Hence, to show $J_{(\mathbf{P}_e)}(p) \leq J_{(\mathbf{P}_e)}(p_0)$, it suffices to show $J_{(\mathbf{P}_e)}(p) \leq \liminf_{k \rightarrow \infty} J_{(\mathbf{P}_e)}(p_k)$, which is to show

$$\begin{aligned} &h_f(Tp(t_f)) + \int_0^{t_f} h(Tp(t), t) + g(p(t), t) + \text{Tr}(\Pi(t)) dt \\ &\leq \liminf_{k \rightarrow \infty} h_f(Tp_k(t_f)) + \int_0^{t_f} h(Tp_k(t), t) + g(p_k(t), t) + \text{Tr}(\Pi^k(t)) dt, \end{aligned} \quad (\text{A.55})$$

where $\Pi^k(t)$ is the solution of (2.25) associated with sensor state Tp_k . Since $\{Tp_k\}$ converges to Tp uniformly on $[0, t_f]$, the continuity of $h_f(\cdot)$ implies

$$h_f(Tp(t_f)) = \liminf_{k \rightarrow \infty} h_f(Tp_k(t_f)); \quad (\text{A.56})$$

Fatou's lemma [67] implies

$$\int_0^{t_f} h(Tp(t), t) dt \leq \liminf_{k \rightarrow \infty} \int_0^{t_f} h(Tp_k(t), t) dt; \quad (\text{A.57})$$

and Lemma 2.5 implies

$$\int_0^{t_f} \text{Tr}(\Pi(t)) dt = \liminf_{k \rightarrow \infty} \int_0^{t_f} \text{Tr}(\Pi^k(t)) dt. \quad (\text{A.58})$$

To prove (A.55), based on (A.56)–(A.58), it suffices to show

$$\int_0^{t_f} g(p(t), t) dt \leq \liminf_{k \rightarrow \infty} \int_0^{t_f} g(p_k(t), t) dt. \quad (\text{A.59})$$

By contradiction, assume there is $\lambda > 0$ such that

$$\liminf_{k \rightarrow \infty} \int_0^{t_f} g(p_k(t), t) dt < \lambda < \int_0^{t_f} g(p(t), t) dt. \quad (\text{A.60})$$

There exists a subsequence $\{p_{k_j}\} \subset \{p_k\}$ such that $\{p_{k_j}\} \subset O_\lambda$ for

$$O_\lambda = \{q \in L^2([0, t_f]; \mathbb{R}^m) : \int_0^{t_f} g(q(t), t) dt \leq \lambda\}.$$

We wish to show that O_λ is weakly sequentially closed. By [88, Theorem 6.1.5], it suffices to show that O_λ is convex and closed. Since $g(\cdot, t) : \mathbb{R}^m \rightarrow \mathbb{R}$ is convex for all $t \in [0, t_f]$, it follows that O_λ is convex. Let $\{q_k\} \subset O_\lambda$ and $\|q_k - q\|_{L^2([0, t_f]; \mathbb{R}^m)}$ converges to 0 as $k \rightarrow \infty$. We can choose a subsequence $\{q_{k_j}\} \subset \{q_k\}$ such that q_{k_j} converges to q pointwise almost everywhere on $[0, t_f]$ [92, p. 53]. Now we have

1. $g(q_{k_j}(t), t) \geq 0$ for all $t \in [0, t_f]$ (assumption (E11));
2. $\lim_{j \rightarrow \infty} g(q_{k_j}(t), t) = g(q(t), t)$ almost everywhere on $[0, t_f]$.

By Fatou's lemma [67],

$$\int_0^{t_f} g(q(t), t) dt \leq \liminf_{k \rightarrow \infty} \int_0^{t_f} g(q_{k_j}(t), t) dt \leq \lambda, \quad (\text{A.61})$$

where the last inequality holds due to the fact that $\{q_{k_j}\} \subset O_\lambda$. Hence, $q \in O_\lambda$ and O_λ is closed.

Since O_λ is weakly sequentially closed, $p_{k_j} \rightharpoonup p$ implies that $p \in O_\lambda$, which contradicts (A.60). Hence, $J_{(\mathbf{Pe})}(p) \leq J_{(\mathbf{Pe})}(p_0)$ is proved, and we conclude Condition-2.

Proof of Condition-3: We now show that the mapping $J_{(\mathbf{Pe})}(\cdot) : \mathcal{P} \rightarrow \mathbb{R}$ is weakly sequentially lower semicontinuous on \mathcal{P}_0 . Suppose $\{p_k\} \subset \mathcal{P}_0$ and $p_k \rightharpoonup p \in \mathcal{P}_0$. We wish to establish $J_{(\mathbf{Pe})}(p) \leq \liminf_{k \rightarrow \infty} J_{(\mathbf{Pe})}(p_k)$, which can be shown using the technique of proving Condition-2 (starting from (A.55)).

So we conclude the existence of a solution of problem (Pe). □

A.10 Proof of Theorem 4.2

Proof. Since $\text{Tr}(\Pi_N(t)) \geq 0$ ($\Pi_N(t)$ is nonnegative and self-adjoint for all $t \in [0, t_f]$) and the mapping $K_N^e : C([0, t_f]; \mathbb{R}^n) \rightarrow \mathbb{R}$ is continuous (see Lemma 2.5), the proof is analogous to that of Theorem 4.1, where $\Pi(t)$ is replaced by $\Pi_N(t)$. □

A.11 Proof of Theorem 4.3

To prove Theorem 4.3, recall that the notation $J_{(\mathbf{APe})}^*(p_N^*)$ means the optimal value of (APe) evaluated at its optimal solution p_N^* , where the dimension of approximation applied to (APe) is N (as indicated by the subscript of p_N^*). In the proof, we attach a subscript to (APe), such as $J_{(\mathbf{APe})_N}(p)$, to indicate its dimension when it is not reflected by the argument, e.g., $J_{(\mathbf{APe})_N}(p)$ means that the cost of (APe) using an N -dimensional approximation evaluated at a guidance function p . The following

lemma will be used in the proof of Theorem 4.3

Lemma A.2. *Consider problems (Pe) and its approximation (APe). Let assumptions (E4)–(E12) hold. Then the following results hold:*

1. For $p \in C([0, t_f]; \mathbb{R}^m)$, $\lim_{N \rightarrow \infty} J_{(\text{APe})_N}(p) = J_{(\text{Pe})}(p)$;
2. The mapping $J_{(\text{Pe})} : C([0, t_f]; \mathbb{R}^m) \rightarrow \mathbb{R}^+$ such that $J_{(\text{Pe})}(p) = \int_0^{t_f} \text{Tr}(\Pi(t)) dt + J_m(\zeta, p)$ is continuous, where ζ is the sensor state steered by p under the dynamics (2.4) and $\Pi(\cdot)$ is the covariance operator obtained through (2.25) with sensor state ζ .

Proof of Lemma A.2. 1. We first prove that for $p \in C([0, t_f]; \mathbb{R}^m)$,

$$\lim_{N \rightarrow \infty} |J_{(\text{APe})_N}(p) - J_{(\text{Pe})}(p)| = 0. \quad (\text{A.62})$$

To establish (A.62), it suffices to show

$$\lim_{N \rightarrow \infty} \left| \int_0^{t_f} \text{Tr}(\Pi_N(t)) - \text{Tr}(\Pi(t)) dt \right| = 0. \quad (\text{A.63})$$

We have

$$\begin{aligned} \left| \int_0^{t_f} \text{Tr}(\Pi_N(t)) - \text{Tr}(\Pi(t)) dt \right| &\leq \int_0^{t_f} \left| \|\Pi_N(t)\|_{\mathcal{J}_1(\mathcal{H})} - \|\Pi(t)\|_{\mathcal{J}_1(\mathcal{H})} \right| dt \\ &\leq \int_0^{t_f} \|\Pi_N(t) - \Pi(t)\|_{\mathcal{J}_1(\mathcal{H})} dt \\ &\leq \sup_{t \in [0, t_f]} \|\Pi_N(t) - \Pi(t)\|_{\mathcal{J}_1(\mathcal{H})} t_f. \end{aligned} \quad (\text{A.64})$$

By Lemma 2.8, $\sup_{t \in [0, t_f]} \|\Pi_N(t) - \Pi(t)\|_{\mathcal{J}_q(\mathcal{H})} \rightarrow 0$ as $N \rightarrow \infty$. And specifically, when $q = 1$, the convergence in (A.62) holds due to (A.64).

2. The cost function of (Pe) is the sum of two parts: the uncertainty cost $\int_0^{t_f} \text{Tr}(\Pi(t))dt$, cast as a continuous mapping $K^e : C([0, t_f]; \mathbb{R}^n) \rightarrow \mathbb{R}^+$ (see Lemma 2.5) and the mobility cost $J_m(\zeta, p)$, cast as a mapping $\bar{J}_m : C([0, t_f]; \mathbb{R}^m) \rightarrow \mathbb{R}^+$ which we define below. The mapping \bar{J}_m is the single argument version of the original mobility cost by defining the sensor state as a mapping of the sensor guidance. Here, we redefine the domain of the map T in the proof of Theorem 4.1 such that $T : C([0, t_f]; \mathbb{R}^m) \rightarrow C([0, t_f]; \mathbb{R}^n)$. The continuity of T still holds [88], i.e., for $p_1, p_2 \in C([0, t_f]; \mathbb{R}^m)$ there exist $c_9 > 0$ such that

$$\|Tp_1 - Tp_2\|_{C([0, t_f]; \mathbb{R}^n)} \leq c_9 \|p_1 - p_2\|_{C([0, t_f]; \mathbb{R}^m)}. \quad (\text{A.65})$$

Let $\bar{J}_m(p) = J_m(Tp, p)$ and we show \bar{J}_m is continuous. Define mappings $G : C([0, t_f]; \mathbb{R}^m) \rightarrow \mathbb{R}^+$, $H : C([0, t_f]; \mathbb{R}^n) \rightarrow \mathbb{R}^+$, and $H_f : C([0, t_f]; \mathbb{R}^n) \rightarrow \mathbb{R}^+$ such that

$$G(p) = \int_0^{t_f} g(p(t), t)dt, \quad (\text{A.66})$$

$$H(p) = \int_0^{t_f} h(Tp(t), t)dt, \quad (\text{A.67})$$

$$H_f(p) = h_f(Tp(t_f)). \quad (\text{A.68})$$

Since $\bar{J}_m(p) = G(p) + H(p) + H_f(p)$, we shall proceed with showing that the mappings G , H , and H_f are continuous.

Let $p_1, p_2 \in \mathcal{P}(p_{\max}, a_{\max})$. Both the set of admissible guidance's values $P_0 = \cup_{t \in [0, t_f]} \{p(t) : p \in \mathcal{P}(p_{\max}, a_{\max})\}$ and the interval $[0, t_f]$ are closed and bounded (hence compact). Since $g : P_0 \times [0, t_f] \rightarrow \mathbb{R}^+$ is continuous, by the Heine-Cantor Theorem [76, Proposition 5.8.2], g is uniformly continuous, i.e., for all $\epsilon > 0$ there exists $\delta > 0$ such that for all $t \in [0, t_f]$, $|p_1(t) - p_2(t)| < \delta$ implies $|g(p_1(t), t) - g(p_2(t), t)| < \epsilon$. Hence, it follows that

$$\begin{aligned} \|p_1 - p_2\|_{C([0, t_f]; \mathbb{R}^m)} &= \sup_{t \in [0, t_f]} |p_1(t) - p_2(t)| < \delta, \\ \Rightarrow |g(p_1(t), t) - g(p_2(t), t)| &< \epsilon, \quad \forall t \in [0, t_f]. \end{aligned} \quad (\text{A.69})$$

Therefore, for all $\epsilon > 0$ there exists $\delta > 0$ such that $\|p_1 - p_2\|_{C([0, t_f]; \mathbb{R}^m)} < \delta$ implies

$$\int_0^{t_f} |g(p_1(t), t) - g(p_2(t), t)| dt < \epsilon t_f, \quad (\text{A.70})$$

which concludes the continuity of the mapping G .

Since the continuous image of a compact set is compact [76, Proposition 5.5.1], the image set $T(\mathcal{P}(p_{\max}, a_{\max}))$ is compact, i.e., the set $\Xi = \{\zeta \in C([0, t_f]; \mathbb{R}^n) : \zeta = Tp, p \in \mathcal{P}(p_{\max}, a_{\max})\}$ is compact. The compactness of Ξ implies that the set of sensor state's values $\zeta(t)$, $\Xi_0 = \cup_{t \in [0, t_f]} \{\zeta(t) | \zeta \in \Xi\}$, is closed. Furthermore, since $\|Tp\|_{C([0, t_f]; \mathbb{R}^n)}$ is bounded (see (A.65)) and Ξ_0 is finite dimensional, the set Ξ_0 is compact. The compactness of Ξ_0 and continuity of the function $h : \Xi_0 \times [0, t_f] \rightarrow \mathbb{R}^+$ implies that h is uniformly continuous by the Heine-Cantor Theorem [76, Proposition 5.8.2]. Hence, for all $\epsilon > 0$ there exists $\delta > 0$ such that if

$\|p_1 - p_2\|_{C([0,t_f];\mathbb{R}^m)} < \delta/c_9$, which implies $\|Tp_1 - Tp_2\|_{C([0,t_f];\mathbb{R}^n)} < \delta$, then

$$\int_0^{t_f} |h(Tp_1(t), t) - h(Tp_2(t), t)| dt \leq \epsilon t_f, \quad (\text{A.71})$$

which concludes the continuity of the mapping H .

The mapping H_f is continuous because for all $\epsilon > 0$ there exists $\delta > 0$ such that if $\|p_1 - p_2\|_{C([0,t_f];\mathbb{R}^m)} < \delta/c_9$, which implies $\sup_{t \in [0,t_f]} |Tp_1(t) - Tp_2(t)| < \delta$, then

$$|Tp_1(t_f) - Tp_2(t_f)| < \delta. \quad (\text{A.72})$$

Furthermore, $|H_f(p_1) - H_f(p_2)| = |h_f(Tp_1(t_f)) - h_f(Tp_2(t_f))| < \epsilon$ holds due to the continuity of h_f .

Hence, we conclude the continuity of \bar{J}_m , which, together with the continuity of $K^e(\cdot)$ and (A.65), implies the continuity of $J_{(\mathbf{P}e)}(\cdot)$. \square

Proof of Theorem 4.3. We start with proving (4.8), i.e., $|J_{(\mathbf{A}P\mathbf{e})}^*(p_N^*) - J_{(\mathbf{P}e)}^*(p^*)| \rightarrow 0$ as $N \rightarrow \infty$. First,

$$\begin{aligned} J_{(\mathbf{A}P\mathbf{e})}^*(p_N^*) &= \min_{p \in \mathcal{P}(p_{\max}, a_{\max})} J_{(\mathbf{A}P\mathbf{e})_N}(p) \\ &\leq J_{(\mathbf{A}P\mathbf{e})_N}(p^*) \\ &\leq |J_{(\mathbf{A}P\mathbf{e})_N}(p^*) - J_{(\mathbf{P}e)}^*(p^*)| + J_{(\mathbf{P}e)}^*(p^*). \end{aligned}$$

It follows that

$$\limsup_{N \rightarrow \infty} J_{(\text{APe})}^*(p_N^*) \leq J_{(\text{Pe})}^*(p^*), \quad (\text{A.73})$$

because $|J_{(\text{APe})_N}(p^*) - J_{(\text{Pe})}^*(p^*)| \rightarrow 0$ as $N \rightarrow \infty$ (see Lemma A.2-1).

To proceed with proving (4.8), in addition to (A.73), we shall show

$$\liminf_{N \rightarrow \infty} J_{(\text{APe})}^*(p_N^*) \geq J_{(\text{Pe})}^*(p^*).$$

Choose a convergent subsequence $\{J_{(\text{APe})}^*(p_{N_k}^*)\}_{k=1}^\infty$ such that

$$\lim_{k \rightarrow \infty} J_{(\text{APe})}^*(p_{N_k}^*) = \liminf_{N \rightarrow \infty} J_{(\text{APe})}^*(p_N^*). \quad (\text{A.74})$$

Since the subsequence $\{p_{N_k}^*\}_{k=1}^\infty \subset \mathcal{P}(p_{\max}, a_{\max})$ which is uniformly equicontinuous and uniformly bounded, by the Arzelà-Ascoli Theorem [67], there is a (uniformly) convergent subsequence of $\{p_{N_k}^*\}_{k=1}^\infty$. We denote this convergent subsequence with the same indices $\{N_k\}_{k=1}^\infty$ to simplify notation. Denote the limit of $\{p_{N_k}^*\}_{k=1}^\infty$ by p_{inf}^* , i.e.,

$$\lim_{k \rightarrow \infty} \|p_{N_k}^* - p_{\text{inf}}^*\|_{C([0, t_f]; \mathbb{R}^m)} = 0. \quad (\text{A.75})$$

Next, we show

$$\lim_{k \rightarrow \infty} |J_{(\text{APe})}^*(p_{N_k}^*) - J_{(\text{Pe})}^*(p_{\text{inf}}^*)| = 0. \quad (\text{A.76})$$

First notice that for all $p \in \mathcal{P}(p_{\max}, a_{\max})$, $J_{(\text{APe})_N}(p)$ converges to $J_{(\text{Pe})}(p)$ point-wise as the dimension of approximation N goes to infinity (see (A.62)). Furthermore, since the sequence of approximated uncertainty cost $\{\int_0^{t_f} \text{Tr}(\Pi_N(t))dt\}_{N=1}^\infty$ is a monotonically increasing sequence, the sequence $\{J_{(\text{APe})_N}(p)\}_{N=1}^\infty$ is a monotonically increasing sequence for each p on the compact set $\mathcal{P}(p_{\max}, a_{\max})$. By Dini's Theorem [68, Theorem 7.13], $|J_{(\text{APe})_N}(p) - J_{(\text{Pe})}(p)| \rightarrow 0$ uniformly on $\mathcal{P}(p_{\max}, a_{\max})$ as $N \rightarrow \infty$. By Moore-Osgood Theorem [68, Theorem 7.11], this uniform convergence and the convergence $p_{N_k}^* \rightarrow p_{\text{inf}}^*$ as $k \rightarrow \infty$ (see (A.75)) imply that

$$\lim_{k \rightarrow \infty} J_{(\text{Pe})}(p_{N_k}^*) = \lim_{j \rightarrow \infty} \lim_{k \rightarrow \infty} J_{(\text{APe})_j}^*(p_{N_k}^*). \quad (\text{A.77})$$

And the iterated limit in (A.77) equals the double limit [78, p. 140], i.e.,

$$\lim_{j \rightarrow \infty} \lim_{k \rightarrow \infty} J_{(\text{APe})_j}^*(p_{N_k}^*) = \lim_{j \rightarrow \infty} \lim_{k \rightarrow \infty} J_{(\text{APe})_j}^*(p_{N_k}^*) = \lim_{k \rightarrow \infty} J_{(\text{APe})}^*(p_{N_k}^*). \quad (\text{A.78})$$

By (A.77), (A.78), and the fact that $J_{(\text{Pe})}(p_{\text{inf}}^*) = \lim_{k \rightarrow \infty} J_{(\text{Pe})}(p_{N_k}^*)$ holds (due to the continuity of $J_{(\text{Pe})}(\cdot)$, see Lemma A.2-2), we conclude that (A.76) holds and

$$\begin{aligned} \liminf_{N \rightarrow \infty} J_{(\text{APe})}^*(p_N^*) &= \lim_{k \rightarrow \infty} J_{(\text{APe})}^*(p_{N_k}^*) \\ &= J_{(\text{Pe})}(p_{\text{inf}}^*) \\ &\geq J_{(\text{Pe})}^*(p^*). \end{aligned} \quad (\text{A.79})$$

Therefore, we conclude from (A.73) and (A.79)

$$\lim_{N \rightarrow \infty} J_{(\mathbf{A}\mathbf{P}\mathbf{e})}^*(p_N^*) = J_{(\mathbf{P}\mathbf{e})}^*(p^*). \quad (\text{A.80})$$

Next, we prove (4.9), i.e., $|J_{(\mathbf{P}\mathbf{e})}(p_N^*) - J_{(\mathbf{P}\mathbf{e})}^*(p^*)| \rightarrow 0$ as $N \rightarrow \infty$. We start with $J_{(\mathbf{P}\mathbf{e})}^*(p^*) \leq J_{(\mathbf{P}\mathbf{e})}(p_N^*)$ for all N , which implies that

$$J_{(\mathbf{P}\mathbf{e})}^*(p^*) \leq \liminf_{N \rightarrow \infty} J_{(\mathbf{P}\mathbf{e})}(p_N^*). \quad (\text{A.81})$$

To prove (4.9), what remains to be shown is $J_{(\mathbf{P}\mathbf{e})}^*(p^*) \geq \limsup_{N \rightarrow \infty} J_{(\mathbf{P}\mathbf{e})}(p_N^*)$. Choose a convergent subsequence $\{J_{(\mathbf{P}\mathbf{e})}(p_{N_j}^*)\}_{j=1}^\infty$ such that

$$\lim_{j \rightarrow \infty} J_{(\mathbf{P}\mathbf{e})}(p_{N_j}^*) = \limsup_{N \rightarrow \infty} J_{(\mathbf{P}\mathbf{e})}(p_N^*). \quad (\text{A.82})$$

Since $\{p_{N_j}^*\}_{j=1}^\infty \subset \mathcal{P}(p_{\max}, a_{\max})$ is uniformly equicontinuous and uniformly bounded, by Arzelà-Ascoli Theorem [67], $\{p_{N_j}^*\}_{j=1}^\infty$ has a (uniformly) convergent subsequence which we denote with the same indices $\{N_j\}_{j=1}^\infty$ to simplify notation. Denote the limit of $\{p_{N_j}^*\}_{j=1}^\infty$ by p_{\sup}^* such that

$$\lim_{j \rightarrow \infty} \left\| p_{N_j}^* - p_{\sup}^* \right\|_{C([0, t_f]; \mathbb{R}^m)} = 0. \quad (\text{A.83})$$

Due to the continuity of $J_{(\mathbf{P}\mathbf{e})}(\cdot)$ (see Lemma A.2-1):

$$J_{(\mathbf{P}\mathbf{e})}(p_{\sup}^*) = \lim_{j \rightarrow \infty} J_{(\mathbf{P}\mathbf{e})}(p_{N_j}^*) = \limsup_{N \rightarrow \infty} J_{(\mathbf{P}\mathbf{e})}(p_N^*). \quad (\text{A.84})$$

Now we have

$$\begin{aligned}
J_{(\mathbf{P}\mathbf{e})}(p_{\text{sup}}^*) &\leq |J_{(\mathbf{P}\mathbf{e})}(p_{\text{sup}}^*) - J_{(\mathbf{P}\mathbf{e})}^*(p^*)| + J_{(\mathbf{P}\mathbf{e})}^*(p^*) \\
&= |J_{(\mathbf{P}\mathbf{e})}(p_{\text{sup}}^*) - \lim_{N \rightarrow \infty} J_{(\mathbf{A}\mathbf{P}\mathbf{e})}^*(p_N^*)| + J_{(\mathbf{P}\mathbf{e})}^*(p^*) \\
&= |J_{(\mathbf{P}\mathbf{e})}(p_{\text{sup}}^*) - \lim_{j \rightarrow \infty} J_{(\mathbf{A}\mathbf{P}\mathbf{e})}^*(p_{N_j}^*)| + J_{(\mathbf{P}\mathbf{e})}^*(p^*). \tag{A.85}
\end{aligned}$$

Since the sequence of approximated uncertainty cost $\{\int_0^{t_f} \Pi_N(t) dt\}_{N=1}^\infty$ is a monotonically increasing sequence, the sequence $\{J_{(\mathbf{A}\mathbf{P}\mathbf{e})_N}(p)\}_{N=1}^\infty$ is a monotonically increasing sequence for each p on the compact set $\mathcal{P}(p_{\text{max}}, a_{\text{max}})$. Since $\lim_{N \rightarrow \infty} J_{(\mathbf{A}\mathbf{P}\mathbf{e})_N}(p) = J_{(\mathbf{P}\mathbf{e})}(p)$ for all $p \in \mathcal{P}(p_{\text{max}}, a_{\text{max}})$ (see Lemma A.2-1), by Dini's Theorem [68, Theorem 7.13], the limit holds uniformly on $\mathcal{P}(p_{\text{max}}, a_{\text{max}})$ as $N \rightarrow \infty$. By Moore-Osgood Theorem [68, Theorem 7.11], this uniform convergence and the convergence $p_{N_j}^* \rightarrow p_{\text{sup}}^*$ as $j \rightarrow \infty$ (see (A.83)) imply that

$$J_{(\mathbf{P}\mathbf{e})}(p_{\text{sup}}^*) = \lim_{k \rightarrow \infty} \lim_{j \rightarrow \infty} J_{(\mathbf{A}\mathbf{P}\mathbf{e})_k}^*(p_{N_j}^*). \tag{A.86}$$

Furthermore, the iterated limit equals the double limit [78, p. 140], i.e.,

$$\lim_{k \rightarrow \infty} \lim_{j \rightarrow \infty} J_{(\mathbf{A}\mathbf{P}\mathbf{e})_k}^*(p_{N_j}^*) = \lim_{j \rightarrow \infty} \lim_{k \rightarrow \infty} J_{(\mathbf{A}\mathbf{P}\mathbf{e})_k}^*(p_{N_j}^*) = \lim_{j \rightarrow \infty} J_{(\mathbf{A}\mathbf{P}\mathbf{e})}^*(p_{N_j}^*).$$

Hence,

$$J_{(\mathbf{P}\mathbf{e})}(p_{\text{sup}}^*) = \lim_{j \rightarrow \infty} J_{(\mathbf{A}\mathbf{P}\mathbf{e})}^*(p_{N_j}^*), \tag{A.87}$$

which, combined with (A.85), implies

$$J_{(\mathbf{P}_e)}^*(p^*) \geq J_{(\mathbf{P}_e)}(p_{\text{sup}}^*) = \limsup_{N \rightarrow \infty} J_{(\mathbf{P}_e)}(p_N^*). \quad (\text{A.88})$$

The desired convergence $\lim_{N \rightarrow \infty} J_{(\mathbf{P}_e)}(p_N^*) = J_{(\mathbf{P}_e)}^*(p^*)$ follows from (A.81) and (A.88). □

Bibliography

- [1] S. Afshar, K. Morris, and A. Khajepour. Comparison of different observer designs for heat equation. In Proceedings of the 54th IEEE Conference on Decision and Control, pages 1136–1141, 2015.
- [2] A. Aish, J. Ashworth, B. Barrio-Frojan, S. Benjamins, S. Bolam, P. Brazier, S. Brockington, P. Chaniotis, A. Clements, R. Coggan, et al. Marine habitats. In UK Marine Monitoring and Assessment Strategy (2010) Charting Progress 2 Healthy and Biological Diverse Seas Feeder Report, pages 68–271. Department for Environment Food and Rural Affairs, 2010.
- [3] A. Bensoussan. Filtrage optimal des systèmes linéaires. Dunod, 1971.
- [4] A. Bensoussan. Optimization of sensors’ location in a distributed filtering problem. In Stability of Stochastic Dynamical Systems. Lecture Notes in Mathematics, volume 294, pages 62–84. Springer, 1972.
- [5] A. Bensoussan, G. Da Prato, M. C. Delfour, and S. K. Mitter. Representation and control of infinite dimensional systems, volume 1. Birkhäuser Boston, 1992.
- [6] R. Bhatia. Matrix Analysis, volume 169. Springer Science & Business Media, 1996.
- [7] E. Buckingham. On physically similar systems; illustrations of the use of dimensional equations. Physical review, 4(4):345, 1914.
- [8] F. Bullo, J. Cortés, and S. Martínez. Distributed Control of Robotic Networks. Applied Mathematics Series. Princeton University Press, 2009.
- [9] J. Burns, E. Cliff, C. Rautenberg, and L. Zietsman. Optimal sensor design for estimation and optimization of PDE systems. In Proceedings of the 2010 American Control Conference, pages 4127–4132, 2010.
- [10] J. A. Burns and C. N. Rautenberg. The infinite-dimensional optimal filtering problem with mobile and stationary sensor networks. Numerical Functional Analysis and Optimization, 36(2):181–224, 2015.

- [11] J. A. Burns and C. N. Rautenberg. Solutions and approximations to the Riccati integral equation with values in a space of compact operators. SIAM Journal on Control and Optimization, 53(5):2846–2877, 2015.
- [12] J. A. Burns and C. N. Rautenberg. The infinite-dimensional optimal filtering problem with mobile and stationary sensor networks. Numerical Functional Analysis and Optimization, 36(2):181–224, 2015.
- [13] J. A. Burns, E. W. Sachs, and L. Zietsman. Mesh independence of Kleinman-Newton iterations for Riccati equations in Hilbert space. SIAM Journal on Control and Optimization, 47(5):2663–2692, 2008.
- [14] L. Carotenuto, P. Muraca, and G. Raiconi. Optimal location of a moving sensor for the estimation of a distributed-parameter process. International Journal of Control, 46(5):1671–1688, 1987.
- [15] S. Cheng and D. A. Paley. Optimal control of a 1D diffusion process with a team of mobile actuators under jointly optimal guidance. In Proceedings of the 2020 American Control Conference, pages 3449–3454, 2020.
- [16] S. Cheng and D. A. Paley. Cooperative estimation and control of a diffusion-based spatiotemporal process using mobile sensors and actuators. Submitted, 2021.
- [17] S. Cheng and D. A. Paley. Optimal control of a 2D diffusion-advection process with a team of mobile actuators under jointly optimal guidance. To appear in Automatica, 2021.
- [18] S. Cheng and D. A. Paley. Optimal guidance and estimation of a 1D diffusion process by a team of mobile sensors. In Proceedings of the 59th IEEE Conference on Decision and Control, pages 1222–1228, 2021.
- [19] S. Cheng and D. A. Paley. Optimal guidance and estimation of a 2D diffusion-advection process by a team of mobile sensors. Submitted, 2021.
- [20] S. Cheng and D. A. Paley. Optimal guidance of a team of mobile actuators for controlling a 1D diffusion process with unknown initial conditions. In Proceedings of the 2021 American Control Conference, pages 1493–1498, 2021.
- [21] R. F. Curtain and H. Zwart. An introduction to infinite-dimensional linear systems theory, volume 21. Springer Science & Business Media, 2012.
- [22] M. A. Demetriou. Closed-loop guidance of mobile sensors for the estimation of spatially distributed processes. In Proceedings of the 2018 American Control Conference, pages 931–936, 2008.
- [23] M. A. Demetriou. Guidance of mobile actuator-plus-sensor networks for improved control and estimation of distributed parameter systems. IEEE Transactions on Automatic Control, 55(7):1570–1584, 2010.

- [24] M. A. Demetriou. Domain decomposition methods in the distributed estimation of spatially distributed processes with mobile sensors. In Proceedings of the 2016 American Control Conference, pages 1649–1654, 2016.
- [25] M. A. Demetriou. Gain adaptation and sensor guidance of diffusion PDEs using on-line approximation of optimal feedback kernels. In Proceedings of the 2016 American Control Conference, pages 2536–2541, 2016.
- [26] M. A. Demetriou. Incorporating impact of hazardous and toxic environments on the guidance of mobile sensor networks used for the cooperative estimation of spatially distributed processes. In Proceedings of the 57th IEEE Conference on Decision and Control, pages 1317–1322, 2018.
- [27] M. A. Demetriou. Using modified Centroidal Voronoi Tessellations in kernel partitioning for optimal actuator and sensor selection of parabolic PDEs with static output feedback. In Proceedings of the 56th IEEE Conference on Decision and Control, pages 3119–3124, 2018.
- [28] M. A. Demetriou and E. Bakolas. Navigating over 3D environments while minimizing cumulative exposure to hazardous fields. Automatica, 115:108859, 2020.
- [29] M. A. Demetriou and J. Borggaard. Optimization of a joint sensor placement and robust estimation scheme for distributed parameter processes subject to worst case spatial disturbance distributions. In Proceedings of the 2004 American Control Conference, pages 2239–2244, 2004.
- [30] M. A. Demetriou and N. A. Gatsonis. Scheduling of static sensor networks and management of mobile sensor networks for the detection and containment of moving sources in spatially distributed processes. In Proceedings of the 17th Mediterranean Conference on Control and Automation, pages 187–192, 2009.
- [31] M. A. Demetriou, N. A. Gatsonis, and J. R. Court. Lyapunov based guidance of a mobile sensing agent for state estimation of a gaseous source in a 3D spatial domain. In Proceedings of the 50th IEEE Conference on Decision and Control, pages 1986–1992, 2011.
- [32] M. A. Demetriou, N. A. Gatsonis, and J. R. Court. Model-based detection of a moving gaseous source in a 2D spatial domain using a sensor-based grid adaptation approach. In Proceedings of the 2011 American Control Conference, pages 2374–2380, 2011.
- [33] M. A. Demetriou and I. I. Hussein. Estimation of spatially distributed processes using mobile spatially distributed sensor network. SIAM Journal on Control and Optimization, 48(1):266–291, 2009.
- [34] M. A. Demetriou, A. Paskaleva, O. Vayena, and H. Doumanidis. Scanning actuator guidance scheme in a 1-D thermal manufacturing process. IEEE Transactions on Control Systems Technology, 11(5):757–764, 2003.

- [35] S. Dubljevic, M. Kobilarov, and J. Ng. Discrete mechanics optimal control (DMOC) and model predictive control (MPC) synthesis for reaction-diffusion process system with moving actuator. In Proceedings of the 2010 American Control Conference, pages 5694–5701, 2010.
- [36] Z. Emirsjlow and S. Townley. From PDEs with boundary control to the abstract state equation with an unbounded input operator: a tutorial. European Journal of Control, 6(1):27–49, 2000.
- [37] Heron Systems Inc. OpenMACE – Multi-Agent Collaborative Ecosystem. <https://github.com/heronsystems/OpenMACE>. [Online; accessed 28-April-2021].
- [38] W. Honig, J. A. Preiss, T. K. Kumar, G. S. Sukhatme, and N. Ayanian. Trajectory planning for quadrotor swarms. IEEE Transactions on Robotics, 34(4):856–869, 2018.
- [39] M. Hoy, A. S. Matveev, and A. V. Savkin. Algorithms for collision-free navigation of mobile robots in complex cluttered environments: a survey. Robotica, 33(3):463–497, 2015.
- [40] W. Hu, K. Morris, and Y. Zhang. Sensor location in a controlled thermal fluid. In Proceedings of the 55th IEEE Conference on Decision and Control, pages 2259–2264, 2016.
- [41] L. Imsland. Partially distributed optimization for mobile sensor path-planning. In Proceedings of the 56th IEEE Conference on Decision and Control, pages 3101–3106, 2017.
- [42] D. Karagiannis and V. Radisavljevic-Gajic. A backstepping boundary observer for a simply supported beam. IEEE Transactions on Automatic Control, 64(9):3809–3816, 2019.
- [43] D. Kasinathan and K. Morris. H_∞ -optimal actuator location. IEEE Transactions on Automatic Control, 58(10):2522–2535, 2013.
- [44] A. Khapalov. L^∞ -exact observability of the heat equation with scanning pointwise sensor. SIAM Journal on Control and Optimization, 32(4):1037–1051, 1994.
- [45] A. Y. Khapalov. Continuous observability for parabolic system under observations of discrete type. IEEE Transactions on Automatic Control, 38(9):1388–1391, 1993.
- [46] R. Khodayi-Mehr, W. Aquino, and M. M. Zavlanos. Model-based active source identification in complex environments. IEEE Transactions on Robotics, 35(3):633–652, 2019.

- [47] D. E. Kirk. Optimal control theory: an introduction. Courier Corporation, 2012.
- [48] M. Krstic and A. Smyshlyaev. Boundary control of PDEs: A course on backstepping designs, volume 16. SIAM, 2008.
- [49] I. Lasiecka and R. Triggiani. Control theory for partial differential equations: continuous and approximation theories, volume 1. Cambridge University Press Cambridge, 2000.
- [50] F. L. Lewis, D. Vrabie, and V. L. Syrmos. Optimal control. John Wiley & Sons, 2012.
- [51] D. Liberzon. Calculus of variations and optimal control theory: a concise introduction. Princeton University Press, 2011.
- [52] C. E. Luis and A. P. Schoellig. Trajectory generation for multiagent point-to-point transitions via distributed model predictive control. IEEE Robotics and Automation Letters, 4(2):375–382, 2019.
- [53] M. McAsey, L. Mou, and W. Han. Convergence of the forward-backward sweep method in optimal control. Computational Optimization and Applications, 53(1):207–226, 2012.
- [54] J. S. Meditch. Least-squares filtering and smoothing for linear distributed parameter systems. Automatica, 7(3):315–322, 1971.
- [55] N. Michael, D. Mellinger, Q. Lindsey, and V. Kumar. The GRASP multiple micro-UAV testbed. IEEE Robotics Automation Magazine, 17(3):56–65, 2010.
- [56] K. Morris. Control of systems governed by partial differential equations. In The Control Systems Handbook: Control System Advanced Methods, Second Edition, pages 1519–1556. CRC press, 2010.
- [57] K. Morris. Linear-quadratic optimal actuator location. IEEE Transactions on Automatic Control, 56(1):113–124, 2010.
- [58] K. Morris, M. A. Demetriou, and S. D. Yang. Using H_2 -control performance metrics for the optimal actuator location of distributed parameter systems. IEEE Transactions on Automatic Control, 60(2):450–462, 2015.
- [59] K. Morris and S. Yang. Comparison of actuator placement criteria for control of structures. Journal of Sound and Vibration, 353:1–18, 2015.
- [60] K. Morris and S. Yang. A study of optimal actuator placement for control of diffusion. In Proceedings of the 2016 American Control Conference, pages 2566–2571, 2016.
- [61] K. A. Morris. Optimal output estimation for infinite-dimensional systems with disturbances. Systems and Control Letters, 146:104803, 2020.

- [62] S. J. Moura and H. K. Fathy. Optimal boundary control & estimation of diffusion-reaction PDEs. In Proceedings of the 2011 American Control Conference, pages 921–928, 2011.
- [63] Y. Nie, O. Faqir, and E. C. Kerrigan. ICLOCS2: Try this optimal control problem solver before you try the rest. In 2018 UKACC 12th International Conference on Control, pages 336–336, 2018.
- [64] K. K. Oh, M. C. Park, and H. S. Ahn. A survey of multi-agent formation control. Automatica, 53:424–440, 2015.
- [65] S. Omatu and J. H. Seinfeld. Distributed parameter systems: theory and applications. Clarendon Press, 1989.
- [66] Y. Privat, E. Trélat, and E. Zuazua. Optimal shape and location of sensors for parabolic equations with random initial data. Archive for Rational Mechanics and Analysis, 216(3):921–981, 2015.
- [67] H. Royden and P. Fitzpatrick. Real analysis (4th edition). New Jersey: Prentice-Hall Inc, 2010.
- [68] W. Rudin. Principles of mathematical analysis, volume 3. McGraw Hill, 1964.
- [69] J. Saak and P. Benner. Efficient numerical solution of the LQR-problem for the heat equation. PAMM:Proceedings in Applied Mathematics and Mechanics, 4(1):648–649, 2004.
- [70] M. Schranz, M. Umlauft, M. Sende, and W. Elmenreich. Swarm robotic behaviors and current applications. Frontiers in Robotics and AI, 7:36, 2020.
- [71] A. Schroeder. Mitigating harmful algal blooms using a robot swarm. PhD thesis, University of Toledo, 2018.
- [72] M. Schwager, M. P. Vitus, S. Powers, D. Rus, and C. J. Tomlin. Robust adaptive coverage control for robotic sensor networks. IEEE Transactions on Control of Network Systems, 4(3):462–476, 2017.
- [73] A. Smyshlyaev and M. Krstic. Backstepping observers for a class of parabolic PDEs. Systems and Control Letters, 54(7):613–625, 2005.
- [74] A. Smyshlyaev and M. Krstic. Adaptive control of parabolic PDEs. Princeton University Press, 2010.
- [75] Z. Song, Y. Q. Chen, J. S. Liang, and D. Uciński. Optimal mobile sensor motion planning under non-holonomic constraints for parameter estimation of distributed systems. International Journal of Intelligent Systems Technologies and Applications, 3(3-4):277–295, 2007.
- [76] W. A. Sutherland. Introduction to metric and topological spaces. Oxford University Press, 2009.

- [77] N. Sydney and D. A. Paley. Multivehicle coverage control for a nonstationary spatiotemporal field. Automatica, 50(5):1381–1390, 2014.
- [78] A. E. Taylor. General theory of functions and integration. Courier Corporation, 1985.
- [79] C. Tricaud, M. Patan, D. Uciński, and Y. Q. Chen. D-optimal trajectory design of heterogeneous mobile sensors for parameter estimation of distributed systems. In Proceedings of the 2008 American Control Conference, pages 663–668, 2008.
- [80] F. Tröltzsch. Optimal control of partial differential equations: theory, methods, and applications, volume 112. American Mathematical Society, 2010.
- [81] D. Ucinski. Optimal measurement methods for distributed parameter system identification. CRC press, 2004.
- [82] D. Ucinski and Y. Chen. Time-optimal path planning of moving sensors for parameter estimation of distributed systems. In Proceedings of the 44th IEEE Conference on Decision and Control, pages 5257–5262, 2005.
- [83] D. Uciński and J. Korbicz. Path planning for moving sensors in parameter estimation of distributed systems. In Proceedings of the First Workshop on Robot Motion and Control, pages 273–278, 1999.
- [84] D. W. Veldman, R. H. Fey, H. J. Zwart, M. M. Van De Wal, J. D. Van Den Boom, and H. Nijmeijer. Sensor and actuator placement for proportional feedback control in advection-diffusion equations. IEEE Control Systems Letters, 4(1):193–198, 2020.
- [85] J. W. Wang, Y. Guo, M. Fahad, and B. Bingham. Dynamic Plume Tracking by Cooperative Robots. IEEE/ASME Transactions on Mechatronics, 24(2):609–620, 2019.
- [86] J. W. Wang, Y. Q. Liu, Y. Y. Hu, and C. Y. Sun. A spatial domain decomposition approach to distributed H^∞ observer design of a linear unstable parabolic distributed parameter system with spatially discrete sensors. International Journal of Control, 90(12):2772–2785, 2017.
- [87] L. Wang, A. D. Ames, and M. Egerstedt. Safety barrier certificates for collisions-free multirobot systems. IEEE Trans. Robotics, 33(3):661–674, 2017.
- [88] J. Werner. Optimization theory and applications. Springer-Verlag, 2013.
- [89] A. Wolek, S. Cheng, D. Goswami, and D. A. Paley. Cooperative mapping and target search over an unknown occupancy graph using mutual information. IEEE Robotics and Automation Letters, 5(2):1071–1078, 2020.

- [90] A. Wolek, S. Cheng, D. Goswami, and D. A. Paley. Cooperative mapping and target search over an unknown occupancy graph using mutual information. IEEE Robotics and Automation Letters, 5(2):1071–1078, 2020.
- [91] Y. Xu, J. Choi, and S. Oh. Mobile sensor network navigation using Gaussian processes with truncated observations. IEEE Transactions on Robotics, 27(6):1118–1131, 2011.
- [92] K. Yosida. Functional analysis, volume 123. springer, 1988.
- [93] H. Yu, M. Diagne, L. Zhang, and M. Krstic. Bilateral boundary control of moving shockwave in lwr model of congested traffic. IEEE Transactions on Automatic Control, 2020.
- [94] H. Yu, K. Meier, M. Argyle, and R. W. Beard. Cooperative path planning for target tracking in urban environments using unmanned air and ground vehicles. IEEE/ASME Transactions on Mechatronics, 20(2):541–552, 2015.
- [95] F. Zeng and B. Ayalew. Estimation and coordinated control for distributed parameter processes with a moving radiant actuator. Journal of Process Control, 20(6):743–753, 2010.
- [96] M. Zhang and K. Morris. Sensor choice for minimum error variance estimation. IEEE Transactions on Automatic Control, 63(2):315–330, 2018.